

**A conditional mouse model for the characterization of  
mTORC1 function in muscle and brain**

**Inauguraldissertation**

zur

Erlangung der Würde eines Doktors der Philosophie

Vorgelegt der

Philosophisch-Naturwissenschaftlichen Fakultät

Der Universität Basel

Von

**Dimitri Yves Reto Cloëtta**

Aus Zürich (ZH) und Bergün (GR)

Basel, 2010

Genehmigt von der Philosophisch-Naturwissenschaftlichen Fakultät

Auf Antrag von

**Prof. Dr. Markus A. Rüegg**

**Prof. Dr. Bernhard Bettler**

Basel, den 17. Februar 2009

Prof. Dr. Eberhard Parlow  
Dekan

## Table of contents

<b>1. Summary</b> .....	3
<b>2. General introduction</b> .....	4
<b>2.1. The mTORC1 and mTORC2 pathway</b> .....	4
2.1.1. Upstream factors of mTOR .....	4
2.1.2. Downstream effectors and general functions of mTOR .....	5
<b>2.2. Functions of mTOR in muscle</b> .....	7
<b>2.3. Functions of mTOR in the developing and adult brain</b> .....	8
<b>2.4. Aim of this study and contributions</b> .....	9
<b>3. Results</b> .....	10
<b>3. 1. Paper 1</b> .....	10
3.1.1. Summary .....	11
3.1.2. Introduction .....	12
3.1.3. Results .....	14
3.1.4. Discussion .....	20
3.1.5. Materials and methods .....	24
3.1.6. Figures and tables.....	27
<b>3.2. Paper 2</b> .....	34
3.2.1. Summary .....	35
3.2.2. Introduction .....	36
3.2.3. Results .....	37
3.2.4. Discussion .....	44
3.2.5. Experimental procedures .....	48
3.2.6. Acknowledgements .....	49
3.2.7. Figures and tables.....	50
3.2.8. Supplemental data .....	58
<b>4. Concluding remarks</b> .....	71
<b>5. References</b> .....	73
<b>6. Acknowledgements</b> .....	82
<b>Curriculum vitae</b> .....	83

# 1. Summary

The Ser/Thr kinase mammalian target of rapamycin (mTOR) regulates cell growth in response to extracellular stimulation with growth factors and to intracellular factors that sense the nutritional and the energy state of the cell. mTOR forms two distinct multiprotein complexes, the rapamycin-sensitive mTOR complex 1 (mTORC1) and mTORC2. Most characterized functions of mTOR are mediated by mTORC1. However, direct investigation of the *in vivo* function in most tissues including brain and muscle has been occluded by the early embryonic lethality of deficient mice for all mTORC1 members. Here, I describe the generation and characterization of mice that are deficient for *raptor*, an essential component of mTORC1, in skeletal muscle fibers and the developing brain.

Analysis of the *raptor*-deficient brain reveals a general growth defect that evenly affects the whole organ. A decrease in cell size and cell number underlies the observed microcephaly. This is in accordance to earlier studies which assign to mTORC1 a role as controller of cell size and cell cycle. Beside this, mTORC1 controls several more specific aspects of brain development. Glial differentiation is disturbed and this is paralleled by a decrease of Stat3 activity, a member of the Jak/Stat pathway that was previously involved in gliogenesis. Loss of the glial network in the dentate gyrus likely causes malformations of the developing granule cell layer. Furthermore, I describe an unexpected role of mTORC1 in the formation of hippocampal and cortical layers.

Muscle-specific knockout (ko) mice develop a progressive muscle dystrophy and show changes in muscle metabolism. Based on alterations in the activation state and expression levels, we provide evidence that this phenotype is accounted for by PGC1 $\alpha$  as well as Akt/PKB.

In summary, this work provides evidence, that raptor is important for postnatal survival both, in muscle and the brain. Beside the generalized changes in cell growth, both ko models provide first evidence *in vivo* that mTORC1 regulates specific aspects of metabolism and that it differentially affects both glial and neuronal differentiation by affecting cell-specific pathways.

## 2. General introduction

The macrolide rapamycin is produced by the bacterium *Streptomyces hygroscopicus* as an antifungal agent [1]. The bacterium was isolated from an Easter Island (indigenous name: Rapa Nui) soil sample and the antibiotic purified and characterized [2-4]. Later, the immunosuppressant activity of rapamycin was discovered [5] and manifested by identification of its ability to inhibit T-cell proliferation [6]. Like for the other immunosuppressant drugs cyclosporin A and FK-508, its primary receptor is the immunophilin FKBP [7]. In a genetic screen for targets of the complex of FKBP and rapamycin in the budding yeast *Sachharomyces cerevisiae*, two homologous proteins were identified and termed target of rapamycin 1 (TOR1) and TOR2 [8].

The *TOR* gene was subsequently identified in other eukaryotes, but occurred only in one copy [9]. The mammalian ortholog of TOR is called mTOR, which was previously also named FRAP, RAFT, RAP or SEP [10]. In parallel to the situation in yeast [11], mTOR forms two distinct multiprotein complexes [12, 13]. mTOR complex 1 (mTORC1) consists of mTOR, raptor (*regulatory associated protein of mTOR*), mLST8 and PRAS40 [14]. Beside mTOR, mTORC2 harbors rictor (*rapamycin insensitive companion of mTOR*), mSIN1 and mLST8. mTORC1 is sensitive to acute application of rapamycin, whereas long term treatment may interfere with the new formation of mTORC2 by titrating away free mTOR [15]. Analysis of the TOR pathway “from yeast to man” revealed a conserved role of TOR as nutrient sensor and as controller of cell growth [16].

### 2.1. The mTORC1 and mTORC2 pathway

Due to the ease of rapamycin application and probably also because of the more prominent and more severe phenotypes that are associated with deletion of mTORC1, mTORC2 was much later described and its function is still less characterized. The two mTOR complexes, however, are probably differentially regulated and have different effectors [12, 13].

#### 2.1.1. Upstream factors of mTOR

mTORC1 reacts on extracellular and on intracellular signals that bear information about the nutritional state of the cell and the organism [16]. Best characterized is its function as sensor for growth factors, ATP levels and amino acid levels.

In numerous studies, mTOR was described to mediate insulin and IGF signaling via a signaling cascade consisting of the Insulin or IGF receptor, IRS, PI3K, PDK1, Akt/PKB, the TSC1/TSC2 complex and Rheb [10]. The TSC1/TSC2 complex and its direct downstream target Rheb thereby play a central role in linking the PI3K – Akt/PKB branch of the insulin signaling with mTOR [17]. In its GTP bound state, the small GTPase Rheb activates mTORC1, whereas nucleotide-free Rheb inhibits mTOR [18, 19]. The TSC complex, which is negatively regulated by Akt/PKB-mediated phosphorylation, acts as a GTPase activating protein (GAP) towards Rheb and thereby promotes GTP unloading from Rheb and inactivation of mTOR [17]. Unlike the growth factor pathway, amino acids do not signal through TSC [20] and do not change the Rheb-GTP levels [21]. Instead of class 1 PI3K like in the insulin signaling pathway, a role for the class 3 PI3K hVps34 was established in amino acid sensing and regulation of mTORC1, although the mechanism remains unclear [22, 23]. Recently, the Rag proteins, a family of four GTPases was identified to interact with mTOR and to be essential for amino acid induced mTORC1 activation [24]. The energy status of the cell is reflected by the activity level of AMPK. Low energy levels that go together with a high intracellular AMP/ATP level activate AMPK [25]. Activated AMPK can directly phosphorylate TSC in a way that enhances its GAP activity towards Rheb and inhibits mTORC1 [26].

Availability of insulin/IGF, amino acids and energy all regulate mTORC1 activity in a way that allows for an appropriate adjustment of cell growth. But these factors are by far not the only input on mTOR. In different cells and contexts, additional physiological signals can activate the mTOR pathway. For example, BDNF [27], Reelin [28], Leptin [29] and REDD-mediated oxidative stress [30] have been shown to modulate mTORC1 activity.

Insulin and the PI3K pathway activate mTORC2. The TSC-complex promotes mTORC2 kinase activity in a manner that is independent of its GAP-mediated Rheb activation [31]. TSC2 physically interacts with mTORC2 but the mechanism of activation is not currently understood [32].

### **2.1.2. Downstream effectors and general functions of mTOR**

The TOR pathway is a controller of eukaryotic cell growth. It collects input signal from various extracellular and intracellular sources and mediates a diverse set of cellular functions via several effectors [16]. Several principal mechanisms are known so far by which mTOR regulates appropriate cell growth. These include promotion of translation via enhanced

ribosome biogenesis and translation initiation, control of transcription and metabolism as well as the inhibition of autophagy.

The best characterized direct mTORC1 downstream targets are S6K and 4E-BP1. They contribute at least to a substantial part to mTORC1 controlled translation. Via phosphorylation of 4E-BP1, mTOR regulates cap-dependent translation initiation. In the phosphorylated state, 4E-BP1 dissociates from eIF4E which in turn associates with eIF4G and initiates translation [33]. Phosphorylated S6K also acts on the formation of the translation initiation complex. It phosphorylates eIF4B and ribosomal protein S6 [34]. eIF4B phosphorylation mediates its recruitment into the initiation complex and allows for the build up of the eIF4F translation initiation complex [35]. In contrast to previous belief, rapamycin-sensitive translation of 5'-TOP RNA, a subgroup of mRNAs which encode ribosomal proteins and translation elongation factors, is not dependent on S6K [36]. For the interaction of mTORC1 with S6K and 4E-BP1, the protein raptor plays an important role. It mediates efficient binding specifically to a conserved 5 amino acid sequence in the N-terminal region of S6K and the C-terminal region of 4E-BP1, the so called TOR signaling (TOS) motif [37].

In addition to the short term activation of translation initiation, mTORC1 regulates also ribosome biogenesis which is required for long term growth [36]. mTOR promotes several steps of biosynthesis including production of rRNA by RNA Polymerase (Pol) I, ribosomal proteins by RNA Pol II and 5S rRNA by RNA Pol III [38]. S6K is necessary for Pol I activation and phosphorylation of the transcription factors UBF and Rrn3 are also involved in mTORC1 mediated activation [39, 40]. But the exact mechanism by which all three RNA polymerases are controlled by mTOR remains unclear.

mTOR also regulates transcription of many genes involved in metabolic and biosynthetic pathways [16]. Beside the regulation of ribosome biogenesis, mTORC1 also directly activates Stat1 and Stat3 [41]. By downregulation of the transcription factors PGC1 $\alpha$  and PPAR $\gamma$ , mTORC1 is also involved in transcriptional control of mitochondrial and fat metabolism, respectively [42, 43]. TORC1 is an inhibitor of autophagy in several eukaryotes [44]. The role of mTOR in autophagy of mammals, its physiological importance and the mechanisms of regulation still need to be investigated. mTORC2 regulates phosphorylation of the kinases Akt/PKB [45], PKC [13] and SGK [46] at their hydrophobic motifs and modulates the actin cytoskeleton [12]. Loss of mTORC2 dependent Akt/PKB phosphorylation at Ser473 affects activity of only a subset of Akt targets, including FoxO1/3a [47], but not the mTORC1 upstream regulator TSC1/TSC2.

The downstream effects of mTOR are much more diverse than the ones depicted in the upper paragraph. Other mechanisms and physiological actions associated with mTOR signaling for example comprise cell cycle progression [48, 49], differentiation [50], local translation together with cell compartment restricted growth [51] and memory formation [52, 53]. There is also an additional level of mTOR downstream effects which ignores the borders of the cell membrane. Whereas in single cell organisms, TOR regulates cell size and polarization [11], in multicellular organisms it controls cell and organ growth, but not exclusively via cell autonomous actions. For example, deletion of an amino acid transporter in the *Drosophila* larvae fat body causes inactivation of dTOR. Subsequently, this leads to a humoral response associated with a systemic growth inhibition of other tissues [54]. Under nutrient rich conditions, a factor is released from the fat body that stabilizes *Drosophila* insulin-like peptides (Dilp) and promotes insulin signaling and growth of peripheral tissues. When dTOR is not active, under nutrient poor conditions, this factor is no longer released and insulin signaling is inhibited. Another example of the way how mTOR influences whole organism size is its implication in regulation of appetite and food intake. Increased hypothalamic mTOR activity, due to high amino acid abundance or leptin signaling, decreases food intake and body weight [29].

## **2.2. Functions of mTOR in muscle**

Especially because of its dependence on growth factors and on mTORC1 upstream and downstream factors, mTOR signaling was found to be involved in the control of muscle growth [55]. In the adult muscle, growth is associated with gain of individual fiber size rather than increase of fiber number. A balance of protein synthesis and degradation is especially important for the regulation of muscle growth or wasting.

Deregulation of muscle growth is associated with several pathologic states like muscle wasting of HIV patients, cachexia which accompanies devastating diseases, age-induced sarcopenia or simple disuse atrophy [56]. In many of them, the IGF signaling is involved [57].

Genetic mouse models revealed that ablation of the mTOR-upstream component Akt/PKB [58] and the downstream effector S6K [59] induce atrophy. In contrast, overexpression of Akt/PKB [60, 61] and IGF-1 [62] is sufficient to induce muscle hypertrophy. Mice that overexpress the negative regulator of mTOR, TSC1, in skeletal muscle show growth defects [63]. Further evidence for an involvement of mTORC1 in these mechanisms comes from the observation, that Akt/PKB induced hypertrophy is rapamycin sensitive [64, 65]. Moreover,



branched chain amino acids, but in particular the strong mTORC1 activator leucine, help in the build-up of muscle by induction of protein synthesis [66].

In addition to the regulation of protein synthesis, activation of the IGF-1/PI3K/Akt/PKB pathway was found to prevent induction of the atrophy mediators MAFbx and MuRF1 via Akt-mediated inhibition of FoxO1 [67] or via mTOR [68].

### **2.3. Functions of mTOR in the developing and adult brain**

During brain growth, mTOR is thought to exert many functions. *In vitro* experiments implicate mTOR in mechanisms that are supposed to be crucial for several stages of brain development.

In cultured neural stem cells, mTORC1 was found to drive differentiation either into the neuronal or the glial lineage [50, 69, 70]. Many studies addressed mTORC1 functions in postmitotic neurons [71]. Neurons are highly organized cells. Axons and dendrites determine the structural and functional polarization. In addition to global cell growth, local mechanisms guide the formation of the cell compartments [72, 73]. mTORC1-dependent mechanisms were suggested to underlie specification and growth of axons [51, 74], growth and maintenance of dendrites [27, 75], growth cone guidance [76] and synaptogenesis [27, 77]. Mechanistically, regulation of local translation is believed to account for these effects [78, 79]. Among the activity- and mTORC1-dependent newly synthesized proteins in synaptodendritic preparations, factors previously involved in dendrite growth or synaptogenesis were identified.

In the adult brain, mTORC1 plays a role in synaptic plasticity and memory formation [71]. Expression of late-phase of LTP was found to be sensitive to rapamycin [80, 81]. This was the case even in dendrites that were severed from their somas, further supporting the concept of local translation in synaptic plasticity [82]. Localized rapamycin application into the auditory cortex of Mongolian gerbils prevents consolidation of long term memory [53]. In an additional study, rats that were subjected to post-training infusion of rapamycin performed worse in the Morris water maze paradigm, a typical test for hippocampus dependent long-term memory formation [52].

## 2.4. Aim of this study and contributions

The goal of this study was to characterize the role of mTORC1 in brain development and in the muscle. Investigation of the function of mTORC1 in these tissues was previously prevented by the fact that null mutants of the individual mTORC1 components mTOR, raptor or mLST8 are embryonically lethal [83-85]. Therefore, a mouse model for the conditional deletion of *raptor*, an essential component of mTORC1, was generated.

In order to specifically delete *raptor* in brain or muscle, we crossed our floxed mice to *Nestin-Cre* and *HSA (human skeletal actin)-Cre* mice, respectively. Specificity of both Cre driver lines was previously described [86, 87]. Analysis of the *raptor*-deficient brain revealed several functions of mTORC1 during brain development. Phenotypes comprise global as well as specific aspects of brain development. In addition to the confirmation of the importance of mTORC1 in muscle growth, study of the *raptor*-deficient muscle phenotype revealed interesting new details of the role of mTORC1 in muscle physiology and metabolism.

Analysis of the muscle was principally performed by Conrad Florian Bentzinger and Klaas Romanino. For examination of the function of mTOR in the muscle, *riCTOR* floxed mice were used which we had generated simultaneously to the *raptor* floxed mice.

## **3. Results**

### **3. 1. Paper 1**

**Ablation of mTORC1 in the developing brain induces microcephaly, defects in glial differentiation and cortical layering**

Dimitri Cloëtta<sup>1</sup>, Venus Thomanetz<sup>1</sup>, Regula Lustenberger<sup>1</sup>, Shuo Lin<sup>1</sup>, Filippo Oliveri<sup>1</sup>, Markus A. Ruegg<sup>1</sup>

<sup>1</sup>Biozentrum, University of Basel, CH-4056 Basel, Switzerland

*in preparation*

### 3.1.1. Summary

The mammalian target of rapamycin (mTOR) regulates cell growth in response to various intracellular and extracellular signals. It assembles into two multiprotein complexes, the rapamycin-sensitive mTOR complex 1 (mTORC1) and the rapamycin-insensitive mTORC2. In this study, we deleted the gene of the functionally crucial mTORC1 component raptor in the developing mouse central nervous system. Such mice are viable for a few hours after birth. Analysis of the brain reveals that mTORC1-deficiency causes severe microcephaly due to both, a reduction of cell size and number. Experiments with cultured neurospheres show that the decreased cell number is due to decreased proliferation. Further, differentiation of neural stem cells into the glial lineage is inhibited in *raptor*-deficient mice. The underdeveloped radial glial network in the dentate gyrus thereby likely disturbs formation of the granule cell layer. Inhibition of gliogenesis is paralleled by a decreased protein and phosphorylation level of Stat3. In particular, this study establishes an unexpected role of mTORC1 in the migration of neurons in the cortex and hippocampus. Taken together, these results show that postnatal survival, overall brain growth and specific aspects of brain development critically depend on mTORC1 function.

### 3.1.2. Introduction

In eukaryotes, cell growth is regulated by the TOR pathway. The mammalian ortholog mTOR contributes to two distinct multiprotein complexes referred to as mTORC1 and mTORC2 [12, 13]. mTORC1 consists of mTOR, raptor, mLST8 and PRAS40 and is sensitive to acute treatment of the immunosuppressant rapamycin [16]. Like mTORC1, mTORC2 harbours mTOR and mLST8 but further contains rictor and mSIN1. Under prolonged rapamycin application, mTORC2 can be inhibited as well [15]. Whereas knowledge of the role of mTORC2 is sparse, mTORC1 has been implicated in the control of metabolism, protein translation, ribosome biogenesis, autophagy and transcription [16]. However, analysis of the physiological function of mTORC1 *in vivo* was for long time restricted to early embryonic development, due to the lethality of *mTOR*, *raptor* and *mLST8*-deficient embryos. *mTOR*<sup>-/-</sup> and *raptor*<sup>-/-</sup> embryos die shortly after implantation due to proliferation defects [83-85]. *mLST8*<sup>-/-</sup> mice phenocopy *rictor*<sup>-/-</sup> mice and reveal that *mLST8* is not necessary for mTORC1-dependent early embryonic development. Only later, at midgestation (E10.5), embryos die due to vascular defects in the fetal placenta and show additional embryonic defects.

Brain development under conditions of reduced mTOR activity was addressed by a study which characterized a mutation in the *mTOR* gene that resulted in a splicing defect [88]. Mutant embryos lacked telencephali and died at midgestation. This effect was phenocopied by rapamycin application. Interpretation of these results is difficult since mTOR null embryos die much earlier in development [83, 85] and the prolonged rapamycin application does not allow to associate the contribution of either mTOR complex to the phenotype. Only recently, our lab developed mice with floxed *raptor* (*regulatory associated protein of mTOR*) alleles. These models allowed to overcome embryonic lethality and conferred specificity in the analysis of mTOR complexes 1. The floxed mice were used to conditionally ablate mTORC1 in skeletal muscle or fat and these studies showed that mTORC1 exerts distinct functions in different tissues [89, 90].

Many valuable *in vitro* studies, however, have addressed mTOR function in different aspects of brain development. A few studies addressed differentiation of neural stem cells and came to the seemingly conflicting conclusions that mTORC1 is either crucial for commitment into the neuronal or into the glial lineage [50, 69, 70]. The highly defined context of these studies may explain such differences and poses the question to which extent the chosen conditions reflect the physiological situation. A large set of studies addressed consequences of mTOR inhibition or knockdown for growth of the postmitotic neurons [71]. Based on those studies, mTOR seems to be important for polarization, dendrite development and axonal growth or guidance. Complexity of the dendritic tree is reduced upon mTORC1 inhibition [27, 75]. For axons, some show that rapamycin-sensitive local translation in growth cones mediates axon

guidance or regrowth after axotomy [51, 91, 92]. Others show that axon specification and elongation is mTORC1 dependent [74]. In summary, *in vitro* data have resulted in a panoply of potential functions of mTORC1. However, its role *in vivo* has not been addressed.

Prenatal brain development is a highly complex process. Cells proliferate extensively, differentiate and migrate and ultimately organize themselves into layers and nuclei. Many cells have to adopt highly branched structures. Axons have to be responsive to extracellular cues in order to form correct fiber lamination which depends on local translation [92]. For many of these steps of brain development, a role of the cell growth controller mTOR was established *in vitro* or was proposed. To define the physiological function of mTORC1 in brain development, we used a conditional mouse model to specifically delete *raptor* in the developing central nervous system (CNS). We find that *raptor*-deficient brains are smaller than control brains due to decreased cell size and reduced proliferation. Differentiation into the glial lineage and development of the layers is affected in the hippocampus and the cortex by removal of *raptor*. In summary, our results show that global brain growth as well as more specific aspects of brain development depends on mTORC1 function.

### 3.1.3. Results

#### **mTORC1 in the brain is not necessary for embryonic survival and body growth**

Mice that lack mTORC1 in the brain were generated by, crossing *raptor*-floxed mice [89] with mice that express Cre under control of the CNS stem cell-specific enhancer of the Nestin promoter [86, 93]. In the resulting *raptor<sup>fl/fl</sup>;nestin-Cre* mice (herein called RAbKO mice), Cre-mediated recombination deletes exon 6 of the *raptor* gene and induces a frame shift, which causes a precocious stop of translation (Fig. 1A). Genotyping of E19.5 mouse embryos and newborn pups revealed approximately 25% of the offspring to be RAbKO mice, which reflects the Mendelian ratio. This shows that mTORC1 function in the developing CNS is not necessary for embryonic survival (Table 1).

Recombination within the brain was confirmed by PCR (Fig. 1A,B). Genomic DNA of RAbKO mice showed a single band for the *raptor* floxed allele but no *raptor* wild-type band and was positive for the *Cre* gene. Using primers P1 and P3, the band of the Cre-driven recombination was detected in brain but not in tail lysates. PCR with P1 and P2 primers revealed a decreased signal of the unrecombined *raptor* floxed allele in the brain compared to the tail. In contrast, double floxed control mice that were negative for the *Cre* gene showed no decrease of this band in the brain compared to the tail lysates. Equal amount of DNA was used for each PCR and the *riCTOR* wild-type allele served as control. Western blot analysis of brain lysates also showed that the amount of raptor protein was strongly reduced in RAbKO (Fig. 1C). The residual raptor protein was probably present due to expression in meninges and blood vessels. mTOR and the mTORC2 member rictor were unchanged in RAbKO lysates. Loss of mTORC1 function was confirmed by Western blot against ribosomal protein S6, whose phosphorylation is mTORC1 dependent [36]. Whereas the level of the S6 protein was the same in control and RAbKO animals, phosphorylation at serine 235/236 was strongly reduced in RAbKO brains.

RAbKO mice died within several hours after birth. In contrast to their control littermates, they never showed a milk belly. After a few hours, mice breathed improperly, got cyanotic and died (data not shown). Body weight of E19.5 RAbKO mice was normal indicating that mTORC1 in the brain has no role in prenatal body growth (Fig. 1D).

#### ***raptor*-deficient brains are smaller than control brains**

As mTORC1 is well known for its role in cell growth, we examined the brain size of E19.5 mice. Analysis of the brains revealed that RAbKO brains are much smaller than control brains. Brain weight was reduced to 53.7% whereas the weight of heterozygous knockout brains was not changed, showing that one functional *raptor* allele is sufficient to maintain normal brain size during development (Fig. 2A). To investigate whether the reduction in size

was a global effect or attributed to distinct brain regions, brain sections of various levels along the rostral-caudal axis were stained with cresyl violet (Fig 2B). Comparison revealed that all major brain regions were smaller.

The difference in size can be caused either by a decrease in cell size or cell number, mechanisms that are both in good accordance with the known functions of mTORC1 [16]. To discriminate between these two possibilities, we quantified the DNA content in brain lysates. The DNA amount is highly proportional to the number of cells and can be quantified by the enhancement of fluorescence of the fluorochrome Hoechst33258 to DNA [94]. This method was previously used to characterize the mechanisms of brain size changes in Akt3/PKB $\gamma$  knockout mice [95, 96]. The DNA amount per brain was reduced in RAbKO animals to 67.6%, indicating that they contain approximately 30 percent less cells (Fig. 2C). We further determined the amount of DNA per gram of brain tissue (Fig. 2D), which is a measure for cell density [96, 97]. DNA amount per gram of brain was increased to 124.4%, indicating that cell density is increased by the same ratio. Thus, cell size must be reciprocally decreased to about 80%. Neither cell number nor cell density was changed in the heterozygous RAbKO mice. As mTOR and mTORC1 deficiency or dysfunction causes proliferation defects in ES cells and early mouse embryonic development [83-85], we next asked whether the loss of cells in the RAbKO brain was caused by a reduced proliferation rate of neural stem- or progenitor cells. To address this question, we cultured P0 telencephalic neural stem cells of control and RAbKO mice as freely floating neurospheres. *Raptor*-deficient primary neurospheres grew much more slowly than spheres derived from control. To investigate the role of mTORC1 in neurosphere formation and growth, the same number of cells originating from control and RAbKO primary spheres were plated at clonal density and analyzed for their ability to generate secondary spheres. The number of secondary neurospheres was similar in RAbKO cultures (Fig. 2G), indicating that the number of self-renewing stem cells was unchanged [98]. The size of the neurospheres, however, was strongly reduced (Fig. 2E,F). The size distribution in RAbKO spheres is shifted towards smaller diameters compared to controls (Fig. 2F) and the Wilcoxon two sample test showed that the difference is highly significant ( $p < 1.384 \times 10^{-12}$ ). This shows that the proliferative capacity of neural stem- or progenitor cells is decreased. Taken together, these data show that mTORC1 is necessary for proper brain growth which involves both, proliferation and cell growth.

### **Glial differentiation is impaired in *raptor* deficient brains**

*In vitro*, mTORC1 has been suggested to regulate differentiation of neural stem cells and precursor cells towards the neuronal or glial lineage [50, 69, 70]. To investigate whether this would also apply *in vivo*, or whether the observed reduced proliferation rate would affect a particular precursor line, we analyzed the cellular composition of the RAbKO brain, using



Western blot analysis of E19.5 control and RAbKO brains (Fig. 3A). The signal of the neuron-specific isoform  $\beta$ -tubulin III was not decreased in RAbKO brain lysates indicating that the proportion of neurons was unchanged. Similarly, brain lipid-binding protein (BLBP), a radial glial marker reflecting the number of neuronal precursors was not altered [99]. The same was the case for GAD65/67, a marker for the neuronal subpopulation of inhibitory interneurons with their distinct origin in the ganglionic eminence. These data indicate that mTORC1 is not essential for the differentiation of neural stem cells into the neuronal lineage. The astrocytic marker GFAP, however, was strongly reduced in RAbKO brain lysates, which led us to further investigate the glial lineage.

To investigate the distribution of GFAP-positive cells in the brain, we made stainings of brain sections from newborns (Fig. 3B). At this time of development, GFAP-positive cells would only just start to populate the brain. Indeed, the signal was only apparent in a few regions. In the dentate gyrus of control brains, the GFAP-signal was quite prominent at the granule cell layer, whereas in RAbKO animals, the signal was much weaker. Distinct populations of early GFAP-positive cells are the three groups of cells that form the midline glial structures: the indusium griseum glia (IGG), the midline zipper glia (MZG) and the glial wedge (GW). They are thought to play a role in callosal axon guidance and some of them are GFAP-positive as early as E13 [100]. These populations were less pronounced in RAbKO mice when stained with an antibody against GFAP. This shows that glial cell populations in mTORC1-deficient brains are not efficiently generated or do not acquire an important glial characteristic, namely the expression of the intermediate filament protein GFAP.

mTOR was previously linked to glial differentiation via its ability to phosphorylate Stat3 [50, 101], which regulates astrocyte development [102, 103]. For maximal activation, phosphorylation of Stat3 at two residues, Tyr705 and Ser727 is required. Tyr705 is phosphorylated by members of the Jak/Tyk family, whereas Ser727 can be phosphorylated by mTORC1. Hence, we analyzed the expression and phosphorylation state of Stat3, in brain lysates of newborns (Fig. 3C). We found that the protein level as well as phosphorylation of both sites was decreased in RAbKO lysates, indicating that the overall activity of Stat3 is decreased. This result suggests that failure of mTORC1 mediated activation of Stat3 may underlie the depletion of GFAP-positive cells.

To further analyze whether the lack of astrocytes represents a deficit of the *raptor*-deficient neural stem cells to differentiate into the glial lineage, we differentiated neurosphere cultures from RAbKO and control mice. Differentiation was achieved by culturing the dissociated spheres as attached cultures and removal of growth factors FGF2 and EGF. Staining with the anti-GFAP antibody revealed a lower fraction of GFAP-positive astrocytes after 5 days of differentiation (Fig. 3D). The fraction of neurons, however was not changed. This was further

confirmed by quantification (Fig. 3E) and Western blot probed for  $\beta$ -tubulin III and GFAP (Fig. 3F).

### **The pyramidal- and the granule cell layer do not form in the *raptor* deficient hippocampus**

One of the most obvious differences between E19.5 RAbKO and control mice apparent in Cresyl violet-stained brain sections was the lack of a proper pyramidal layer in the CA regions of the *raptor*-deficient hippocampus (Fig. 4A). Also, the dentate gyrus was not organized in a distinct C shaped layer and a hylus. We therefore examined the hippocampus closer at an earlier time point using several markers (Fig. 4A). Cresyl violet staining of E15.5 brains revealed that in RAbKO mice, the hippocampal plate (HP) as well as the cortical plate (CP) were formed. At the same stage, Map2, a marker for dendrites and at early brain development also for the somata of subplate (SP) neurons [104, 105], formed a continuous band along the cortical subplate which ranges far into the control hippocampus. The Map2 SP band in RAbKO brain was fading before it reached the hippocampus (filled arrow head, Fig. 4A). At E19.5, the Map2-positive SP band penetrated the hippocampus.

Cresyl violet and Map2 staining both revealed a layering defect in the hippocampus of RAbKO mice. We therefore wanted to determine the localization of neurons in the hippocampus and stained with an antibody against the neuronal marker NeuN. At E15.5, no obvious difference in NeuN distribution was visible between genotypes. The NeuN signal was evenly distributed throughout the hippocampal CA- and dentate gyrus regions but was excluded from the ventricular zone (VZ). In contrast, at E19.5, distribution of postmitotic neurons was different in the RAbKO hippocampus. In the control hippocampus, neurons were densely packed at the ventricular surface of the pyramidal layer of the CA regions (open arrowhead). The dentate gyrus already showed the initial formation of the C shaped granule cell layer (arrow, Fig. 4A) and the hylus (asterisk Fig. 4A). In the RAbKO hippocampus however, neurons did not form a proper pyramidal layer (open arrowhead). In the dentate gyrus, which represents a secondary proliferation zone separated from the VZ, neurons were evenly filling the hylus and did not show the initial formation of the granule cell layer.

We further addressed CA layering by application of BrdU. In control mice, most cells that had incorporated BrdU at E14.5 were integrated into the pyramidal cell layer at E19.5 (Fig. 4B). In the RAbKO hippocampus, BrdU-positive cells were found near and even within the VZ showing that mTORC1 is essential for the formation of a pyramidal layer in the CA regions and a defined granule cell layer in the dentate gyrus.

### **Cortical layer formation is affected by removal of *raptor***

In contrast to the hippocampal organization, cortical layering of *raptor*-deficient brains was grossly normal when comparing Cresyl violet stained E19.5 brain sections (Fig. 5A). Map2-stained brain sections revealed normal preplate splitting and SP formation in RAbKO brains (Fig 5B). When we further stained E19.5 brain sections for the neuronal marker NeuN, we found strongly positive neurons only in the SP and the upper CP for both genotypes (Fig. 5C). This is in agreement with a previous study where rapamycin application did not interfere with preplate splitting and early cortical plate formation [28].

To further investigate whether and how cortical layering was affected, we injected BrdU into timed pregnant dams at different stages of embryonic development and analyzed the position of BrdU-positive cells at E19.5 or in newborns (Fig. 5D). When injected at E12.5, which is around preplate splitting, no obvious difference could be observed between control and RAbKO mice (data not shown). The BrdU signal was relatively concentrated at the SP and faded gradually towards the MZ. Only a few labeled cells were visible within the IZ. Cells that were generated at E14.5, however, showed a different pattern in the *raptor*-deficient cortex. Similar to the situation in the hippocampus (Fig. 4B), the signal was relatively concentrated in the VZ and IZ, below the SP, and relatively deprived from the CP (Fig. 5D,E). Within the control cortex however, they were localized more in the upper CP. When injected at E17.5, a time where the CP layer is almost complete [106], fewer BrdU-positive cells were localized in the CP of E19.5 RAbKO mice (data not shown). This indicates that neurons developing at E14.5 or later do migrate less efficiently into the CP.

### **Raptor is necessary for normal formation of axonal tracts and dendritic complexity**

mTORC1 has previously been linked to axonal growth in several conditions [51, 74, 91]. According to these studies, initial specification as well as axonal elongation and steering are influenced by mTORC1 which would serve as regulator of local cell growth. We therefore examined the developing axonal tracts in E19.5 brains. Cresyl violet stainings of brain sections revealed that the size of several major axon tracts was reduced in *raptor*-deficient brains as shown for the corpus callosum (CC), the anterior commissure (AC) and the fimbria (Fig. 6A). Quantification of the CC thickness and the AC diameter showed strong and significant decreases in RAbKO brains (Fig. 6B). To exclude the possibility that reduced CC thickness was simply caused by a depletion of neurons in the cortex, we used Western blot analysis with the neuronal marker  $\beta$ -tubulin III (Fig. 6C). Several studies using rapamycin or RNAi against mTOR have shown that mTOR restricts dendrite development and maintenance [27, 75]. To quantify the reduction in a cell-autonomous system, we cultured hippocampal neurons from homozygously floxed E16.5 mice and transfected them at DIV4 with an expression plasmid encoding Cre or a control plasmid. Both vectors were

cotransfected with a GFP-expressing plasmid to visualize the whole cell for the measurement. Sholl blot analysis at DIV 14 showed a significant decrease in the complexity of the dendritic tree (Fig. 6D). In conclusion, raptor-deficient neurons show growth defects including a simplification of the dendritic tree and an inability of the axons to form properly sized tracts in the brain.

### 3.1.4. Discussion

In this study, we used *Nestin-Cre* mice together with the floxed *raptor* mice to delete *raptor* in the developing CNS. The resulting RAbKO mice showed a phenotype that affects cell size and proliferation in the entire brain which causes microcephaly. Beside this global effect, we also found several more specific aberrations affecting glia differentiation and radial migration of neurons in the cortex and hippocampus.

#### **Requirement of mTORC1 for normal brain growth**

RAbKO mice were born alive and were viable for several hours, indicating that the previously described embryonic death of the mTOR mutants or after rapamycin treatment during embryonic development was not mediated solely by mTORC1 ablation in the brain [88]. Analysis of the *raptor* deficient brain revealed that mTORC1 was not essential for telencephalon formation or initial formation of any other large brain structure. However, the size of the entire brain was smaller. The change in size was reminiscent of the brains of mice where Akt3/PKB $\gamma$ , an mTORC1-upstream component, was knocked out [96]. However, the effect of the Akt3/PKB $\gamma$  deletion is milder and these mice are viable. This might be due to the compensation of the other two Akt/PKB isoforms. Similar to the Akt3/PKB $\gamma$  ko, we found that both cell size and number were decreased in *raptor*-deficient brains. Reduced cell size might be due to decreased activity of the well characterized mTORC1 effectors S6K/S6. A slower rate of proliferation was found to underlie the loss in cell number. Defects in proliferation are supposed to cause early embryonic death of *mTOR* and *raptor* null mice [84]. mTORC1 was previously associated with cell cycle control via G1 progression. A recent study defined a molecular mechanism whereby mTORC1 acts on the cell cycle by modulation of p27 activity via direct phosphorylation of SGK [49].

The fact that the entire brain was homogenously smaller from early on suggested that already the earliest neural stem cells and all subsequent progenitors would be affected in a proportional way. However, the reduction in the number of glial cells was disproportional. This suggested that in addition to the regulation of proliferation, further mTORC1 dependent mechanisms regulate differentiation.

#### **mTORC1 is essential for the efficient gliogenesis and formation of the granule cell layer in the dentate gyrus**

The first GFAP-positive cells in the mouse brain appear at the corticoseptal boundary in the GW at E13 and are proposed to be part of the cortical radial glial network [100]. Later, they will become astrocytes. The other midline glial structures seem to have a different origin and to differentiate directly into astrocytes. Later in development, after the neurogenic to gliogenic

switch, radial glia cells also produce astrocytes in the cortex and hippocampus [107]. Among these are also the astrocyte stem cells that are responsible for adult neurogenesis in the subgranular zone of the dentate gyrus and the subventricular zone of the lateral ventricles. The fact that in RAbKO mice, both early and late generated GFAP populations are affected in a similar way shows that development is not simply delayed. Rather, glial differentiation is inhibited which was further proven by experiments with neural stem cell cultures from RAbKO mice or cultures from homozygously floxed mice that were transduced with a Cre-expressing virus (Fig. 3D-F, Supplementary Figure 1).

Whereas there is consensus that GFAP is not expressed in rodent radial glia [108], some work has shown that the radial glial scaffold in the dentate gyrus expresses GFAP during late embryonic development [109, 110]. Granule cell migration in the dentate gyrus is somewhat different from neuronal migration in the neocortex. Migration does not start directly in the ventricular zone but originates from the hylus of the dentate gyrus which represents a secondary proliferation zone. Therefore, it is not the classical radial glia scaffold which mediates migration and layer formation but a separate glial network in the hylus. Thus, a decrease in organization of the glial network of the dentate gyrus causes malformation of the granule cell layer [111]. In our mouse model, the malformation of the granule cell layer formation coincides with a generally decreased GFAP signal in the dentate gyrus. It was also obvious that cells were much more bound to the pial surface than in the control where many processes reached perpendicularly far into the hylar region (Fig. 3B). Elongation and organization of glia in the dentate gyrus depends on reelin. Parts of the effects of reelin were shown to be rapamycin sensitive, for example induction of dendrite growth [28]. It might therefore be that ablation of mTORC1 hits granule cell migration in two ways. First, it inhibits differentiation of the radial glial cells in the dentate gyrus. Subsequently, it might also influence growth of glial processes and formation of a proper migration scaffold.

### **Reduction of GFAP positive cells correlates with decreased expression and mTORC1 dependent activation of the Jak-Stat signaling member Stat3**

Activity of Stat3 is regulated both by phosphorylation at Tyr705 and Ser727 [101]. mTORC1 was previously shown to be the kinase for Stat3 Ser727. Indeed, in brain lysates of RAbKO brains, we found phosphorylation of Stat3 at this site to be strongly reduced. Protein level of Stat3, however, was also decreased. This was probably caused by a failed induction of the positive autoregulatory feedback loop of activated Stat3 on transcription of genes of the Jak-Stat pathway [112]. It was shown that the Stat pathway has to be activated first in order to allow for increased induction of transcription. This activation of the pathway came along with the switch of the neurogenic to the gliogenic period. It had been previously shown that the Jak-Stat pathway induces differentiation of astrocytes and can directly activate expression

from the GFAP promoter [102, 103]. This indicates that reduced GFAP in mTORC1-deficient brains is due to the inability of Stat3 to be phosphorylated and activated and thereby to initiate an enhanced Jak/Stat signaling that ultimately induces efficient gliogenesis. Interestingly, loss of the mTORC1 inhibitor TSC, a model for the genetic disease tuberous sclerosis in humans, induces Stat3 activation and GFAP expression [113]. By promotion of astrocyte differentiation or radial glial differentiation in the dentate gyrus, mTORC1 activated Stat3 should also mediate generation of neural stem cells responsible for adult neurogenesis. CNTF or Stat3 deletion, which inhibits generation of GFAP-positive cells, both cause reduced neurogenesis and reduce the size of the granule cell layer in the adult mouse [114]. Also deletion of *Igf1*, a classical upstream factor of mTOR results in loss of granule cells in the hippocampus [115]. This suggests that mTORC1 may play a pivotal role in adult neurogenesis.

### **A novel role for mTORC1 in cortical cell migration**

In *raptor*-deficient brain, both the developing granule cell layer of the dentate gyrus and the pyramidal cell layer of the CA regions were perturbed. Whereas layering in the hippocampus was clearly deficient, malformations in the cortex were not obvious in cresyl violet stained RAbKO brain sections. BrdU birthdating experiments revealed that early born neurons migrate properly which is in agreement with a previous slice culture study where rapamycin had no effect on preplate splitting and early CP layering [28]. Interestingly, we found now that mTORC1 deficiency affected cortical and hippocampal architecture at a later stage. When BrdU was injected at E14.5, a fraction of labeled cells remained in the VZ/IZ of mTORC1 depleted brains whereas in control brains, BrdU puncta were much more abundant in the CP. This suggests that in contrast to earlier generated cells, neurons born after E14.5 are partially trapped in the VZ/IZ. Before newly generated neurons penetrate the SP and migrate through the CP, they gather in the IZ and change their morphology from multipolar to bipolar [116]. Interference with this transition takes place in several mouse models with cortical migration defects due to inhibited CP penetration [117-119]. This is also the case for the cortex specific *Cdk5* ko mouse, the hippocampus of which shows a similar phenotype like the one of RAbKO mice [120]. In addition, axonal trajectories of *Cdk5* mutants were abnormal, a phenotype that also occurs in the *raptor* deficient brain. This suggests that a polarity defect which inhibits the transition of the multipolar to dipolar state might account for the observed migration defects in RAbKO brains. The fact that we find the dendritic complexity to be reduced *in vitro* together with studies that manifest the role of mTORC1 in dendritic growth or in axon specification further support this view.

In conclusion, our data shows that mTORC1 is crucial for normal brain growth and postnatal survival. Several aspects of brain development are affected by mTORC1 ablation and may in

sum be responsible for death of the newborns. Regulation of cell size and division, which are both affected in RAbKO mice, are processes that are known to be associated with mTORC1 signaling. mTORC1 induced phosphorylation of Stat3 allows for normal differentiation of GFAP positive glia and thereby probably promotes normal layering in the dentate gyrus. Our results further uncover a novel role for mTORC1 in cortical layering, the detailed mechanism of which is not entirely clear. The multiple phenotypes of this mouse reflect the central position of mTORC1 in processing signals of several pathways and forwarding the output to various downstream effectors.



### 3.1.5. Materials and methods

#### Brain-specific *raptor* knockout mice

Mice homozygous for the floxed *raptor* allele were mated with mice that were heterozygous for the floxed allele and further expressed Cre under the control of the CNS-specific enhancer of the Nestin promoter. Time matings were made and E15.5, E19.5 embryos or newborns were taken for analysis. Genotyping was performed on tail or brain lysates using primers depicted in Fig. 1A. P1: 5'-ATG GTA GCA GGC ACA CTC TTC ATG; P2: 5'-GCT AAA CAT TCA GTC CCT AAT C; P3: 5'-CAG ATT CAA GCA TGT CCT AAG C; Cre-forward: 5'-TGT GGC TGA TGA TCC GAA TA; Cre-backward: 5'-GCT TGC ATG ATC TCC GGT AT. For comparative PCR, 2.5 µg template DNA was used for each PCR reaction. Mice that were heterozygous or homozygous for the floxed *raptor* allele and were negative for Cre were taken as control.

#### Antibodies

The following rabbit polyclonal antibodies were used: mTOR, S6 Ribosomal Protein, P-S6 Ribosomal Protein (Ser235/236), P-Stat3 (Ser727) from Cell Signaling, BLBP, Map2 from Chemicon and GAD65/67 from Sigma. Rabbit monoclonal antibodies were as follows: *raptor*, *riCTOR*, P-Stat3 (Tyr705) and  $\beta$ -Actin from Cell Signaling. Mouse monoclonal antibodies were as follows: Stat3 from Cell Signaling, NeuN and GFAP from Chemicon,  $\beta$ -Tubulin III from Sigma. Rat monoclonal antibodies are were follows: BrdU from AbD Serotec.

#### Brain lysates for Western blots

Brains of embryos or newborns were dissected, washed in ice-cold PBS and combined with 10x (volume/weight) lysis buffer (50 mM Tris at pH 8, 150 mM NaCl, 1mM EDTA, 1% Triton-X100) supplemented with protease inhibitor cocktail tablets (Roche) and phosphatase inhibitor cocktail I and II (Sigma). Brains were passed several times through a 1 ml pipette tip and homogenized with a glass-teflon homogenizer by using 12 strokes at 800 rpm. Lysates were centrifuged at at 13600 rpm for 15 min at 4°C. Total protein levels were then determined using the BCA protein assay (Pierce) and supplied with sample buffer. Equal amounts of protein were loaded onto SDS gels, transferred to nitrocellulose membranes and probed for the indicated antibodies.

#### Brain sections, histochemistry and immunohistochemistry

For fresh frozen sections, dissected brains were embedded in OCT reagent and directly frozen on dry ice. 10 µm-thick brain sections were prepared with a cryostat, dried and frozen at -70°C or directly postfixed with 4% PFA in PBS for 20 min and washed in PBS for further

analysis. For paraffin sections, brains were fixed for at least two days in 4% PFA in PBS, then dehydrated in a graded alcohol series and embedded in paraffin. 4µm-thick sections were prepared on a microtome. For further applications, mounted sections were deparaffinized by heating for 20 min at 65°C, then immediately immersed twice in Xylol for 5 min each. Sections were rehydrated and either directly subjected to cresyl violet staining and haematoxylin/eosin staining or antigen retrieval was performed. For this, slides were boiled in sodium citrate buffer (10 mM sodium citrate, 0.05% Tween 20, pH 6) for 20 min and allowed to cool slowly for another 20 min at room temperature. Sections were washed with PBS for further analysis. For immunohistochemistry, sections were blocked for 30 min in PBS containing 5% BSA and 0.25% Triton-X100. Slices were incubated over-night at 4°C in blocking buffer with one of the following primary antibodies: GFAP (1:200), NeuN (1:200), Map2 (1:400), BrdU (1:2000). Subsequently, slides were washed 3 x with PBS for 5 min each and incubated with appropriate secondary antibodies and DAPI in blocking buffer for 1 h at room temperature. After washing in PBS, coverslips were mounted with Kaiser's glycerol gelatine.

### **Birthdating analysis**

For birthdating analysis in the cortex, 50 mg BrdU/kg was applied by intraperitoneal injection to pregnant mice at indicated stages. Embryos were removed at E19.5 and fresh frozen brain sections were prepared. After postfixation and PBS wash, sections were incubated in 2 M HCl for 1h at 37°C. Afterwards, sections were washed 3 x in PBS and incubated for 10 min in borate buffer (0.1 M, pH 8.5) at room temperature. Sections were then washed 3 x with PBS and processed for immunohistochemistry as described.

### **DNA quantification**

DNA was quantified in tissue homogenates as previously described [94]. Briefly, whole brains were homogenized by Polytron for 20 s at low strength in detection buffer (0.05 M NaPO<sub>4</sub>, 2.0 M NaCl, 2 mM EDTA, 1 µg/ml Hoechst 33258 (Sigma), pH 7.4), followed by sonication for 20 s. Samples were excited at 356 nm and emission at 492 nm was determined. DNA concentration of homogenates was determined relative to a standard curve using calf thymus DNA (Sigma).

### **Neurospheres**

Neurospheres were prepared from P0 telencephali. Briefly, telencephali were dissected in HBSS, the meninges and the olfactory bulbs were removed. The tissue was triturated with a 1 ml pipette tip in neurosphere medium consisting of DMEM/F12 (1:1), 0.2 mg/ml L-glutamine, 1% penicillin/streptomycin, 2% B27, 2 µg/ml heparin, 20 ng/ml EGF and 10 ng/ml

FGF2. The homogenate was diluted twice in the ratio 1:1 with fresh neurosphere medium and each time triturated shortly.  $5 \times 10^4$  cells were plated in a 5 cm dish. After 7 days, cultures were collected, and passaged. For determination of the capacity of secondary neurosphere formation and growth, cells were plated at a clonal density of 3000 cells/ml [121]. Six representative images were taken for each well of a 6-well plate to count neurospheres and measure the diameter. For differentiation, neurospheres were splitted after 5 to 6 days and plated on coverslips coated with 15  $\mu\text{g/ml}$  Poly-L-Ornithin and 40  $\mu\text{g/ml}$  Laminin at a density of 150,000 cells/cm<sup>2</sup>. The dispersed cultures were differentiated in neurosphere medium lacking FGF2, EGF and Heparin and fixed after 5 days with 4% PFA. For staining, cells were washed 3 x with PBS, incubated for 10 min in 0.25% TritonX and then blocked for 30 min in PBS containing 5% BSA. Staining was performed with the same procedure as described above for the brain sections.

### 3.1.6. Figures and tables

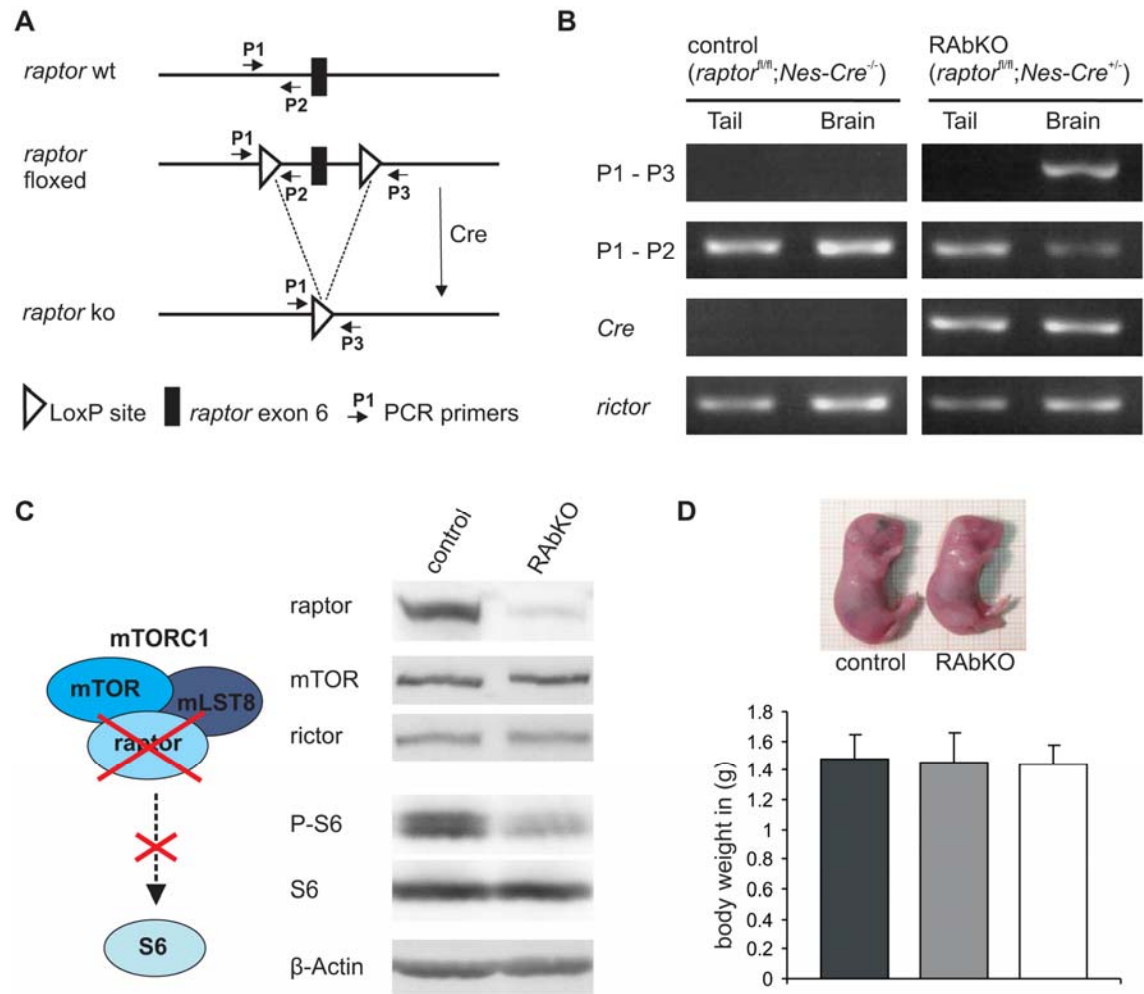


**Figure 1: Generation of RAbKO mice.** (A) Schematic representation of the wild-type (*raptor wt*) and targeted *raptor* allele before (*raptor floxed*) and after (*raptor ko*) expression of Cre recombinase from the Nestin promoter in CNS cells. Localization of PCR primers P1, P2 and P3 used in (B) are indicated. (B) Analysis of recombination in brain and tail lysates of newborn RAbKO (*raptor<sup>fl/fl</sup>*; *Nes-Cre<sup>+/-</sup>*) and control (*raptor<sup>fl/fl</sup>*; *Nes-Cre<sup>-/-</sup>*) mice. The recombined *raptor ko* allele (PCR product of P1 and P3, first lane) is only found in the brain of mice that are positive for the Cre recombinase under the Nestin promoter (*Cre*, third lane). The *raptor floxed* allele signal (PCR product of P1 and P2, second lane) is strongly decreased in RAbKO brain lysates. The residual signal indicates occurrence of unrecombined non-CNS cells in the brain. The *rictor* allele served as loading control. (C) Schematic representation of the impaired mTORC1 in knockout cells. Western blots of brain lysates of RAbKO and control mice probed for members of mTORC1 and mTORC2 and downstream signaling. Phosphorylation of S6 is strongly decreased in RAbKO lysates. (D) Photographs of newly born control and RAbKO mice are shown in the top panel. The lower panel shows the body weight of E19.5 control (dark grey), heterozygous RAbKO (light grey) and RAbKO mice (white). Bars (D) represent means  $\pm$  standard deviation.

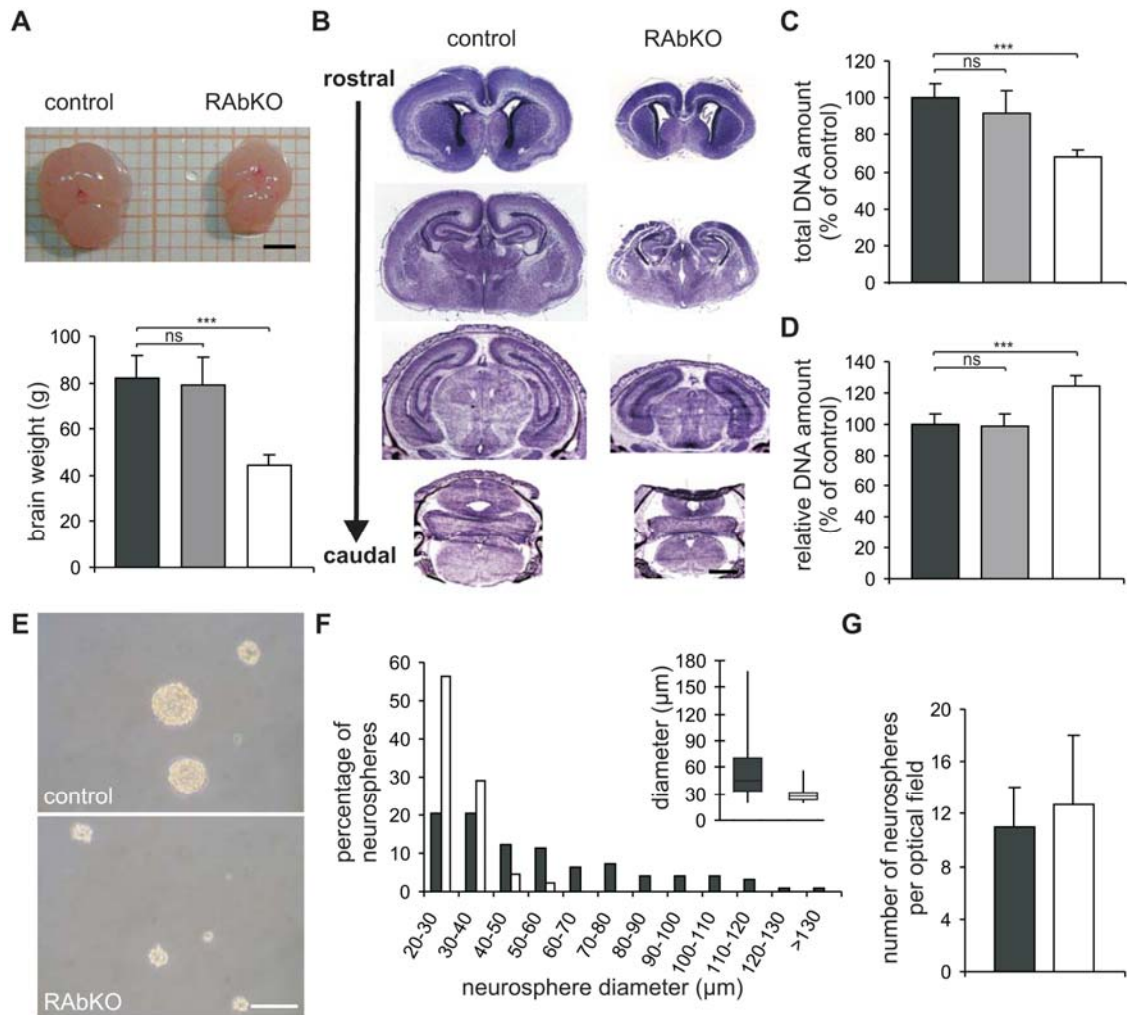


**Figure 2: *raptor* deficient brains are smaller than control brains due to reduced cell size and defects in proliferation.** (A) Brain weight of control (dark grey), heterozygous RAbKO (light grey) and RAbKO (white) mice. (B) Nissl staining of control and RAbKO brain sections at different rostral-caudal levels reveals that all major structures are evenly reduced in size. (C and D) Both, a decreased cell number and size contribute to decreased brain size. Determination of DNA amount (C) and concentration (D) in control (dark grey), heterozygous RAbKO (light grey) and RAbKO brains (white). (E) Representative micrographs of control and RAbKO neurosphere cultures. (F) Distribution of diameters of control (dark grey) and RAbKO (white) neurospheres. Size distribution of RAbKO neurospheres is strongly shifted to the left. Inset: box plot of the same data. The bottom and the top of the boxes represent the lower and the upper quartile, the middle band represents the median. Whiskers represent minimum and maximum. (G) Number of control (dark grey) and RAbKO (white) neurospheres per visual field. Bars (A, B, C, D and G) represent means  $\pm$  standard deviation. n (A and B) = 22 (control), 9 (heterozygous RAbKO) and 8 (RAbKO). n (C and D) = 5 (control), 5 (heterozygous RAbKO) and 4 (RAbKO). n (F) = 100 (control), 91 (RAbKO). n (G) = 18 (control), 15 (RAbKO). p-values (from two-tailed t-Test): \*\*  $p < 0.01$ , \*\*\*  $p < 0.001$ , ns:  $p > 0.05$ . Scale bars: (B) = 1 mm, (E) = 100  $\mu$ m.

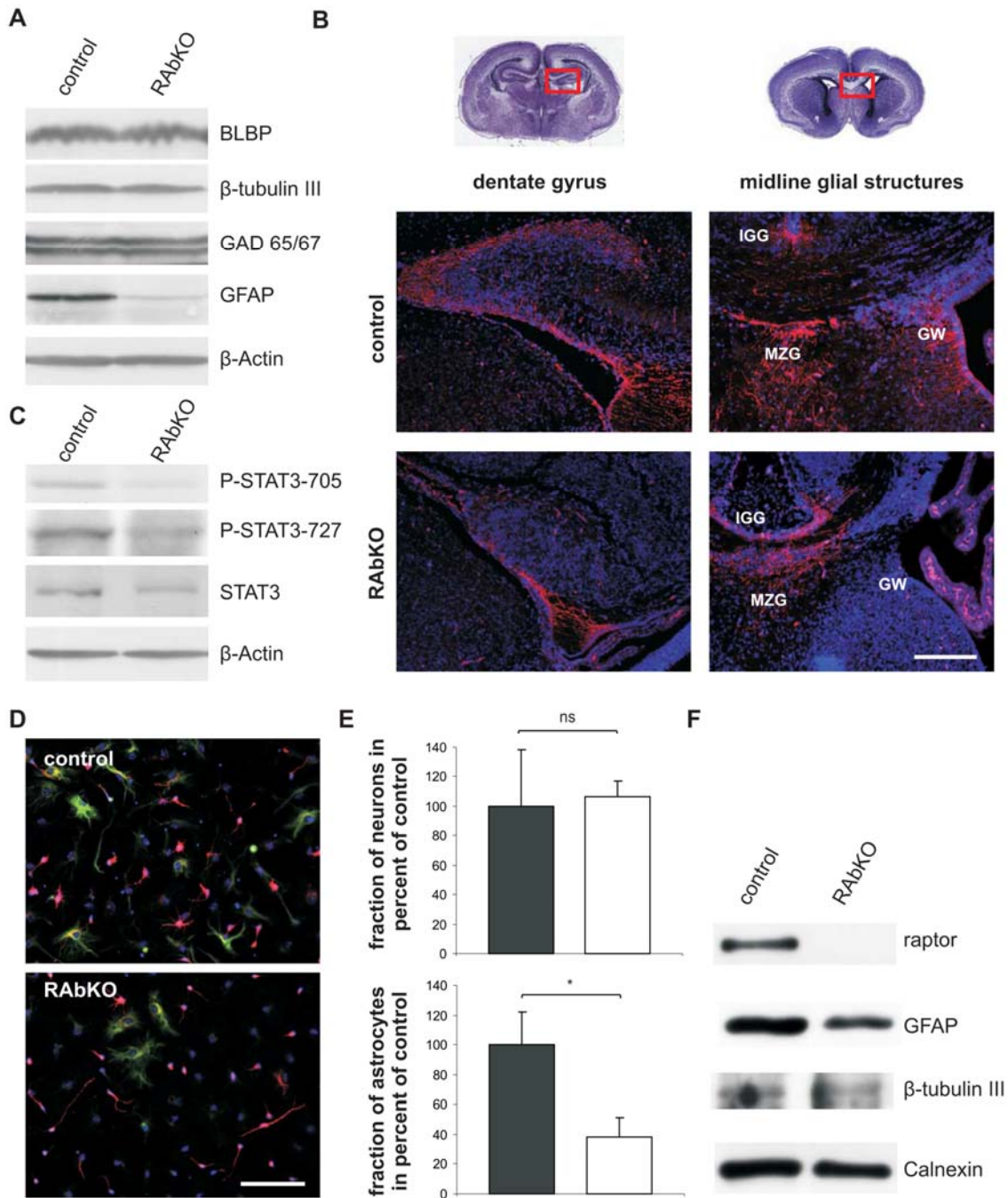


**Figure 3: Astrocytic differentiation is impaired in RAbKO brains.** (A) Western blot analysis of brain lysates from control and RAbKO brains probed for indicated markers of neural development and β-Actin as loading control. (B) Upper part: Cresyl violet stainings of brain sections. Red boxes represent regions shown below. Micrographs show dentate gyrus and midline glial structure regions of control and RAbKO brain sections stained with GFAP antibody (red) and DAPI (blue). IGG: indusium griseum; MZG: midline zipper glia; GW: glial wedge. (C) Western blot analysis of protein concentration adjusted control and RAbKO lysates probed for Stat3 and its different phosphorylation states. Detection of β-Actin serves as loading control. (D) Micrographs of differentiated neurosphere derived cells from control and RAbKO, stained with β-tubulin III antibody (red), GFAP antibody (green) and DAPI (blue). (E) Quantification of the fraction of neurons (upper panel) and astrocytes (lower panel) in percent of control. (F) Western blot analysis of lysates from cultures grown under the same conditions as in (D) probed for the indicated markers. n (E) = 3 control and 3 RAbKO. p-values (from paired t-Test): \*\* p < 0.01, ns: p > 0.05. Scale bars: (B) = 200 μm, (D) = 100 μm.



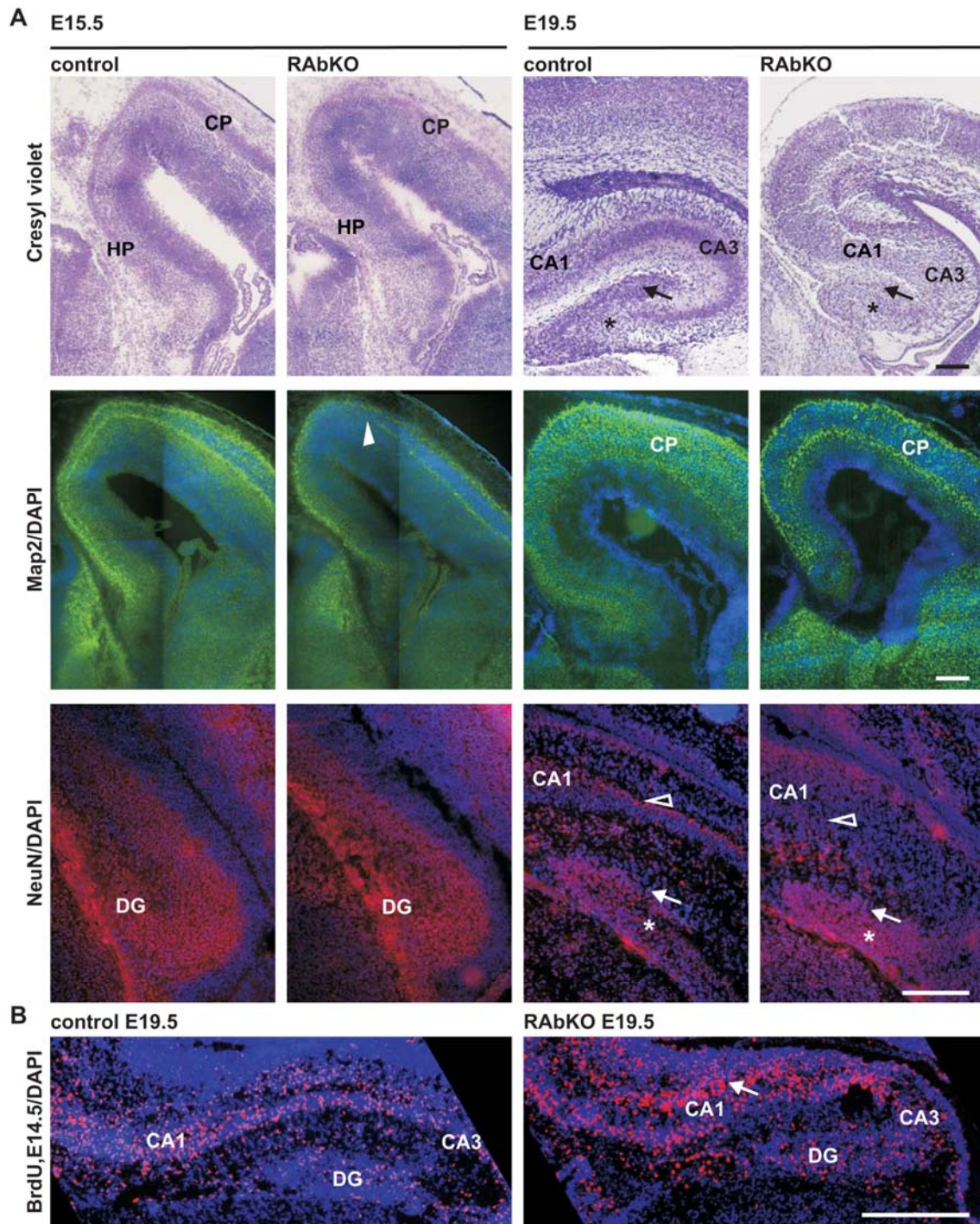


**Figure 4: Defects in hippocampal layering.** (A) Micrographs of cresyl violet stained and Map2 (green)/DAPI (blue) or NeuN (red)/DAPI (blue) costained E15.5 and E19.5 RAbKO and control hippocampus. Asterisks depict the position of the hylus which is filled with NeuN-positive cells in RAbKO sections, arrows the region of the developing granular cell layer, which is distinctly formed only in the control. The filled arrowhead points towards the fading of the SP in RAbKO. Open arrowheads point to the pyramidal layer (control) or the place where the pyramidal layer is missing (RAbKO). CA1, CA3, dentate gyrus (DG) and cortical plate (CP) and hippocampal plate (HP) are indicated. (B) BrdU (red)/DAPI (blue) staining of brain sections of E19.5 embryos which incorporated BrdU at E14.5. The arrow depicts the ectopic layer of BrdU-positive cells in the RAbKO hippocampus. Scale bars (A,B) = 200  $\mu$ m.

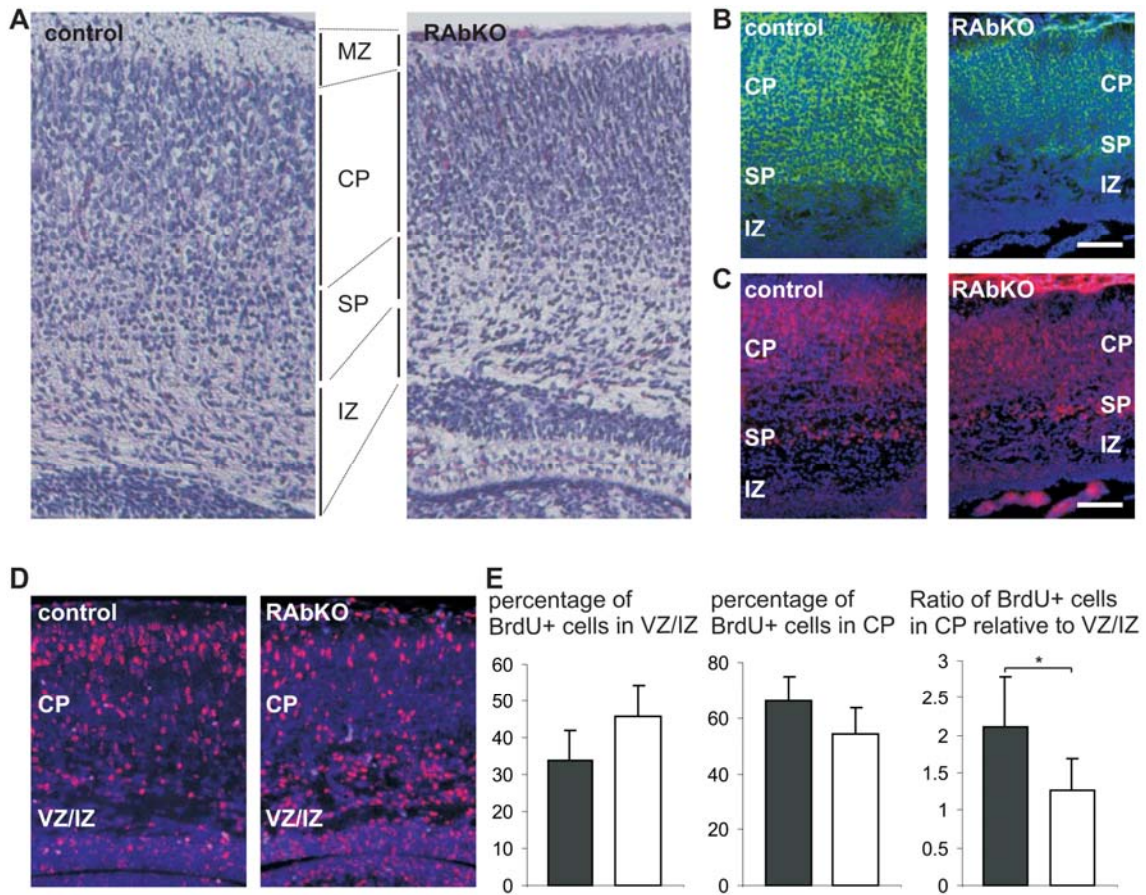


**Figure 5: Defects in cortical layering.** (A) Cresyl violet staining of RAbKO and control cortices. (B) Map2 (green)/DAPI (blue) stainings of RAbKO and control cortices. (C) NeuN (red)/DAPI (blue) stainings of RAbKO and control cortices. (D) BrdU was injected into pregnant dams at E14.5 of embryonic development and brain sections prepared from E19.5 embryos. BrdU (red)/DAPI (blue) staining shows a difference in the distribution of newly formed cells. (E) Quantification of the distribution of BrdU-positive cells. The first two panels show the percentage of BrdU-positive cells in VZ/IZ and in the CP, respectively. The last panel shows the ratio of BrdU-positive cells found in the CP in relation to the cells located in the VZ/IZ. MZ: marginal zone; CP: cortical plate; SP: subplate; IZ: intermediate zone; VZ: ventricular zone. Scale bars (A,B,C,D) = 100  $\mu$ m.



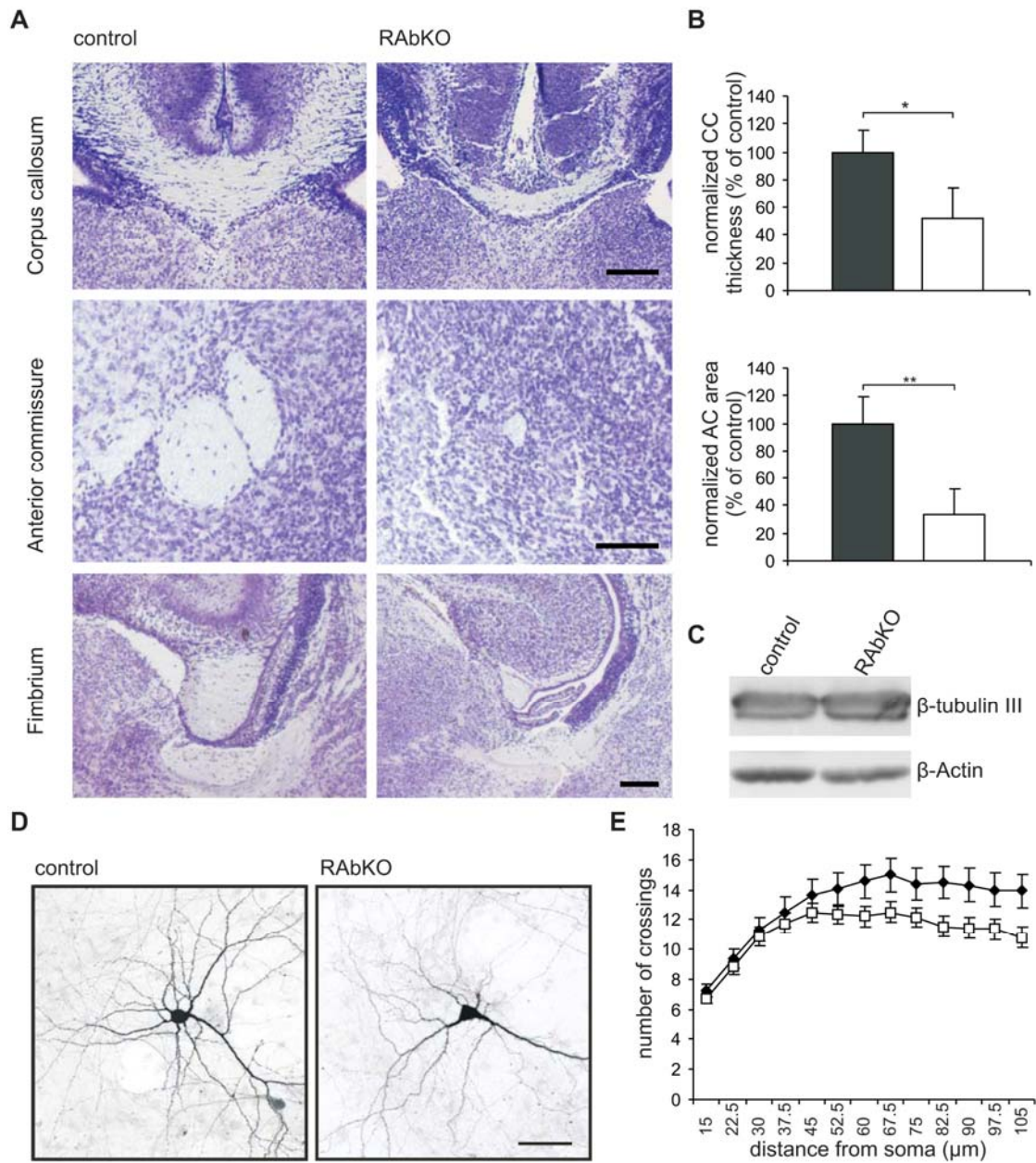


**Figure 6: Several axon tracts are smaller in raptor-deficient brains and dendritic complexity is reduced in culture.** (A) Micrographs of indicated axon tracts of comparable sections stained with cresyl violet. (B) Quantifications of control (dark grey) and RAbKO (white) corpus callosum (CC) thickness, which was normalized to dorsoventral axis length of the section and anterior commissure (AC) area, which was normalized to section area. (C) Western blots of cortical lysates of control and RAbKO brains probed with the neuronal marker  $\beta$ -tubulin III and  $\beta$ -Actin as control. (D and E) Hippocampal neurons double floxed for *raptor* were cultured from E16.5 embryos and cotransfected at 4 DIV with either a Cre expressing plasmid or a control vector together with a GFP expressing plasmid. Neurons were fixed at 14 DIV and analyzed by confocal microscopy. (D) Representative images from control and Cre-transfected neurons. Scale bars, 50  $\mu$ m. (E) Sholl analysis of knockout and control neurons. Concentric circles of indicated radius were drawn around the soma. The number of crossing dendrites was determined for each circle. n (B) = 5 (control) and 4 (RAbKO). p-values (from two-tailed T-test): \*  $p < 0.05$ , \*\*  $p < 0.01$ . Error bars in (E) are confidence intervals. Scale bars in (A) CC: 0.5 mm; AC: 100  $\mu$ m; Fimbrium: 250  $\mu$ m. Scale bars in (D): 50  $\mu$ m.

Table I. Number and percentage of E19 embryos or newborns of indicated genotype.

	control	heterozygous	ko
number per genotype	56	27	24
percentage of total	52.3	25.2	22.4

Control mice include those that were positive for one or two copies of the floxed allele and were negative for *Cre* upon genotyping.

## 3.2. Paper 2

### **Skeletal muscle-specific ablation of *raptor*, but not of *riCTOR*, causes metabolic changes and results in muscle dystrophy**

C. Florian Bentzinger<sup>1</sup>, Klaas Romanino<sup>1</sup>, Dimitri Cloëtta<sup>1</sup>, Shuo Lin<sup>1</sup>, Joseph B. Mascarenhas<sup>1</sup>, Filippo Oliveri<sup>1</sup>, Jinyu Xia<sup>2</sup>, Emilio Casanova<sup>3</sup>, Céline F. Costa<sup>1</sup>, Marijke Brink<sup>3</sup>, Francesco Zorzato<sup>2</sup>, Michael N. Hall<sup>1</sup>, Markus A. Ruegg<sup>1</sup>

<sup>1</sup>Biozentrum, University of Basel, CH-4056 Basel, Switzerland;

<sup>2</sup>Departments of Anesthesia and Biomedicine, Basel University Hospital, CH-4031 Basel, Switzerland.

<sup>3</sup>Institute of Physiology, Department of Biomedicine, University of Basel, CH-4056, Basel, Switzerland

Send correspondence to:

Markus A. Ruegg, Ph.D.

Biozentrum, University of Basel

Klingelbergstrasse 70

CH-4056 Basel, Switzerland

Phone: +41 61 267 22 23

Fax: +41 61 267 22 08

E-Mail: markus-a.ruegg@unibas.ch

Published in: **Cell Metab. 2008 Nov;8(5):411-24.**

### **3.2.1. Summary**

Mammalian Target of Rapamycin (mTOR) is a central controller of cell growth. mTOR assembles into two distinct multiprotein complexes called mTOR complex 1 (mTORC1) and mTORC2. Here we show that the mTORC1 component raptor is critical for muscle function and prolonged survival. In contrast, muscles lacking the mTORC2 component rictor are indistinguishable from wild-type controls. Raptor-deficient muscles become progressively dystrophic, are impaired in their oxidative capacity and contain increased glycogen stores, but express structural components indicative of oxidative muscle fibers. Biochemical analysis indicates that these changes are probably due to loss of activation of direct downstream targets of mTORC1, downregulation of genes involved in mitochondrial biogenesis, including PGC1 $\alpha$ , and hyperactivation of PKB/Akt. Finally, we show that activation of PKB/Akt does not require mTORC2. Together, these results demonstrate that muscle mTORC1 has an unexpected role in the regulation of the metabolic properties and that its function is essential for life.

### 3.2.2. Introduction

Growth of an organ during development and during adaptation in the adult can be controlled by alterations either in the number or the size of cells. The two mechanisms are fundamentally different and require distinct regulation. Rapamycin is a cell growth inhibitor used to treat a number of clinical indications including graft rejection and cancer [122]. The molecular target of rapamycin is a Ser/Thr kinase, called TOR in yeast [8] or mTOR in mammals. The evolutionarily conserved TOR pathway controls many cellular processes, including protein synthesis, ribosome biogenesis, nutrient transport and autophagy (reviewed in [16]). mTOR assembles into two distinct multiprotein complexes, termed mTORC1 and mTORC2 [12, 13]. mTORC1 consists of raptor (regulatory associated protein of mTOR), mLST8, PRAS40 and mTOR [16], and is sensitive to rapamycin. mTORC2 consists of rictor (rapamycin insensitive companion of mTOR), mSIN1, mLST8 and mTOR [12, 13].

Changes in the size of adult muscle, in response to external stimuli, are mainly due to the growth of individual muscle fibers and not an increase in fiber number [55]. As mTOR controls cell growth, it has also been implicated in the control of muscle mass. For example, rapamycin inhibits recovery of skeletal muscle from atrophy [64]. Moreover, activation of the mTORC1-upstream component PKB/Akt induces muscle hypertrophy [64, 65, 123] and this increase is rapamycin-sensitive [60]. Conversely, muscle fibers of mice deficient for the mTOR downstream target S6 kinase 1 (S6K1) are atrophic [59]. In contrast, little is known of the function of rapamycin-insensitive mTORC2 whose primary readouts are thought to be the organization of the actin cytoskeleton. Moreover, mTORC2 has been shown to be the kinase that phosphorylates PKB/Akt on Ser473 [45].

To circumvent the early embryonic lethality of mice deficient for raptor or rictor [84, 124], we generated mice with floxed *raptor* or *rictor* alleles. Here we describe the phenotype of mice that lack raptor (i.e. mTORC1), rictor (i.e. mTORC2) or both proteins specifically in skeletal muscle. We find that deletion of mTORC2 does not cause an overt muscle phenotype. In contrast, mTORC1-deficient muscles manifest signs of atrophy and become progressively dystrophic. Moreover, muscles behave metabolically like fast-twitch, glycolytic skeletal muscle, but exhibit structural features and contraction properties indicative of slow-twitch, oxidative muscle fibers. Biochemical analysis indicates that this phenotype can be accounted for by the absence of phosphorylation of the immediate mTORC1 downstream targets S6K/S6 and 4EBP1, the downregulation of PGC1 $\alpha$ , and hyperphosphorylation of PKB/Akt. Finally, deficiency of both raptor and rictor results in a phenotype indistinguishable from that of muscles lacking only raptor. Importantly, PKB/Akt is still hyperphosphorylated under these conditions, suggesting that mTORC2 is not the only kinase able to phosphorylate PKB/Akt on Ser473.

### 3.2.3. Results

#### Skeletal muscle-specific ablation of *raptor* and *ricTOR*

To examine the function of raptor and rictor in skeletal muscle we used the Cre-loxP recombination system. To this end, we introduced loxP sites into the *raptor* and the *ricTOR* locus (Figure 1A). In both cases, Cre-mediated recombination causes a frame shift and early stop of translation. In addition, FRT sites were inserted that flanked a neomycin resistance cassette for the selection of targeted embryonic stem (ES) cells. This cassette was removed using Flp deleter mice (Figure 1A; [125]). Southern blot analysis confirmed successful targeting in ES cells and germ line transmission of resulting chimeras (Figure 1B). Mice homozygous for the floxed allele (*raptor<sup>fl/fl</sup>* or *ricTOR<sup>fl/fl</sup>*) were mated with heterozygous floxed mice that also expressed Cre recombinase under the control of the muscle-specific human skeletal actin (HSA) promoter [87]. Mice positive for the *HSA-Cre* transgene that also carried two floxed alleles were then analyzed. For simplicity, we refer to *HSA-Cre; raptor<sup>fl/fl</sup>* as RAmKO (for raptor muscle knockout) and to *HSA-Cre; ricTOR<sup>fl/fl</sup>* as RImKO (for rictor muscle knockout) mice. Successful recombination of *raptor* or *ricTOR* was confirmed by PCR on genomic DNA isolated from *tibials* muscle (Figure S1A). Western blot analysis of RAmKO and RImKO skeletal muscle revealed a strong reduction of the respective proteins (Figure 1C; Figure S1B and Table S1). Residual expression of these proteins in knockout muscle is not due to leaky recombination of the targeted allele as *raptor<sup>fl/fl</sup>* or *ricTOR<sup>fl/fl</sup>* mice crossed to other Cre-expressing mice led to a complete loss of the respective protein in the targeted tissue (Figure S1B; [90]; M.N. Hall, personal communication). Thus, the low levels of raptor and rictor protein that were detected in the RAmKO and RImKO muscles are ascribable to the expression of raptor or rictor in non-targeted cells, such as fibroblasts, satellite cells, Schwann cells and peripheral nerves, which are also contained in skeletal muscle.

Neither RAmKO nor RImKO mice showed an overt phenotype in the first weeks of life. Starting at the age of approximately 5 weeks, RAmKO mice could be distinguished from their littermates by their lower body weight. The difference became significant after day 63 and the mice remained lighter throughout life (Figure 1D). In contrast, the body weight of RImKO mice did not differ significantly from controls, although at higher age RImKO mice were slightly heavier (Figure 1D). For both RAmKO and RImKO mice, the food consumption was comparable to controls (Figure S1C and data not shown). RAmKO mice developed a pronounced kyphosis starting at the age of approximately 2 months and became markedly lean (Figure 1E; Figure S1D). In contrast, RImKO mice appeared normal. Finally, RAmKO mice began to die at the age of 110 days and none survived for more than 190 days (Figure 1F). RImKO mice did not die prematurely (the oldest RImKO mice now being more than 2 years old).

To examine whether the difference in weight gain was based on reduced muscle mass in RAmKO mice, we weighed different muscles and several other organs at day 90 (i.e. before the mice showed a severe phenotype) and at day 140. As shown in Table 1, all the muscles measured were significantly lighter in 90 and 140 day-old RAmKO mice compared to controls. As RAmKO mice appeared lean (Figure 1E) and only little or no fat was detected in older mice (Figure S1D), we also weighed the epididymal fat pads. Indeed, RAmKO mice contained significantly less adipose tissue at the age of 140 days (Table 1). The loss of adipose tissue does not seem to be due to changes in mitochondrial uncoupling properties as the body temperature of RAmKO mice was not different from control littermates (Figure S1E). The weight of the liver was indistinguishable from controls whereas hearts were again lighter (Table 1). The left ventricle mass of the heart, however, correlated with the difference in body weight (Figure S1F), indicating that the difference in heart weight is probably due to allometric scaling [126]. Moreover, the ejection fraction determined by echocardiography was indistinguishable from littermate controls (data not shown). Finally, we could not detect any recombination events in the hearts of RAmKO mice (Figure S1A). Our data therefore show that raptor deficiency in skeletal muscle causes a progressive, disproportional loss of skeletal muscle and fat.

### **Deficiency of mTORC1 but not mTORC2 causes muscle dystrophy**

Kyphosis and early death are often signs of muscle dystrophy [127]. We therefore examined different skeletal muscles of RAmKO and RImKO mice using hematoxylin & eosin (H&E) staining. No change in the overall architecture of *soleus* and *extensor digitorum longus* (EDL) muscle was found in RImKO mice (Figure 2A). Muscles from RAmKO mice showed signs of a dystrophy, such as mononuclear cells (green arrowheads) and a high number of small and large muscle fibers (blue arrowheads). In *soleus* muscle and to a lower extent in EDL, we also found muscle fibers with centralized nuclei (white arrowheads), indicative of ongoing de- and regeneration, and structures reminiscent of central cores (black arrowheads in Figure 2A and Figure 2B). Quantification showed that the fiber size distribution was strongly altered in both *soleus* and EDL muscle (Figure 2C, D, E, F). In addition, the number of centralized myonuclei (Figure 2G) and the relative percentage of muscle fibers with the central core-like structures (Figure 2H) was higher in RAmKO mice compared to controls. Dystrophic hallmarks seemed more pronounced in *soleus* than in EDL muscle. Interestingly the severity of the dystrophy correlated with the high endogenous expression of raptor, rictor, mTOR or PKB/Akt in wild-type *soleus* muscle (Figure S2A). Muscles of RAmKO mice also showed increased immunoreactivity for tenascin-c and f4/80 (Figure S2B), which mark fibrotic tissue [128] and infiltrating macrophages [129], respectively. However, other dystrophic hallmarks including increased uptake of Evans blue into muscle fibers and increased levels of creatine

kinase in the blood could not be detected (Figure S2C and data not shown). Similarly, the number of muscle fibers was not changed in *soleus* muscle of RAmKO mice compared to controls (Figure S2D). Neuromuscular junctions of RAmKO mice were indistinguishable from those in control mice (Figure S2E). Probably due to ongoing de- and regeneration, many extrasynaptic acetylcholine receptor (AChR) clusters could be detected in the diaphragm of RAmKO mice (Figure S2F). Based on the extensive muscle wasting and the high degree of fibrosis, the dystrophy was particularly severe in the diaphragm of older mice (Figure 2I), suggesting that respiratory failure might be the cause of premature death. In contrast to RAmKO mice, muscles of RImKO mice did not show any alterations in fiber size (Figure S3A) and in the cytoskeletal organization as indicated by the sarcomeric arrangement of  $\alpha$ -actinin (Figure S3B). In summary, our data show that ablation of *raptor* and thus of mTORC1, but not of *riCTOR*, results in a progressive muscle dystrophy.

### **Skeletal muscles of RAmKO mice show alterations in their metabolic and structural properties**

One of the first observations we made during the course of this work was that muscles of RAmKO mice appeared paler than those of RImKO or control mice. This difference was particularly striking for the *soleus* muscle (Figure 3A, arrowhead) and was not based on decreased vascularization, as revealed by staining for laminin- $\alpha$ 5 (data not shown), which is expressed in blood vessels [130]. To test for changes in mitochondrial function, we used an NADH-tetrazolium (NADH-TR) staining. Indeed, the activity of oxidative enzymes appeared lower in both, EDL and *soleus* muscle of RAmKO mice (Figure 3B). Fibers with central core-like structures, which were completely devoid of NADH-TR reactivity, could be found in RAmKO *soleus* muscle (black arrowheads). Such a lack of NADH staining is a diagnostic feature of central core disease [131]. To further test whether the changes in NADH-TR reactivity involved mitochondria, we also examined longitudinal sections of soleus muscle by electron microscopy. Muscle of RAmKO mice was distinguishable from control muscle by a substantial loss of intermyofibrillar mitochondria, which are normally localized perpendicular to the Z disks (arrows in upper panel, Figure 3C). Only few intermyofibrillar mitochondria remained (arrow lower panel, Figure 3C). Moreover, mitochondria localized in the subsarcolemmal space seemed more densely packed and swollen in RAmKO mice (Figure S4A). As a decrease in oxidative properties is often accompanied by a compensatory increase in glycolytic activity, we performed a periodic acid Schiff (PAS) staining. Indeed, the glycogen content was increased in both EDL and *soleus* muscle (Figure 3D). The increase was more pronounced in the fast-twitch EDL muscle. The glycogen content in the *gastrocnemius* muscle, which consists of a mixed population of fast- and slow-twitch fibers, was more than 5 times higher than in control mice (control:  $21 \pm 7 \mu\text{mol glucose/g tissue}$ ;



RAMKO:  $108 \pm 22$   $\mu\text{mol}$  glucose/g tissue; mean  $\pm$  SEM; N = 4 mice). The change in oxidative capacity and glycogen content in skeletal muscle also affected overall metabolism as glucose uptake from the blood was significantly slower in RAMKO mice compared to littermate controls (Figure 3E).

High content of glycogen is indicative of fast-twitch (type II) muscle fibers. To test whether muscles in RAMKO mice also changed their structural properties, we stained EDL and *soleus* muscle for the slow myosin heavy chain (sIMHC), a marker of slow-twitch fibers. Surprisingly, EDL and *soleus* muscle of 140 day-old RAMKO mice contained even more sIMHC-positive muscle fibers (Figure 3F; green) than controls and the increase of sIMHC was regionalized in individual muscles (Figure S4B). In both muscles, the number of sIMHC-positive fibers was approximately 2 to 3 times higher than in controls (Figure 3G & H). In *soleus* muscle of RAMKO mice, almost 100% of the fibers were positive for sIMHC (Figure 3H) and this increase was also seen by Western blot analysis (Figure 3I; Table S1). Moreover, other components characteristic for slow-twitch muscle, such as the slow isoform of troponinT (sITnT) and of troponinI (sITnI), were also increased in *soleus* muscle of RAMKO mice (Figure 3I & J; Table S1). Thus, deletion of mTORC1 in skeletal muscle fibers causes a shift of their metabolic properties from oxidative to glycolytic. However, this change in the metabolic characteristics of muscles is opposite to their structural properties.

### **Functional characterization of muscles in RAMKO mice**

To address whether the observed changes in metabolic and structural characteristics had consequences on the overall performance of muscle, we allowed 90 day-old mice to exercise using voluntary wheel running. The representative activity chart of a single mouse shows that running sessions of RAMKO mice were shorter and less frequent than those of controls (Figure 4A). When averaged over one week, the total distance run per day by RAMKO mice was  $\sim 60\%$  of that of control mice (Figure 4B) and the top running speed was significantly lower (Figure 4C). In contrast to the aerobic wheel running task, RAMKO mice performed equally well as control animals in a grip strength test on a horizontal grid (Figure 4D). To examine the contraction properties of muscles, force measurements were performed on isolated EDL and *soleus* muscles. In line with the observed increase of fibers expressing structural proteins characteristic of slow-twitch muscle, time to peak, half time to peak and relaxation time of the twitch were all increased (Table 2). This difference to control mice did not reach significance in EDL muscle but was highly significant in *soleus* muscle (Table 2). Twitch force and maximal tetanic absolute force for both muscles was, however, significantly lower in RAMKO mice. The decrease of absolute force capacity reflects the decrease of muscle mass (Table 1), since there is no difference of the maximal tetanic force when normalized to the muscle cross-sectional area (Table 2). An intermittent maximal tetanic

stimulation protocol revealed that both EDL and *soleus* muscle from RAmKO mice were more resistant to fatigue (Figure 4E). These data indicate that raptor-deficient muscle fibers have a reduced aerobic capacity (voluntary wheel running) like fast-twitch, glycolytic muscle fibers, but exert contraction properties (isolated muscles) of slow-twitch, oxidative muscle fibers.

### **Inactivation of *raptor* or *ricTOR* affects activation of PKB/Akt**

In search of a mechanistic explanation for the phenotypes, we examined *soleus* muscle of RAmKO and RImKO mice biochemically. In each experiment, at least three different mice were compared with three littermate controls. Deletion of *raptor* or *ricTOR* did not significantly affect the levels of mTOR (Figure 5A, Table S1). The levels of *ricTOR* were not lowered in RAmKO mice and there was a slight decrease of *raptor* in RImKO mice (Figure 5A, Table S1). The amount of S6K, S6 and 4EBP1, which are the main targets of mTORC1, was not changed in RAmKO mice. However, phosphorylation of S6 and 4EBP1 was strongly decreased (Figure 5A; Table S1). In RImKO mice, mTORC1 targets were not changed but the level and activation state of PKB/Akt and PKC $\alpha$ , which are both well characterized substrates of mTORC2 [13, 45], were lower. More importantly, phosphorylation of PKB/Akt on residues Thr308 and Ser473 was strongly increased in RAmKO mice (Figure 5A; Table S1). Furthermore, the total amount of FoxO1 and FoxO3a was increased in RAmKO mice concomitant with an increase in phosphorylation of FoxO1 on Thr24 (Figure 5A; Table S1). In contrast, phosphorylation of FoxO1 on Ser316 and of FoxO3a on Thr32 was not increased. Activation of S6K by mTORC1 causes feedback inhibition of the insulin/IGF1 pathway by affecting the levels and the phosphorylation of IRS-1 [132, 133]. Consistent with this notion, deficiency of mTORC1 and thus absence of S6K/S6 activation abrogated this inhibitory feedback and strongly increased IRS-1 levels in muscles of RAmKO mice (Figure 5B; Table S1). Concomitant with the high protein levels, IRS phosphorylation on Ser636 and Ser639 was increased. On the other hand, both the levels and phosphorylation of the mitogen-activated protein kinase Erk1 and Erk2 were not significantly changed (Figure 5B; Table S1). Thus, activation of PKB/Akt is probably due to the failure of raptor-deficient muscle fibers to activate S6K and thus due to the absence of the inhibitory feedback onto IRS. The release of this feedback in muscle may require prolonged inactivation of mTORC1 as phosphorylation of PKB/Akt was not increased after 8 hour treatment of cultured C2C12 myotubes with rapamycin and was only slightly elevated after 16 hours (Figure S5C).

Next we asked whether part of the phenotype of RAmKO mice could be based on this hyperphosphorylation of PKB/Akt. To determine whether PKB/Akt was indeed activated within muscle fibers and not in non-muscle tissue of RAmKO mice; we stained cross-sections of *soleus* muscle with antibodies specific for PKB/Akt phosphorylated on Ser473 (P-

PKB/Akt<sup>S473</sup>). Indeed, many of the muscle fibers were strongly positive for P-PKB/Akt<sup>S473</sup> (Figure S5A). Akt/PKB has been shown to regulate expression of atrogenes, called atrogen-1/MAFbx and MuRF-1, via the FoxOs [67, 134]. As expected, mRNA levels for both atrogenes were significantly lower in RAMKO mice than in controls (Figure 5C). A further target of PKB/Akt is glycogen synthase kinase3 $\beta$  (GSK3 $\beta$ ), which in turn inhibits glycogen synthase [135]. Whereas the amount of GSK3 $\beta$  was unaffected, phosphorylation of Ser9 was significantly increased (Figure 5C; Table S1). Moreover, glycogen phosphorylase, which is the enzyme that generates free glucose from glycogen, was downregulated (Figure 5C; Table S1). Thus, hyperphosphorylation of PKB/Akt in conjunction with downregulation of glycogen phosphorylase is probably the basis for the increased levels of glycogen observed in RAMKO mice.

In an attempt to identify the pathway that might underlie the increased number of muscle fibers expressing sIMHC, we found a slight increase in the levels of calcineurin and a highly significant increase in myocyte-enhancer factor 2A (Mef2A; Figure 5C; Table S1). A slight, but not significant increase in Mef2D was also observed. The increase in Mef2A is not a consequence of the ongoing de- and regeneration in *soleus* muscle as Mef2A was also increased in the least affected EDL muscle (Figure S5B). In contrast to skeletal muscle *in vivo*, Mef2A and sIMHC were not increased in cultured C2C12 myotubes upon prolonged treatment with rapamycin (Figure S5C).

### **Genes involved in mitochondrial biogenesis are downregulated in RAMKO mice**

One of the most striking features of RAMKO skeletal muscle is its lower oxidative capacity that is probably due to ultrastructural changes and loss of mitochondria. Thus, we also tested whether genes involved in mitochondrial biogenesis were affected by the deletion of *raptor*. Recent evidence indicates a function of mTORC1 in the regulation of mitochondrial function via PGC1 $\alpha$  [42]. Consistent with these findings, transcript levels for PGC1 $\alpha$  and for its target gene myoglobin were significantly reduced in RAMKO muscle (Figure 5E). Moreover, the protein levels of the PGC1 $\alpha$  co-activator PPAR $\gamma$  and the mitochondrial marker cytochrome c oxidase IV (COX IV) were significantly decreased in RAMKO mice (Figure 5F; Table S1). These results are consistent with the low oxidative capacity of muscle from RAMKO mice and they support the notion that this is due to loss of PGC1 $\alpha$ .

### **Activation of PKB/Akt is independent of mTORC2**

To test whether the hyperactivated state of PKB/Akt in RAMKO mice can be prevented by additional deletion of *rictor*, we generated double floxed mice and mated those with *HSA-Cre* mice. The resulting mice, called DmKO, lacked both raptor and rictor in skeletal muscle (Figure 5G; Table S1). Their overall phenotype was indistinguishable from RAMKO mice

(data not shown). Like in RAmKO mice, skeletal muscle of DmKO mice contained high levels of glycogen and was less oxidative (Figure 5H). Levels of mTOR were significantly lower in DmKO mice than in either of the single knockouts (Figure 5G; Table S1). As mTORC2 was shown to phosphorylate PKB/Akt on Ser473 [45], we also tested the activation state of PKB/Akt in DmKO muscle. As shown in Figure 5G and in Table S1, PKB/Akt was still hyperphosphorylated on Thr308 and Ser473 in DmKO mice. Again, phosphorylation of PKB/Akt occurred only in muscle fibers and not in non-muscle tissue (Figure 5J). In summary, these results indicate that mTORC2 is not the only kinase that phosphorylates PKB/Akt on Ser473.

### 3.2.4. Discussion

Our work dissects the role of raptor and rictor (i.e. mTORC1 and mTORC2, respectively) in skeletal muscle. The *HSA-Cre* mice used for our experiments start to express Cre at the earliest stages of skeletal muscle development when the first myotubes are formed. In fully developed muscle, Cre is exclusively expressed in skeletal muscle fibers but not in non-muscle cells, such as Schwann cells, fibroblasts or satellite cells [87]. Neither RAmKO nor RImKO mice showed any abnormalities at birth, indicating that mTORC1 and mTORC2 are not essential for muscle development. Whereas no overt phenotype was detected in RimKO mice throughout adulthood, which is consistent with another report [136], RAmKO mice developed a progressive dystrophy and ultimately died around the age of five months. Interestingly, DmKO mice showed very similar pathological changes as RAmKO mice, indicating that mTOR function in skeletal muscle requires only mTORC1.

The dystrophy in RAmKO mice did not affect all muscles to the same extent. For example, diaphragm and *soleus* muscles were severely affected while EDL showed much less changes. Prominent features of the dystrophy were elevated numbers of muscle fibers with centralized nuclei and the presence of central core-like structures. Central cores are hallmarks of “central core diseases”, which are inherited neuromuscular disorders with a myopathic syndrome. The most frequent causes of this group of diseases are mutations in the ryanodine receptor, which is the main protein responsible for calcium homeostasis in muscle (reviewed in [137]). Thus, the similarity of the pathology in RAmKO to this class of disease suggests that mishandling of intracellular calcium may underlie the disease. The low levels of PGC1 $\alpha$  may additionally contribute to the dystrophic phenotype of RAmKO mice as conditional ablation of *PGC1 $\alpha$*  in skeletal muscle results in a myopathic phenotype [138]. Finally, several metabolic diseases that cause accumulation of glycogen in skeletal muscle, such as Pompe’s and McArdle’s disease, affect skeletal muscle function. The most severely affected patients may even die because of respiratory distress [139]. In summary, RAmKO show changes in muscle homeostasis that together may lead to the progressive muscle dystrophy.

#### **Raptor is required for high oxidative capacity of skeletal muscle**

We found that the severity of the muscle dystrophy correlated with the relative levels of raptor, rictor, mTOR and PKB/Akt in particular muscles. Interestingly, the most affected muscles, such as *soleus* or diaphragm, are also those that are insulin-sensitive [140] and contain a high number of slow-twitch, oxidative fibers. Biochemical and morphological analysis showed that *soleus* muscle expressed little of the oxygen carrier myoglobin and of COXIV, and contained fewer and misshaped mitochondria. A direct role of mTOR and raptor

for the function of mitochondria has recently been suggested using cultured Jurkat cells [141]. Moreover, mTOR has been shown to form a complex with PGC1 $\alpha$  [42], which together with its cofactor PPAR $\gamma$  is a key regulator of mitochondrial biogenesis and function. Consistent with a regulatory function of mTORC1 for mitochondria, mRNA levels for PGC1 $\alpha$  and protein levels of PPAR $\gamma$  were decreased in RAmKO mice. Furthermore, mRNA and protein levels of target genes for PGC1 $\alpha$ /PPAR $\gamma$ , such as myoglobin [142] and glycogen phosphorylase [143] were also reduced in RAmKO mice. Also, very similar to the phenotype of RAmKO mice, a reduced intermyofibrillar mitochondrial content in slow-twitch muscles has been reported in PGC1 $\alpha$  knockout mice [144]. In summary, our data indicate that mTORC1 is essential for the function of mitochondria in skeletal muscle and they link mTORC1 to the regulation of PGC1 $\alpha$  *in vivo*.

### **Segregation of metabolic and structural properties in skeletal muscle of RAmKO mice**

Despite the loss of oxidative capacity and the downregulation of PGC1 $\alpha$ , expression of slow structural proteins (sISP; Figure 5K) was increased in RAmKO mice. Analysis of the mechanical properties in EDL and *soleus* muscle further confirmed that both muscles adapt characteristics indicative of slow-twitch fibers. These results suggest that RAmKO mice induce a structural program for slow-twitch fibers. As muscle-specific inactivation of *PGC1 $\alpha$*  causes a fiber-type switch to fast-contracting muscle fibers [138] and transgenic overexpression causes an increase in oxidative muscle [142], we also tested whether any other pathways that affect muscle differentiation were altered in the RAmKO mice. Besides PGC1 $\alpha$ , the best characterized factors involved in fiber type determination are calcineurin/NFAT and the Mef2 transcription factors [145]. Of those candidate genes, the levels of calcineurin and in particular of Mef2A and Mef2D were increased in RAmKO mice. Thus, facilitated Mef2-mediated transcription may be the basis for the increased levels of sISP despite the low levels of PGC1 $\alpha$ . Opposite regulation of PGC1 $\alpha$  and Mef2A has also been seen in cultured cells when treated with rapamycin [42]. Mef2 has also been shown to be dominant in the regulation of muscle fiber type as transgenic overexpression of a constitutively active form of Mef2 is sufficient to increase the number of slow muscle fibers [146]. Mef2 is generally thought to be controlled by calcium-activated processes acting via calcineurin and CaM kinase IV [147]. In this context it is interesting to note that the increase of the half-relaxation time in RAmKO muscles may result from a lower removal rate of calcium from the myoplasm by the sarcoplasmic reticulum [148]. This prolonged presence of intracellular calcium during contractile activity might contribute to the activation of calcium-dependent signaling pathways, and thus to the upregulation of sISP (Figure 5K). On the other hand, it is possible that Mef2 expression is increased because of hyperactivation of PKB/Akt [149]. Consistent with this notion, failure to induce a pronounced phosphorylation of

PKB/Akt in cultured C2C12 myotubes by treatment with rapamycin coincided with unchanged levels of Mef2A and  $\alpha$ MHC (Figure S5C).

### **Raptor deficiency affects protein synthesis directly and PKB/Akt activation indirectly**

Ablation of mTORC1 in skeletal muscles prevented phosphorylation of S6K/S6 and 4EBP1. This branch of the mTOR signaling pathway is characterized best and has been shown to directly control protein synthesis. Impaired efficacy of protein synthesis in postnatal muscle might also be the reason for the muscles being lighter in RAmKO mice. This effect may also contribute to the shift in fiber size distribution towards smaller values. Our data thus implicate mTORC1 in the maintenance of mass even in fully innervated muscle. Therefore, they extend previous results in which mTOR inhibition by rapamycin was shown to prevent compensatory hypertrophy and recovery from atrophy but not cause atrophy [64]. Our results are also consistent with the findings that skeletal muscles of S6K1-deficient mice are atrophic [59]. The difference in weight of the RAmKO mice became significant only after the age of approximately 2 months, suggesting that the absence of raptor might be compensated for during early periods of muscle growth. One compensatory mechanism could be PKB/Akt-mediated phosphorylation of GSK3 $\beta$  as inhibition of GSK3 $\beta$  has been shown to cause hypertrophy in cultured C2C12 myotubes [150]. We also provide evidence that the lack of S6K activation in RAmKO mice is responsible for the hyperphosphorylation of PKB/Akt on Thr308 and Ser473 as levels of IRS-1 were highly increased. Activation of S6K has been shown to decrease the levels of IRS-1 (reviewed in [151]). Interestingly, the same hyperactivation of PKB/Akt is seen in mice with an adipocyte-specific ablation of *raptor* [90].

### **Raptor-deficient skeletal muscles are small, despite high energy consumption**

Whereas changes in mitochondrial content and function might be based on a direct influence of mTORC1 (Figure 5K), other aspects such as the loss of adipose tissue are probably a consequence of the hyperactivation of PKB/Akt. Muscle-specific overexpression of a constitutively active form of PKB/Akt causes pronounced hypertrophy [60]. Concomitantly with the hypertrophy, mice are lean and do not become obese on a high fat diet [60]. In the RAmKO mice, PKB/Akt was hyperactive resulting in mice that had much less fat than control mice on a normal chow diet (Table 1) or on a high fat diet (KR, CFB and MAR, unpublished observation). In contrast to mice that express the constitutively active form of PKB/Akt, lack of mTORC1 prevented the "translation" of PKB/Akt activation into muscle hypertrophy in RAmKO mice. Thus, RAmKO mice behave metabolically like mice that overexpress activated PKB/Akt but lack the hypertrophic effect on muscle. We hypothesize that the metabolic phenotype of being lean is due to the high need of muscle for glucose because of their high glycogen storage capability and their low capacity for oxidative phosphorylation. If the muscle

of RAmKO mice acts as such a global glucose sink, non-muscle tissues may have to use alternative energy sources such as fatty acids. This, in turn, could result in an increased release and mobilization of fatty acids from adipose tissue. The high content of glycogen is probably based on the hyperactivation of PKB/Akt, which inhibits GSK3 $\beta$ , which in turn, releases inhibition of glycogen synthase (Figure 5H). In addition, inhibition of GSK3 $\beta$  also lowers phosphorylation of NFATc and thus prolongs its activity in the nucleus [152]. NFATc transcription factors, which are also targets of calcineurin (see above), are known to contribute to fiber type selection (reviewed in [153]). Thus, changes in NFATc activity may add to the expression of structural proteins indicative of slow-twitch muscle.

### **Hyperactivation of PKB/Akt does not require rictor/mTORC2**

Our data strongly indicate that the absence of the S6K-mediated inhibitory feedback caused phosphorylation of PKB/Akt on Thr308 and Ser473 in RAmKO mice. While phosphorylation on Thr308 is mediated by 3-phosphoinositide-dependent kinase (PDK1; [154]), mTORC2 has been shown to phosphorylate PKB/Akt on Ser473 [155]. Consistent with such a role for mTORC2, we and others observed a decrease in Ser473 phosphorylation in mice deficient for rictor (Figure 5; [84, 124, 136]). We now show that unexpectedly, muscles from mice lacking both mTORC1 and mTORC2 still showed a marked increase in PKB/Akt phosphorylation on both Thr308 and Ser473. Thus, mTORC2 is not required to phosphorylate PKB/Akt on Ser473 *in vivo*, indicating that skeletal muscles express a PDK2 distinct from mTORC2. A candidate for this kinase is DNA-dependent protein kinase (DNA-PK), which has been shown to phosphorylate PKB $\alpha$ /Akt1 in cells that are deficient for rictor in response to DNA damage [156]. DNA-PK and PKB/Akt are localized in the nucleus of embryonic fibroblasts upon DNA damage [156]. However, PKB/Akt phosphorylated on Ser473 in DmKO mice was expressed along the sarcolemma and not specifically localized in myonuclei. Several additional proteins have been postulated to act as PDK2, some of which are expressed in skeletal muscle and are localized to the sarcolemma (see [155] for a review).

In summary, our data show that mTORC1 is important for the function and maintenance of skeletal muscle. We provide evidence that the different aspects of the phenotype observed in RAmKO mice are probably based either on the direct effect of mTORC1 on its downstream targets S6K and 4EBP1, on the function of mTORC1 to regulate mitochondrial biogenesis and function via PGC1 $\alpha$ , or on an indirect effect on its upstream component PKB/Akt. Our data also suggest that long-term treatment with high doses of rapamycin may have detrimental effects on muscle function.



### **3.2.5. Experimental procedures**

#### **Antibodies**

Rabbit polyclonal antibodies: 4E-BP1 (Phas-I) from Zymed, ERK1&2 pan and ERK1&2 (pTpY185/187) from Biosource, FoxO1a and FoxO1a (phospho S319) from Abcam, P-PKC $\alpha$  (Ser657) and Troponin T-SS (H-55) from Santa Cruz, Phospho-4E-BP1 (Ser65), PAN-actin, Akt, Phospho-Akt (Thr308), Pan-Calcineurin A, Phospho-FoxO1 (Thr24)/ FoxO3a (Thr32), Phospho-GSK-3 $\beta$  (Ser9), Phospho-IRS-1 (S636/639), MEF2A, mTOR, PKC $\alpha$ , S6 Ribosomal Protein, Phospho-S6 Ribosomal Protein (Ser235/236) and p70 S6 kinase from Cell Signaling. Rabbit monoclonal antibodies:  $\beta$ -actin, Phospho-Akt (Ser473), Cox IV, FoxO3a (75D8), GSK-3 $\beta$ , IRS-1, PI3 Kinase p85, Raptor and Rictor from Cell Signaling and PPAR $\gamma$  from Santa Cruz. Mouse monoclonal antibodies:  $\alpha$ -actinin and myosin (skeletal, slow) from sigma,  $\beta$ -tubulin and Mef2D from BD Biosciences. Goat polyclonal antibody: GP from Santa Cruz.

#### **Tissue homogenization, immunoprecipitation, SDS PAGE and Western blot**

Muscles frozen in liquid nitrogen were powdered on dry ice, transferred to cold RIPA buffer supplemented with 1% Triton-X, 10% glycerol, protease inhibitor cocktail tablets (Roche) and phosphatase inhibitor cocktail I and II (Sigma). Cell lysates were incubated on ice for 2 hours, sonicated 2 times for 15 seconds and centrifuged at 13,600g for 30 min at 4°C. Cleared lysates were then used to determine total protein levels (BCA Protein Assay, Pierce). After dilution with sample buffer, equal protein amounts were loaded onto SDS gels.

#### **Histology and immunohistochemistry**

Muscles frozen in liquid nitrogen-cooled isopentane were fixed with 2% PFA and cut into 12  $\mu$ m cross-sections. Cross-sections were permeabilized with 1% Triton/PBS for 5 min, washed with 100 mM glycine/PBS for 15 min, blocked with 1% BSA/PBS for 30 min and incubated with specific primary antibody overnight at 4°C. Samples were subsequently washed with 1% BSA/PBS, 3 times for 1 hour, stained with appropriate fluorescently labeled secondary antibodies for 1 hour at room temperature. After washing with PBS, samples were mounted with Citifluor (Citifluor Ltd). General histology on cross-sections was performed using hematoxylin and eosin (H&E; Merck, Rayway, NJ, USA). NADH staining was done as described [157]. Periodic acid-schiff staining (PAS staining system, Sigma) was performed according to the manufacturer's instruction. After H&E, NADH and PAS staining, samples were dehydrated and mounted with DePeX mounting medium (Gurr, BDH).

### **3.2.6. Acknowledgements**

We thank people of the Transgenic Mouse Core Facility of the University of Basel, in particular D. Klewe Nebenius, for their help in generating the floxed mice. We are indebted to Drs. A. Felley and T. Pedrazzini at the Rodent Cardiovascular Assessment Facility of the University of Lausanne for echocardiography measurements and U. Sauder from the Microscopy Center of the University of Basel for assistance with electron microscopy. We thank Drs. D. Glass, T. Meier and M. Sandri for reading the manuscript. This work was supported by the Cantons of Basel-Stadt and Baselland, grants from the Swiss National Science Foundation (MNH and MAR), the Association Francaise contres les Myopathies (FZ) and the Swiss Foundation for Research on Muscle Disease (MAR). CFB is a recipient of a fellowship from The Roche Research Foundation.

### 3.2.7. Figures and tables

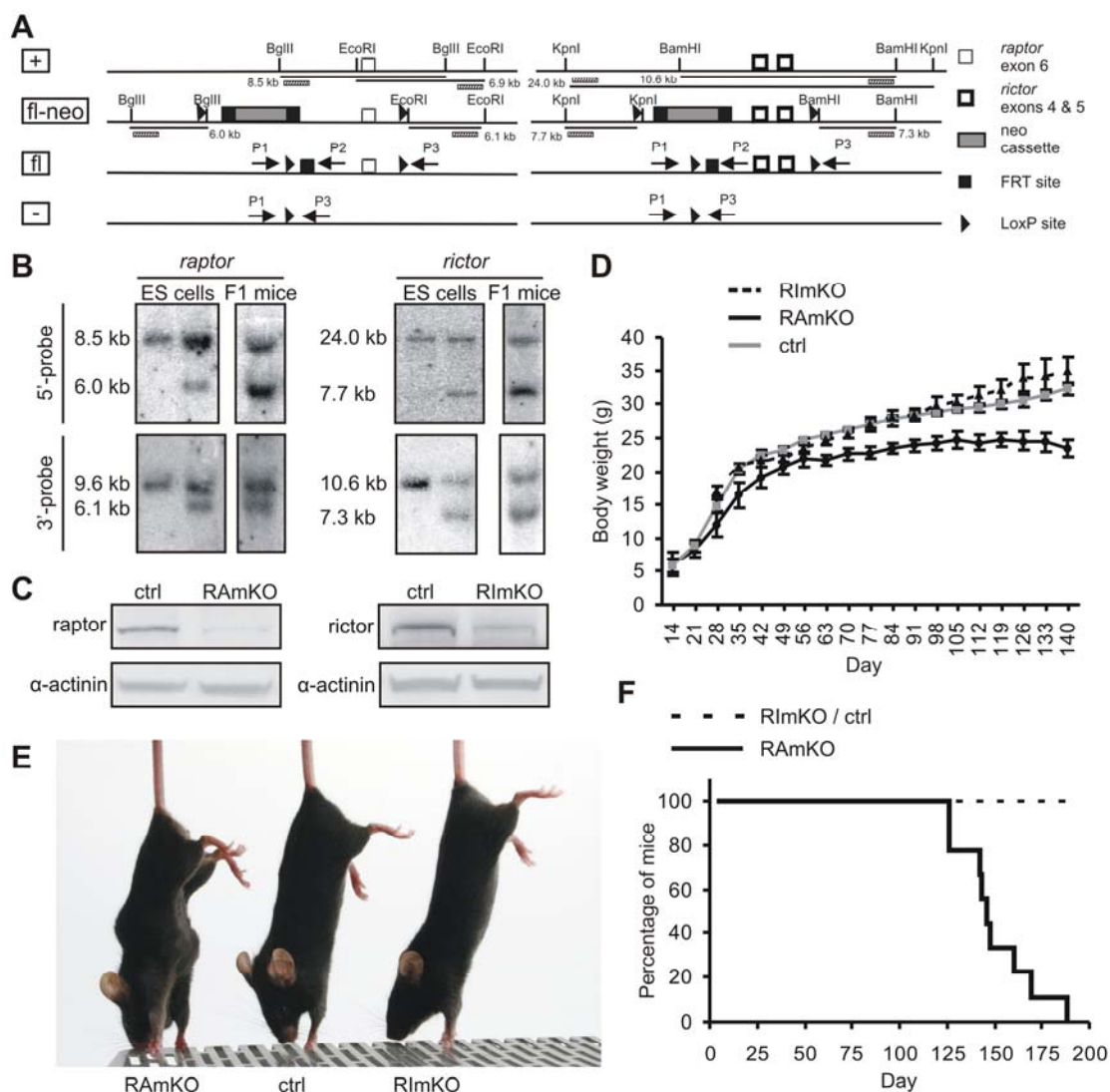


**Figure 1. Targeting strategy and initial characterization of RAmKO and RImKO mice**

(A) Schematic presentation of wild-type and targeted alleles of *raptor* (left panel) and *rictor* (right panel) before and after recombination. Localization and size of DNA fragments generated by particular restriction digests are indicated. Probes used for Southern blot analysis are shown by hatched bars. PCR primers for genotyping are indicated by arrows. +: wild-type allele; fl-neo: targeted allele; fl: alleles after recombination by FRT; -: alleles after recombination by Cre. (B) Southern blot analysis of genomic DNA from ES cells and F1 progeny of resulting chimeras. Correct targeting of the 5' end is indicated by the presence of a 6.0 kb band in the *raptor* locus and a 7.3 kb band in the *rictor* locus. Correct targeting at the 3' end is indicated by a 6.1 kb and a 7.3 kb band, respectively. In each blot of ES cells, wild-type is to the left. (C) Western blot analysis of protein extracts from skeletal muscle of RAmKO and RImKO mice. Controls correspond to muscle extracts from mice that carry the floxed alleles but are negative for *HSA-Cre*. Equal protein loading is confirmed by blotting for  $\alpha$ -actinin. (D) Growth curve of RAmKO, RImKO and control mice. Mice of each genotype were weighed every week. A significant difference between RAmKO and control mice ( $p < 0.05$ ) was observed after the age of 63 days. Individual data points represent means  $\pm$  SEM (N = 5 for RAmKO; N = 3 for RImKO; N = 10 for controls). (E) Photograph of 140 day-old RAmKO, control (ctrl) and RImKO mice. (F) Survival curve of RAmKO, RImKO and control mice.

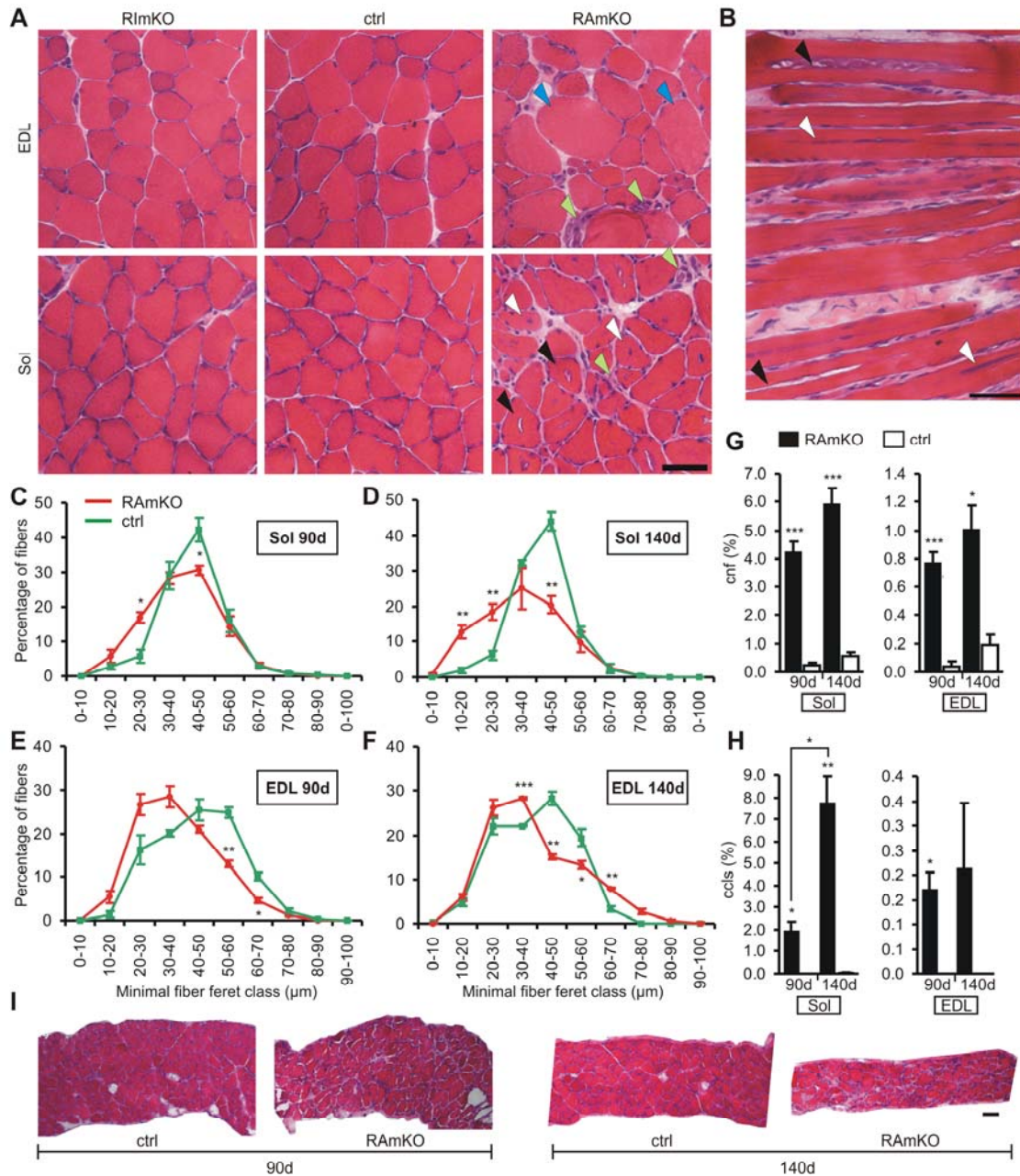
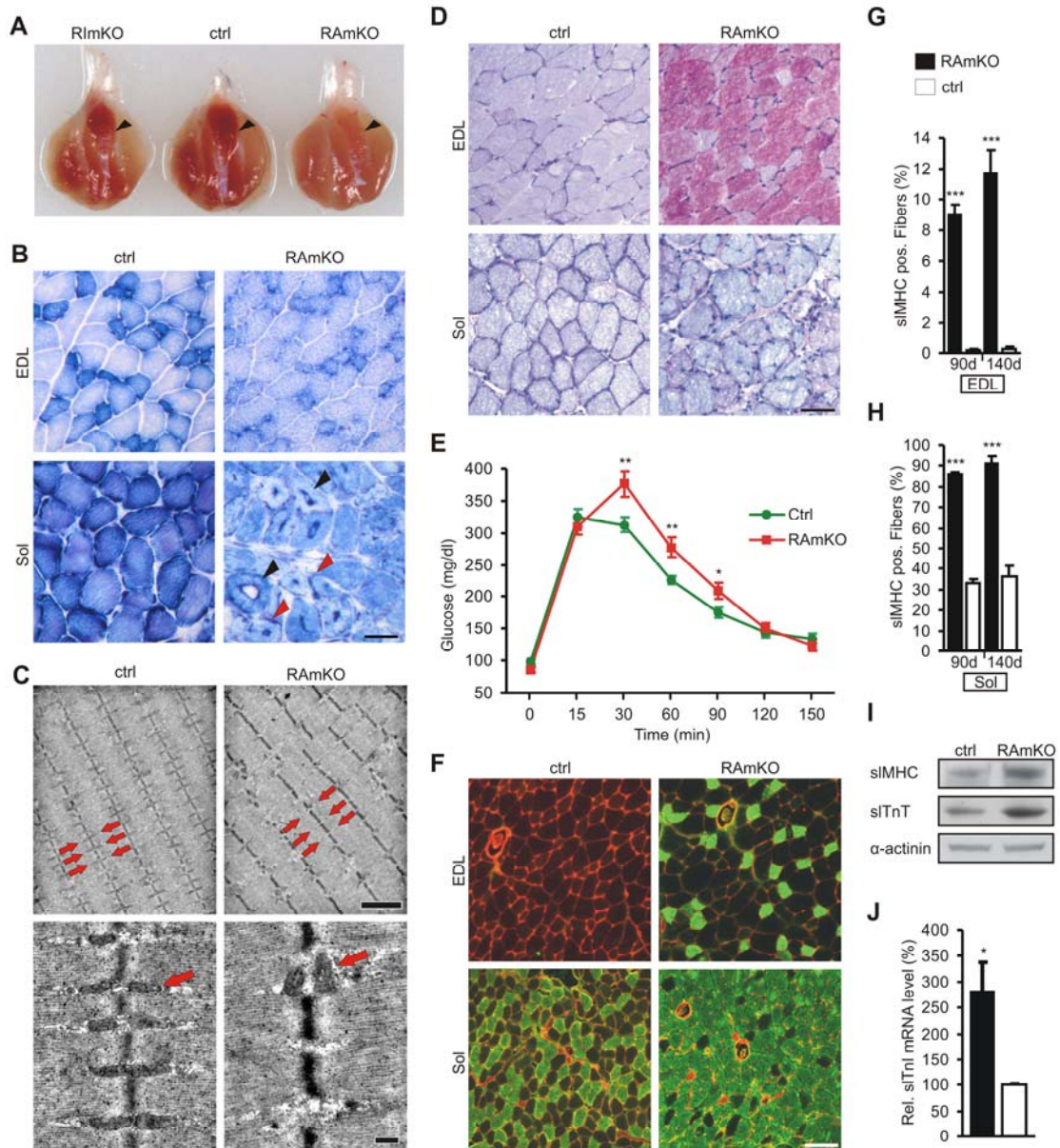


### Figure 2. Muscle of RAmKO mice show signs of a progressive dystrophy

(A) Hematoxylin & Eosin (H&E) staining of muscle cross-sections from the EDL and *soleus* (Sol) muscle of 140 day-old mice. In EDL muscle of RAmKO mice, some large (blue arrowheads) but also small fibers are present. Centralized nuclei (white arrowheads) and central core-like structures (black arrowheads) can be found in *soleus* muscle of RAmKO mice. Both muscles contain many mononuclear cells (green arrowheads). (B) Longitudinal section of *soleus* muscle of a 140 day-old RAmKO mouse. Besides centrally aligned nuclei (white arrowheads), central core-like structures (black arrowheads), which expand longitudinally in muscle fibers are visible. (C, D, E, F) Fiber size distribution in the *soleus* muscle of 90 day- (C) and 140 day-old (D), and in the EDL muscle of 90 day- (E) and 140 day-old (F) RAmKO and control mice. (G) Mean percentage of muscle fibers with centralized nuclei (cnf) in the *soleus* and EDL muscle of RAmKO and control mice. (H) Percentage of muscle fibers containing central core-like structures (ccls) in *soleus* and EDL muscle of RAmKO and control mice. (I) H&E staining of cross-sections of the diaphragm of 90 day- and 140 day-old RAmKO and control mice. Individual data points and bars (C – H) represent mean  $\pm$  SEM (N=4 mice). Scale bars (A, B, I) = 50  $\mu\text{m}$ . P-values are: \*\*\*  $p < 0.001$ ; \*\*  $p < 0.01$ ; \*  $p < 0.05$ .





loading control. (J) Relative mRNA levels of the slow skeletal muscle troponin I isoform (sITnI) in the *soleus* of 90 day-old mice as determined by QRT-PCR (N = 3). Individual data points and bars (E, G, H, J) represent mean  $\pm$  SEM. Scale bars = 50  $\mu$ m (B, D), 2  $\mu$ m (upper pictures C), 250 nm (lower pictures C) and 125  $\mu$ m (F). P-values are: \*\*\* p < 0.001; \*\* p < 0.01; \* p < 0.05.

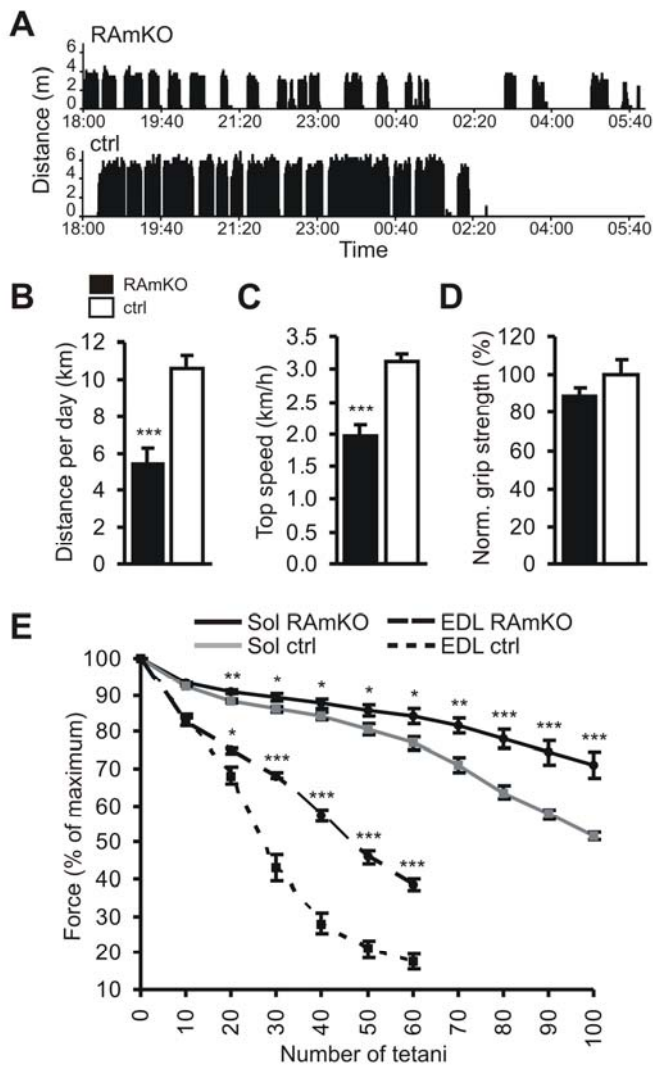


#### Figure 4. Exercise performance and muscle physiology

(A) Representative, activity chart with bins of 10 seconds from a single 95 day-old RAmKO or a control mouse. Charts were measured from 6 pm to 6 am (dark cycle). (B) Average distance run per day determined during one week (starting at the age of 90 days, N = 4 for RAmKO and N = 9 for controls). (C) Average of the top 10% speed measured over one week (starting at the age of 90 days, N = 4 for RAmKO and N = 9 for controls). (D) Grip strength of 90 day-old RAmKO and control mice. Average time mice were able to hold on a horizontal grid was normalized to body weight. Values of control mice were set to 100% (N = 3). (E) Force capacity resistance of EDL or *soleus* muscle isolated from 140 day-old mice was measured during muscle fatigue induced by intermittent tetanic stimulation. Trains of 150 Hz tetani of 350 ms duration were given at 3.6 s intervals. (N = 3 for RAmKO and N = 4 for control mice). Individual data points and bars (B – E) represent mean  $\pm$  SEM. P-values are: \*\*\*  $p < 0.001$ ; \*\*  $p < 0.01$ ; \*  $p < 0.05$ .

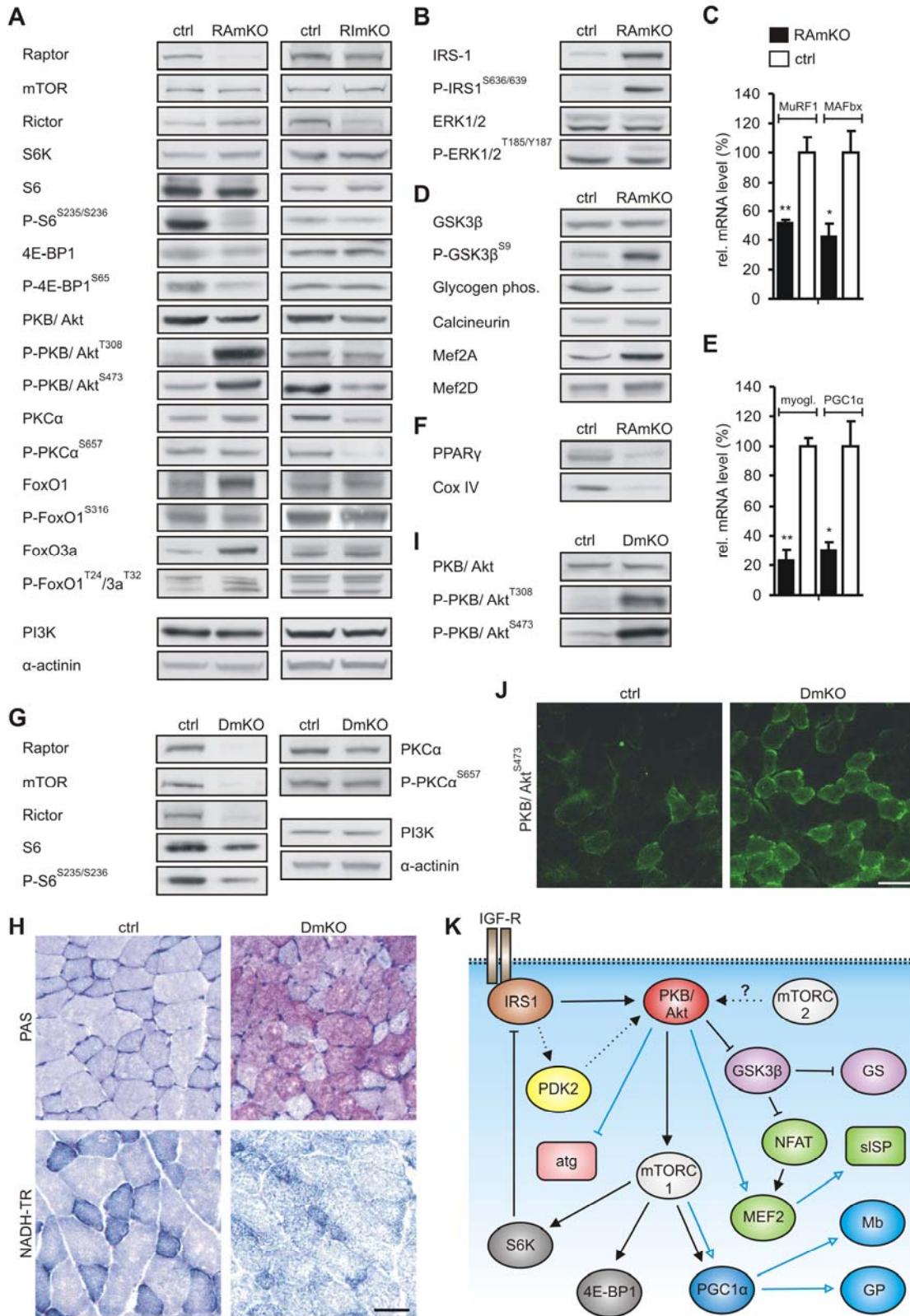




### Figure 5. Biochemical characterization

(A,B,D,F) Western blot analysis of *soleus* muscle from 90 day-old RAmKO, RImKO and control mice using antibodies directed against the proteins indicated (for details see Experimental Procedures). Equal amount of protein was loaded in each lane. Antibodies to  $\alpha$ -actinin and PI3K were in addition used as loading controls. (C & E) Relative mRNA levels of MuRF1, MAFbx, myoglobin (myogl.) and PGC1 $\alpha$  in *soleus* muscle of 90 day-old RAmKO or control mice. Values obtained in controls were set to 100% (N = 3). (G & I) Western blot analysis of *soleus* muscle from 60 day-old DmKO and control mice. (H) PAS and NADH-TR staining on cross-sections of *triceps* muscles from 50 day-old DmKO and control mice. (J) Immunostaining with antibodies specific for P-PKB/Akt<sup>S473</sup> using cross-sections of 60 day-old DmKO and control mice. (K) Schematic of the interactions contributing to the phenotype of RAmKO mice. Signaling pathway downstream of the insulin/IGF receptor is shown. Blue arrows with open arrowheads represent interactions that affect gene transcription; black symbols represent regulation on the protein level that activate or inhibit the targets. Abbreviations are: atg: atrogenes (MuRF1 and MAFbx), GP: glycogen phosphorylase; GS: glycogen synthase; IGF-R: IGF receptor; Mb: myoglobin; sISP: slow structural proteins. Data (C, E) represent mean  $\pm$  SEM. Scale bars (H, J): 50  $\mu$ m. P-values are: \*\* p < 0.01; \* p < 0.05.

Table 1	90d		140d	
	ctrl	RAMKO	ctrl	RAMKO
Tibia length (cm)	2.0 ± 0.1	2.0 ± 0.1	2.0 ± 0.1	2.1 ± 0.1
Lower hindleg (mg)	449.2 ± 19.3	344.0 ± 11.4***	428.0 ± 28.0	331.6 ± 41.3**
<i>Triceps brachii</i> (mg)	98.3 ± 11.3	67.0 ± 10.4***	89.5 ± 14.0	68.8 ± 13.8*
<i>Soleus</i> (mg)	9.7 ± 0.8	7.4 ± 0.6***	9.2 ± 0.8	7.1 ± 1.2*
EDL (mg)	12.7 ± 0.8	10.3 ± 0.7***	12.0 ± 0.7	9.4 ± 1.4*
<i>Tibialis anterior</i> (mg)	58.3 ± 2.7	40.8 ± 2.3***	55.6 ± 1.8	39.0 ± 1.3***
Epididymal fat pad (mg)	566.4 ± 214.9	438.9 ± 93.1	616.0 ± 194.8	242.5 ± 118.7**
Heart (mg)	85.12 ± 6.6	68.1 ± 4.1*	88.5 ± 2.1	72.1 ± 4.4**
Liver (mg)	1350.9 ± 185.0	1187.5 ± 161.0	1232.0 ± 187.5	1055.0 ± 269.1

\* p<0.05, \*\* p<0.01, \*\*\*p<0.001

**Table 1. Analysis of particular tissues in control and RAMKO mice.** Weight or length was measured for different muscles, bones and other organs in 90- and 140 day-old mice. P-values determined by Student's t-test are indicated by asterisks (N = 4 mice). Values represent mean ± SD.

Table 2	EDL		Sol	
	ctrl	RAMKO	ctrl	RAMKO
<b>Twitch</b>				
Time to peak (ms)	10.1 ± 0.9	11.1 ± 1.2	20.3 ± 4.2	39.7 ± 2.4***
Half time to peak (ms)	3.0 ± 0.4	3.5 ± 0.5	5.6 ± 0.6	11.6 ± 1.1***
Half relaxation time (ms)	15.5 ± 2.2	16.8 ± 3.3	30.8 ± 8.7	63.0 ± 5.1***
Absolute force (mN)	54.0 ± 13.2	45.0 ± 9.7	30.0 ± 5.6	21.0 ± 8.1*
<b>Tetanus</b>				
Half contraction time (ms)	16.6 ± 2.0	14.4 ± 1.1*	27.5 ± 5.4	41.0 ± 5.4***
Half relaxation time (ms)	22.1 ± 1.3	24.1 ± 1.6*	55.2 ± 3.9	124.4 ± 13.2***
Absolute force (mN)	311 ± 57.6	224 ± 38.1**	205 ± 20.8	164.0 ± 42.83
Specific force (mN/mm <sup>2</sup> )	380.2 ± 57.2	328.3 ± 62.7	311.6 ± 56.3	264 ± 66.9

\* p<0.05, \*\* p<0.01, \*\*\*p<0.001

**Table 2. Analysis of the contractile properties of EDL and soleus muscles of control and RAMKO mice.** Data were recorded from EDL and soleus muscles of 140 day-old mice. P-values determined by Student's t-test are indicated by asterisks (N = 3 for RAMKO and N = 4 for control mice). Values represent mean ± SD.

### 3.2.8. Supplemental data

#### Supplemental experimental procedures

##### Mice

PAC clones from the RPCI-21 (129S6) mouse genomic DNA library [158] were identified by hybridization with cDNA encoding the targeted exons. For *raptor*, a 6.9 kb SmaI fragment spanning 2.9 kb upstream and 3.8 kb downstream of *raptor* exon 6 was isolated from clone RPCI-21 388E14 and cloned into pBluescript (Stratagene). For the *riCTOR* targeting construct, a 10.3 kb EcoRI fragment that encompassed 4.5 kb upstream of exon 4 and 4.5 kb downstream of exon 5 was isolated from clone RPCI-21 520C16 and ligated into pBluescript. Using homologous recombination (ET cloning) as well as Cre-driven recombination in bacteria and standard cloning procedures, recombination sites, a selection cassette and diagnostic restriction sites were added to the vectors. The neomycin resistance (PGK-TK-neo) cassette flanked by two FRT recombination sites and a 5'-LoxP site was added 283 bp upstream of exon 6 in the *raptor* construct and 304 bp upstream of exon 4 in the *riCTOR* construct [159]. The 3'-LoxP sites were located 277 bp downstream of *raptor* exon 6 and 301 bp downstream of *riCTOR* exon 5, respectively. The targeting vectors were linearized and electroporated into R1 ES cells derived from 129S6 mice [160]. Clones were analyzed for correct integration by Southern blot analysis using both 5'- and 3'-probes (see Figures 1A and B). Chimeric mice were obtained by microinjection of the correctly targeted clones into C57BL/6 blastocysts. Chimeric mice were crossed with C57BL/6 mice to obtain germline transmission. Mice analyzed in this study were backcrossed to C57BL/6 for 4 generations. The backcrosses involved mice constitutively expressing the FLP recombinase to excise the neomycin cassette from the targeted allele [125] and mice expressing the Cre recombinase under the human skeletal actin promoter [87]. As indicated in Figure 1, PCR genotyping of RAmKO mice was performed with primers P1: 5' ATG GTA GCA GGC ACA CTC TTC ATG and P2: 5' GCT AAA CAT TCA GTC CCT AAT C, resulting in an amplicon of 228 bp in case of presence of the FRT site and of 141 bp in case of the wild-type allele. For RImKO mice, primers P1: 5' TTA TTA ACT GTG TGT GGG TTG and P2: 5' CGT CTT AGT GTT GCT GTC TAG, resulting in an amplicon of 295 bp in case of presence of the FRT site and of 197 bp in case of a wild-type allele were used. The monoallelic presence of the Cre recombinase was detected using primers F: 5' TGT GGC TGA TGA TCC GAA TA and B: 5' GCT TGC ATG ATC TCC GGT AT resulting in an amplicon of 249 bp. Tissue-specific LoxP recombination in RAmKO mice was determined with primers P1 and P3: 5' CTC AGA GAA CTG CAG TGC TGA AGG, resulting in an amplicon of 204 bp for the recombined allele and no product for the wild-type or unrecombined allele (Figure 1C). LoxP recombination in RImKO mice was

detected using primers P1 and P3: 5' CAG ATT CAA GCA TGT CCT AAG C resulting in a PCR product of 280 bp in presence of the recombined allele and in no product in wild-type or unrecombined allele. DmKO mice were genotyped with the primers used for RAmKO and RImKO mice. Brain-specific *raptor* and *riCTOR* knockout mice were obtained by crossing floxed mice with *Nestin-Cre* mice [86]. Mdx mice were obtained from the Jackson Laboratory.

### **Animal care, body weight, food intake and body temperature measurements**

Mice were maintained in a conventional facility with a fixed light cycle. Studies were carried out according to criteria outlined for the care and use of laboratory animals and with approval of the Swiss authorities. Body weight, food intake and body temperature were measured weekly. A medical precision thermometer DM 852 from Ellab was used for the body temperature measurements.

### **Real-time PCR**

Total RNA was isolated (SV Total RNA isolation System, Promega) from *soleus* muscles. Reverse transcription was carried out using a mixture of oligodT and random hexamer primers (iScript cDNA Synthesis Kit, Bio-Rad). Sybr Green, real-time PCR analysis (Power SYBR Green Master Mix, Applied Biosystems) was performed using the ABI Prism 7000 Sequence Detector. Expression levels for each gene of interest were normalized to the mean cycle number using real-time PCR for the two housekeeping genes  $\beta$ -actin and Polr2A. In all experiments, the ratio between  $\beta$ -actin and Polr2A was constant. The following primers were used:  $\beta$ -actin sense primer: 5' CAG CTT CTT TGC AGC TCC TT, antisense primer: 5' GCA GCG ATA TCG TCA TCC A; Polr2A sense primer: 5' AAT CCG CAT CAT GAA CAG TG, antisense primer: 5' CAG CAT GTT GGA CTC AAT GC; MAFbx sense primer: 5' CTC TGT ACC ATG CCG TTC CT, antisense primer: 5' GGC TGC TGA ACA GAT TCT CC; MuRF1 sense primer: 5' ACG AGA AGA AGA GCG AGC TG, antisense primer: 5' CTT GGC ACT TGA GAG GAA GG; sITnl sense primer: 5' GTG CCT GGA ACA TCC CTA AT, antisense primer: 5' TGA GAG GCT GTT CTC TCT GC; PGC1 $\alpha$  sense primer: 5' AAC GAT GAC CCT CCT CAC AC, antisense primer: 5' TCT GGG GTC AGA GGA AGA GA; myoglobin sense primer: 5' ATC CAG CCT CTA GCC CAA TC, antisense primer: 5' GAG CAT CTG CTC CAA AGT CC.

### **In vitro muscle strength assessment**

EDL and *soleus* muscles were dissected and mounted into a muscle testing setup (Heidelberg Scientific Instruments). Muscle force assessment was carried out as previously described [161].

### **Voluntary wheel running**

Animals were individually housed in cages equipped with a running wheel carrying a magnet. Wheel revolutions were registered by a reed sensor connected to an I-7053D Digital-Input module (Spectra), and the revolution counters were read by a standard laptop computer via an I-7520 RS-485-to-RS-232 interface converter (Spectra). Digitalized signals were processed by the "mouse running" software developed by Santhera Pharmaceuticals.

### **Assessment of muscle fiber membrane damage**

Mice were forced to run downhill on a treadmill with an inclination of 15°, at the speed of 10 m/min for 10 min. This procedure was repeated for 3 days. After the second running session, Evans blue dye (1 mg / 0.1 ml PBS / 10 g body weight) was injected intraperitoneally. Mice were sacrificed 1 hour after the last running session and cross-sections of the entire hindleg were analyzed [162].

### **Glucose tolerance test**

60 to 65 day-old mice were fasted overnight, followed by an intraperitoneal injection of 2 g/kg glucose. Blood was obtained from the tail vein at the indicated time points and analyzed using a OneTouch UltraMini Meter (Lifescan).

### **Electron microscopy**

Transmission electron microscopy was performed as described [163].

### **Tissue culture**

C2C12 cells were differentiated using DMEM containing 5% horse serum for 72 h before treatments with vehicle or rapamycin (8 or 16 h at 20 nM).

### **Heart weight and function**

Under isoflurane anaesthesia, parasternal short axis M- and B-mode images of the left ventricle were obtained using a VisualSonics 770 machine with a 40-MHz linear transducer. Heart rate (HR), left ventricular end-diastolic diameter (LVEDD), left ventricular end-systolic diameter (LVESD), diastolic and systolic posterior wall and septum thickness were determined. Fractional shortening (%FS) was calculated as  $(LVEDD-LVESD)/EDD \times 100$ . Left ventricular weight was calculated from the cardiac dimensions obtained by the VisualSonics system and confirmed by directly weighing the wet hearts after sacrifice of the mice.

### **Quantifications and statistics**

Muscle glycogen concentration was measured in homogenates after 2 h of hydrolysis in 2N HCl at 100°C. The resulting free glucosyl units were determined using a commercial hexokinase-based assay kit (Sigma). For muscle fiber size quantification, pictures were collected using a Leica DM5000B fluorescence microscope, a digital camera (F-View; Soft Imaging), and analySIS software (Soft Imaging System). Muscle fiber size distribution was determined on laminin- $\gamma$ 1 immunostained muscle cross-sections using the minimum distance of parallel tangents at opposing particle borders (minimal "Feret's diameter") as described elsewhere [164]. Quantification of Western blots was performed using the ImageJ software. Background-corrected grey values were normalized to total protein levels. Compiled data are expressed as mean  $\pm$  SEM. For statistical comparisons of two conditions, the Student's t-test was used. The level of significance is indicated as follows: \*\*\*  $p < 0.001$ , \*\*  $p < 0.01$ , \*  $p < 0.05$ .

Supplementary table S1

	RAmKO	ctrl	ratio	number of replicates	RImKO	ctrl	ratio	number of replicates	DmKO	ctrl	ratio	number of replicates
Raptor	11 ±3*	61 ±11	0.2	3	42 ±1*	51 ±2	0.8	3	2 ±0.5*	35 ±11	0.06	3
mTOR	4 ±2	11 ±4	0.4	4	24 ±5	26 ±1	0.9	3	2 ±1*	17 ±5	0.1	3
Rictor	9 ±1	8 ±1	1.2	4	26 ±1*	59 ±7	0.4	3	17 ±4*	38 ±7	0.4	4
S6K	56 ±5**	27 ±3	2.1	3	24 ±4	90 ±1	0.3	3				
S6	82 ±35	114 ±12	0.7	3	35 ±5	29 ±6	1.2	3	7 ±3	14 ±6	0.5	3
P-S6 <sup>S235/S236</sup>	3 ±1*	21 ±5	0.1	6	19 ±8	57 ±24	0.3	4	21 ±8	44 ±16	0.5	3
4E-BP1	28 ±5	38 ±5	0.7	4	32 ±5	28 ±7	1.1	4				
P-4E-BP1 <sup>S65</sup>	4 ±2*	16 ±2	0.3	4	49 ±12	41 ±10	1.2	4				
PKB/ Akt	104 ±4	129 ±11	0.8	3	14 ±1	27 ±7	0.5	3	12 ±4	15 ±5	0.8	3
P-PKB/ Akt <sup>T308</sup>	9 ±3*	1 ±0.3	8	4	41 ±1*	55 ±3	0.7	3	24 ±6*	0.6 ±3	40	3
P-PKB/ Akt <sup>S473</sup>	9 ±1.5**	1 ±0.5	9.6	4	37 ±6**	98 ±11	0.4	3	22 ±5*	10 ±3	2.3	4
PKCα	31 ±5	25 ±3	1.2	5	11 ±3***	49 ±6	0.2	4	17 ±5	24 ±7	0.7	3
P-PKCα <sup>S657</sup>	26 ±9	40 ±7	0.6	6	6 ±1**	58 ±11	0.1	3	48 ±17	35 ±10	1.4	3
FoxO1	61 ±4***	20 ±3	3.1	3	27 ±3	17 ±8	1.6	3				
P-FoxO1 <sup>S316</sup>	29 ±10	37 ±7	0.8	5	62 ±5	62 ±11	1	3				
FoyO3a	70 ±6***	22 ±3	3.3	4	34 ±3	38 ±6	0.9	4				
P-FoyO1 <sup>T24/T23/3a</sup>	35 ±7*/ 27 ±4	8 ±2/ 28 ±1	4.5/ 1	4	30 ±2/ 31 ±4	33 ±6/ 29 ±7	0.9/ 1.1	4				
IRS-1	74 ±6***	11 ±1	6.7	3								
P-IRS-1 <sup>S636/639</sup>	41 ±14**	3 ±1	13.7	4								
Erk1/2	104 ±10 / 59 ±13	86 ±3/ 29 ±4	1.2/ 2	3								
P-Erk1/2 <sup>T185/Y187</sup>	3 ±1.5 / 16 ±2	2 ±0.5/ 18 ±4	2/ 0.9	3								
GSK3β	80 ±4	69 ±4	1.2	3								
P-GSK3β <sup>S9</sup>	39 ±13*	8 ±1	4.9	3								
Glycogen phos.	15 ±7*	51 ±7	0.3	3								
Calcineurin	31 ±4	21 ±2	1.5	4								
Mef2A	126 ±12*	64 ±11	2	3								
Mef2D	36 ±3	30 ±5	1.2	4								
PPARγ	19 ±3**	41 ±3	0.5	3								
COX IV	10 ±2**	20 ±2	0.5	6								
siMHC	42 ±0.5**	15 ±6	2.7	4								
siTnT	73 ±4***	36 ±2	2.0	4								

\* p<0.05, \*\* p<0.01, \*\*\*p<0.001

**Supplementary table S1.** Quantification of Western blot analysis for the proteins indicated. Proteins analyzed were extracted from *soleus* muscle of 90 day-old RAmKO, RImKO or control (ctrl) littermates. For the analysis of the DmKO mice, 60 day-old mice were compared with control littermates. Amount of total protein loaded onto the SDS-PAGE was adjusted and Western blots were additionally normalized with antibodies to  $\alpha$ -actinin. Numbers given represent average grey values  $\pm$  SEM after subtraction of the background. "Ratio" represents the average grey value obtained from a knockout animal divided by the grey values from the control littermates. "Number of replicates" represents the number of knockout animals analyzed. The number of control littermates was always the same or higher than the values given. P-values were determined by student's t-test.



## Supplemental figures

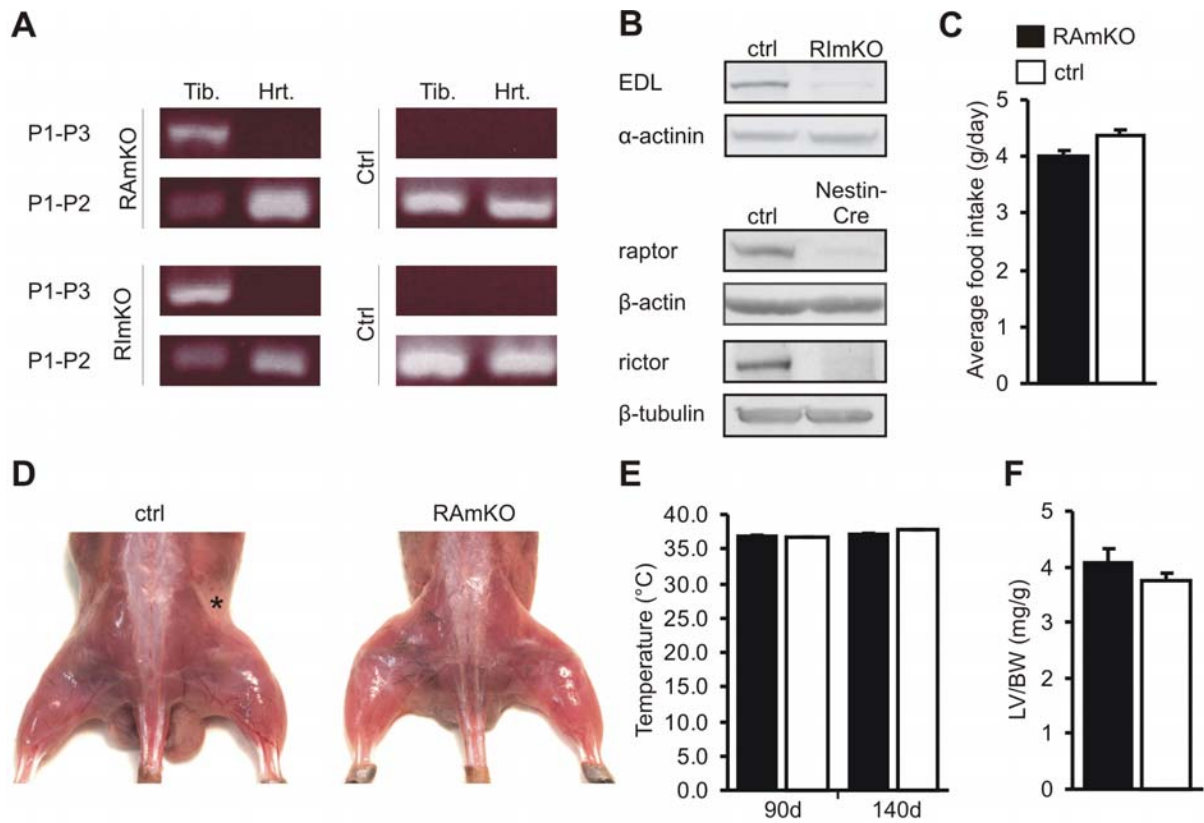


**Figure S1. Specificity of recombination and characterization of RAMKO mice.** (A) PCR on 40 ng of genomic DNA extracted from *tibialis* muscle (Tib.) or the heart (Hrt.) of 60 day-old RAMKO, RImKO or control (ctrl) littermates. The PCR product indicating successful recombination by Cre recombinase (primers P1 and P3, see Fig. 1A for details) is only observed in *tibialis* muscle and not in the heart of RAMKO or RImKO mice. Note that as a result of recombination, less PCR product than in control mice was detected of the non-recombined locus (P1-P2 primers). (B) Western blot analysis of EDL muscle from 90 day-old RImKO and control mice and with brain lysates isolated from mice homozygously carrying either the floxed *ric1* or *raptor* alleles and expressing the Cre recombinase under control of the nestin promoter (*Nestin-Cre*).  $\alpha$ -actinin,  $\beta$ -actin and  $\beta$ -tubulin were used as loading controls. (C) Average daily food intake of RAMKO and control (ctrl) mice between the age of 42 to 140 days (N = 5 for RAMKO; N = 8 for controls). (D) Dorsal view on a 140 day-old skinned, male RAMKO or control mouse. Hindleg muscles of the RAMKO mouse appear thinner and no fat pads (asterisk in ctrl mouse) can be detected. (E) Basal body temperature measured at the age of 90 and 140 days does not differ between RAMKO and control mice (N=4). (F) Left ventricular mass divided by the total body weight (LV/BW) does not change between 140 day-old control and RAMKO mice (N = 3 mice). Bars represent mean  $\pm$  SEM.

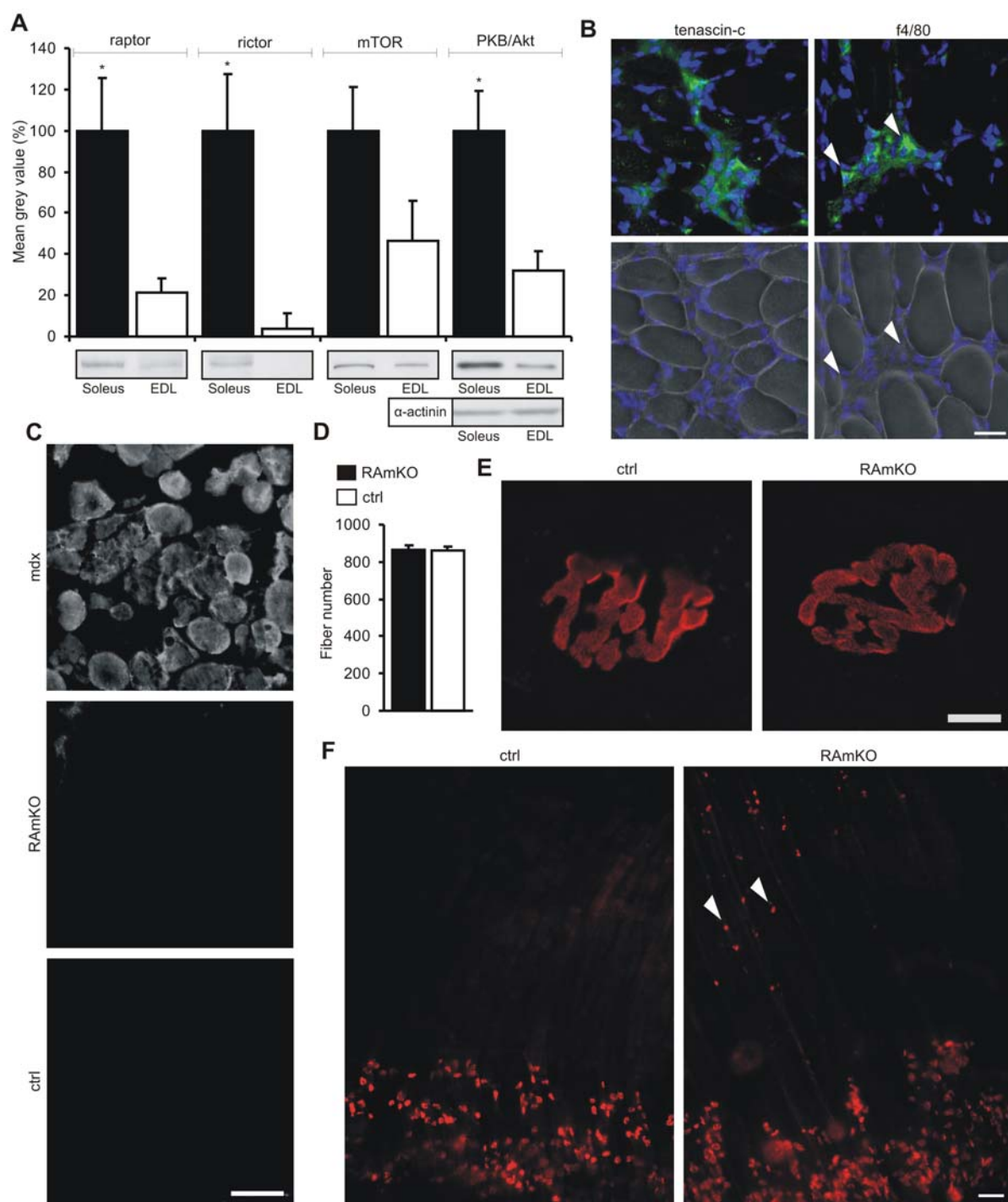


**Figure S2. Expression pattern and assessment of muscular dystrophy parameters in RAMKO mice.** (A) Expression of selected proteins of the PKB/Akt and mTOR pathway in *soleus* and EDL muscle of wild-type C57/BL6 mice. Amount of total protein loaded was adjusted and additionally normalized to the levels of  $\alpha$ -actinin. For quantification, grey values relative to  $\alpha$ -actinin were measured for each protein and set to 100% for *soleus* (N = 3 mice). (B)

Immunohistochemistry for tenascin-c and f4/80 (green) and DAPI staining (blue) reveals increased formation of fibrotic tissue and the presence of inflammatory monocytes (white arrowheads) in the *soleus* muscle of 140 day-old RAmKO mice. (C) Evans blue dye (EBD) incorporation in the lower hindleg of 90 day-old RAmKO and control (ctrl) mice after 3 days of forced treadmill running. No EBD positive fibers could be found in control or RAmKO muscles. In mdx mice, which served as an experimental control, massive incorporation of EBD was observed. (D) The number of fibers in the *soleus* of 180 day-old RAmKO mice is the same as in control littermates (N=4). (E) Maximal intensity projection using confocal microscopy of a whole mount preparation of neuromuscular junctions of the diaphragm of a 90 day-old control (ctrl) or RAmKO mouse. Acetylcholine receptors (AChRs) were visualized by TRITC-conjugated  $\alpha$ -bungarotoxin. There is no difference between the two genotypes. (F) Low magnification pictures of diaphragms of 90 day-old mice stained with TRITC- $\alpha$ -bungarotoxin. The innervation band can be discerned at the bottom of each picture. Extrasynaptic AChR clusters (white arrowheads) are found in the diaphragm of RAmKO mice. Bars represent mean  $\pm$  SEM. Scale bars = 50  $\mu$ m (B & C), 10  $\mu$ m (D), 100  $\mu$ m (E). P-value: \*  $p < 0.05$ .

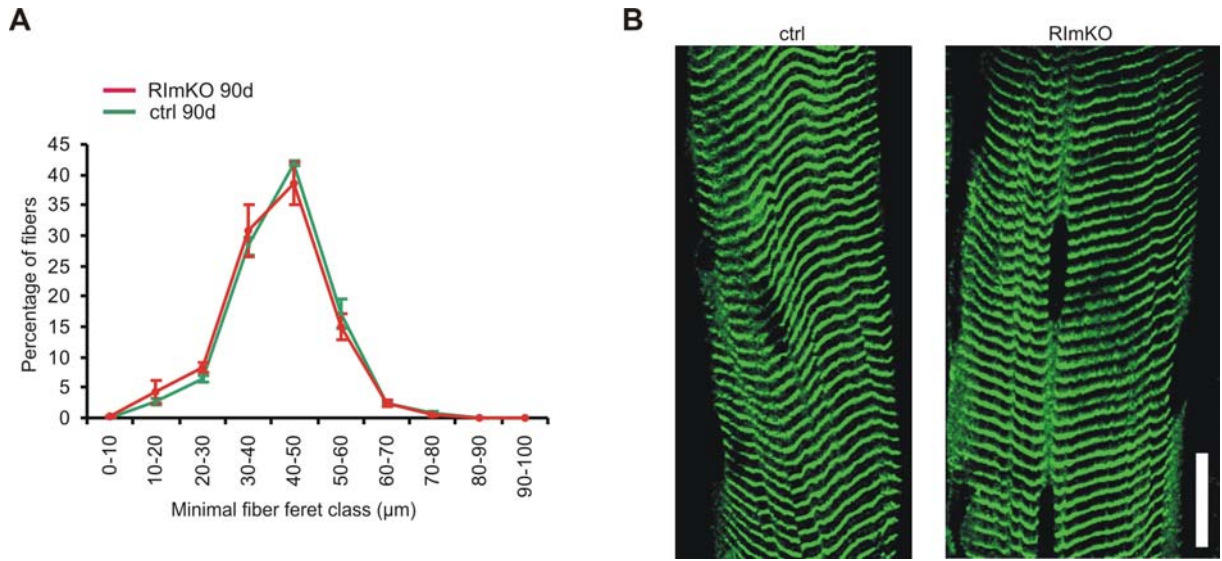


**Figure S3. Fiber size distribution and cytoskeletal architecture in RImKO mice.**

(A) Fiber size distribution in *soleus* muscle of 90 day-old RImKO and control mice. There is no difference between the two genotypes. Data points represent mean  $\pm$  SEM (N = 3 mice). (B) Maximal intensity projection using confocal microscopy of muscle fibers from 90 day-old mice stained with antibodies to  $\alpha$ -actinin. No difference in the sarcomeric organization was observed. Scale bar = 20  $\mu$ m.



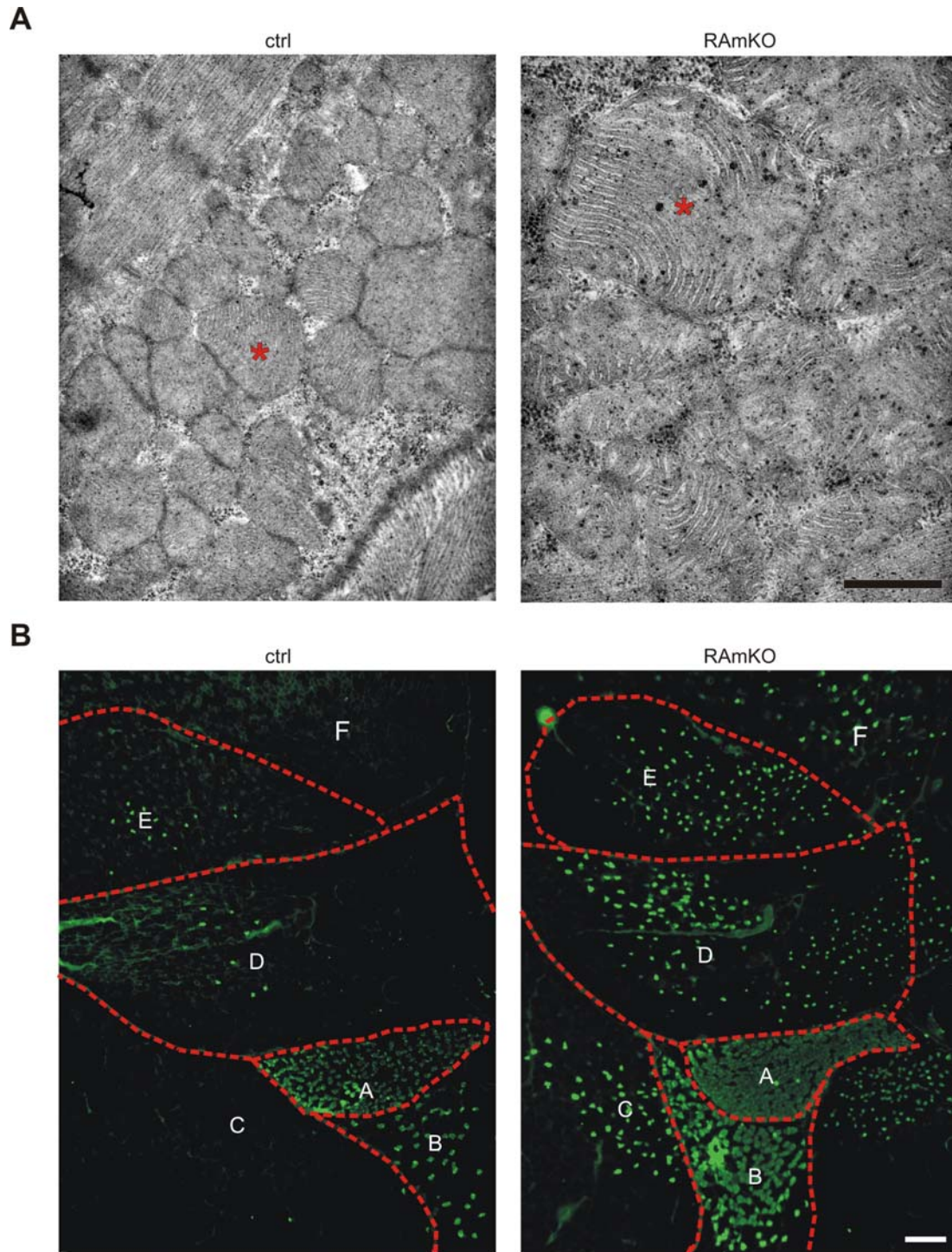


**Figure S4. Subsarcolemmal accumulation of misshaped mitochondria and regionalized sIMHC expression in RAMKO mice.** (A) Representative high power electron micrographs of RAMKO and control (ctrl) *soleus* muscle. Subsarcolemmal mitochondria in RAMKO mice are morphologically abnormal (asterisk marks a single mitochondrion) and mitochondria are more densely packed than in control mice. (B) Immunostaining for sIMHC (green) using cross-sections

of the entire hindleg of RAmKO and control mice. Individual muscles are outlined by red, dotted lines. A: *soleus*; B: plantaris-adjacent *gastrocnemius*; C: *gastrocnemius*; D: *peroneus longus* and *peroneus brevis*; E: *extensor digitorum longus* (EDL); F: *tibialis anterior*. Note that the expression of sIMHC in RAmKO mice is high in particular regions of muscles. Scale bars = 1  $\mu\text{m}$  (A), 200  $\mu\text{m}$  (B).

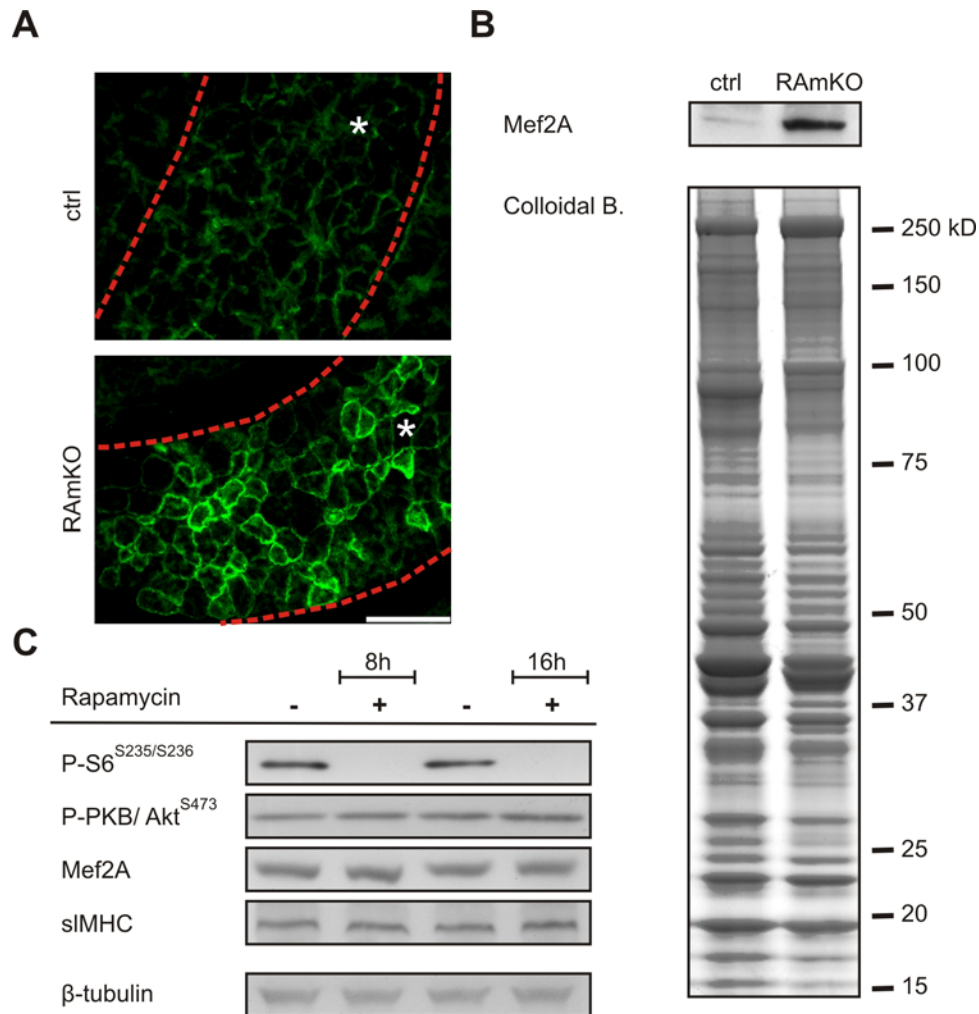


**Figure S5. *In-vivo* and *in-vitro* alterations of Ser473-phosphorylated PKB/Akt, Mef2A and sIMHC.** (A) Cross-sections of the hindleg isolated from 90 day-old RAmKO or control (ctrl) mice were stained with antibodies directed against PKB/Akt phosphorylated on Ser473 (P-PKB/Akt<sup>S473</sup>). *Soleus* muscle (asterisk) shows particularly high levels of P-PKB/Akt<sup>S473</sup> along the sarcolemmal membrane in RAmKO mice. Scale bar = 125 μm. (B) Western blot analysis of EDL muscle from 90 day-old RAmKO and control (ctrl) mice using antibodies to Mef2A. Amount of total protein loaded was adjusted and SDS gels were stained with colloidal blue (bottom) as a loading control. Levels of Mef2A are increased in RAmKO compared to control mice. (C) Western blot analysis of C2C12 cells that were treated for either 8 or 16 hours with rapamycin. β-tubulin was used as a loading control. As determined by quantification of grey-values (N=3), treatment of C2C12 cells with rapamycin for eight or sixteen hours caused a significant loss of S6 phosphorylation. A slight, non-significant increase in P-PKB/Akt<sup>S473</sup> was observed after 16 hour treatment. None of the other proteins was changed.

## 4. Concluding remarks

In this study, we knocked out the gene of the essential mTORC1 component raptor specifically in muscle fiber and in the developing CNS. In both mouse models, growth defects contributed substantially to the phenotype. Whereas in the brain, mTORC1 is necessary during prenatal brain growth, body weight of muscle-specific ko mice is normal at birth. A progressive dystrophy of skeletal muscle and loss of fat causes weight loss which increases with age.

In the newborn brain-specific ko mice, brain size is massively decreased to 55%. The whole brain is evenly affected. Smaller cells and a slower proliferation rate are responsible for this growth deficit. Several more specific phenotypes are superimposed to this pronounced microcephaly. Stat3 was previously described as a direct downstream target of mTORC1. In the CNS, Stat3 is involved in the neurogenic to gliogenic switch and drives glial differentiation. A positive feedback mechanism allows activated (phosphorylated) Stat3 to induce expression of itself and other members of the Jak/Stat pathway. In the *raptor*-deficient brain, phosphorylation- and protein-levels are indeed reduced. In line with this observation, gliogenesis is reduced in mutant brains. The glial network of the dentate gyrus which mediates proper formation of the granule cell layer is largely absent and neurons in the dentate gyrus are dispersed throughout the hilus. In the cortical plate, the signal for the dendritic marker Map2 is decreased and dendritic complexity is reduced in dissociated hippocampal cultures. Further, this study shows that mTORC1 is crucial for normal migration of neurons in the prenatal cortex and hippocampus.

Progressive loss of muscle mass may be accounted for by a decreased mTORC1 dependent protein synthesis. mTORC1-independent anabolic functions of hyper-activated Akt/PKB also contributed to the overall phenotype. This combination from catabolic effects resulting from 4EBP1-, S6K/S6- and PGC1 $\alpha$ -inactivation and anabolic effects from active Akt/PKB may explain some of the seemingly conflicting results. Defects in mitochondrial biogenesis and concurrent reductions in oxidative capacity of the muscle is caused by downregulation of the mTORC1-downstream component PGC1 $\alpha$ . A direct or indirect activation of Mef2 by Akt/PKB, however, may account for the



expression of slow structural proteins. Additionally to the reduced oxidative capacity, hyperactive Akt/PKB may cause the high glucose need of *raptor*-deficient muscles by disinhibition of the glycogen synthase causing glycogen accumulation. This may ultimately also explain the observed loss of fat.

Both models reveal novel and partially unexpected physiological functions of mTORC1 in the respective tissues. Ablation of mTORC1 in both tissues shortens life, most dramatically when deleted in the brain. Partially via regulation of its direct downstream-effectors, mTORC1 is essential for growth and the correct cellular composition as well as organization of muscle and brain.

## 5. References

1. Vezina, C., A. Kudelski, and S.N. Sehgal, *Rapamycin (AY-22,989), a new antifungal antibiotic. I. Taxonomy of the producing streptomycete and isolation of the active principle*. J Antibiot (Tokyo), 1975. **28**(10): p. 721-6.
2. Baker, H., et al., *Rapamycin (AY-22,989), a new antifungal antibiotic. III. In vitro and in vivo evaluation*. J Antibiot (Tokyo), 1978. **31**(6): p. 539-45.
3. Sehgal, S.N., H. Baker, and C. Vezina, *Rapamycin (AY-22,989), a new antifungal antibiotic. II. Fermentation, isolation and characterization*. J Antibiot (Tokyo), 1975. **28**(10): p. 727-32.
4. Singh, K., S. Sun, and C. Vezina, *Rapamycin (AY-22,989), a new antifungal antibiotic. IV. Mechanism of action*. J Antibiot (Tokyo), 1979. **32**(6): p. 630-45.
5. Martel, R.R., J. Klicius, and S. Galet, *Inhibition of the immune response by rapamycin, a new antifungal antibiotic*. Can J Physiol Pharmacol, 1977. **55**(1): p. 48-51.
6. Dumont, F.J., et al., *Distinct mechanisms of suppression of murine T cell activation by the related macrolides FK-506 and rapamycin*. J Immunol, 1990. **144**(1): p. 251-8.
7. Harding, M.W., et al., *A receptor for the immunosuppressant FK506 is a cis-trans peptidyl-prolyl isomerase*. Nature, 1989. **341**(6244): p. 758-60.
8. Heitman, J., N.R. Movva, and M.N. Hall, *Targets for cell cycle arrest by the immunosuppressant rapamycin in yeast*. Science, 1991. **253**(5022): p. 905-9.
9. Abraham, R.T. and G.J. Wiederrecht, *Immunopharmacology of rapamycin*. Annu Rev Immunol, 1996. **14**: p. 483-510.
10. Martin, D.E. and M.N. Hall, *The expanding TOR signaling network*. Curr Opin Cell Biol, 2005. **17**(2): p. 158-66.
11. Loewith, R., et al., *Two TOR complexes, only one of which is rapamycin sensitive, have distinct roles in cell growth control*. Mol Cell, 2002. **10**(3): p. 457-68.
12. Jacinto, E., et al., *Mammalian TOR complex 2 controls the actin cytoskeleton and is rapamycin insensitive*. Nat Cell Biol, 2004. **6**(11): p. 1122-8.
13. Sarbassov, D.D., et al., *Rictor, a novel binding partner of mTOR, defines a rapamycin-insensitive and raptor-independent pathway that regulates the cytoskeleton*. Curr Biol, 2004. **14**(14): p. 1296-302.
14. Thedieck, K., et al., *PRAS40 and PRR5-like protein are new mTOR interactors that regulate apoptosis*. PLoS ONE, 2007. **2**(11): p. e1217.
15. Sarbassov, D.D., et al., *Prolonged rapamycin treatment inhibits mTORC2 assembly and Akt/PKB*. Mol Cell, 2006. **22**(2): p. 159-68.
16. Wullschleger, S., R. Loewith, and M.N. Hall, *TOR signaling in growth and metabolism*. Cell, 2006. **124**(3): p. 471-84.
17. Li, Y., et al., *TSC2: filling the GAP in the mTOR signaling pathway*. Trends Biochem Sci, 2004. **29**(1): p. 32-8.
18. Long, X., et al., *Rheb binds and regulates the mTOR kinase*. Curr Biol, 2005. **15**(8): p. 702-13.
19. Long, X., et al., *Rheb binding to mammalian target of rapamycin (mTOR) is regulated by amino acid sufficiency*. J Biol Chem, 2005. **280**(25): p. 23433-6.
20. Smith, E.M., et al., *The tuberous sclerosis protein TSC2 is not required for the regulation of the mammalian target of rapamycin by amino acids and certain cellular stresses*. J Biol Chem, 2005. **280**(19): p. 18717-27.

21. Rocco, M., J.L. Bos, and F.J. Zwartkruis, *Regulation of the small GTPase Rheb by amino acids*. *Oncogene*, 2006. **25**(5): p. 657-64.
22. Gulati, P., et al., *Amino acids activate mTOR complex 1 via Ca<sup>2+</sup>/CaM signaling to hVps34*. *Cell Metab*, 2008. **7**(5): p. 456-65.
23. Nobukuni, T., et al., *Amino acids mediate mTOR/raptor signaling through activation of class 3 phosphatidylinositol 3OH-kinase*. *Proc Natl Acad Sci U S A*, 2005. **102**(40): p. 14238-43.
24. Sancak, Y., et al., *The Rag GTPases bind raptor and mediate amino acid signaling to mTORC1*. *Science*, 2008. **320**(5882): p. 1496-501.
25. Hardie, D.G., D. Carling, and M. Carlson, *The AMP-activated/SNF1 protein kinase subfamily: metabolic sensors of the eukaryotic cell?* *Annu Rev Biochem*, 1998. **67**: p. 821-55.
26. Inoki, K., T. Zhu, and K.L. Guan, *TSC2 mediates cellular energy response to control cell growth and survival*. *Cell*, 2003. **115**(5): p. 577-90.
27. Kumar, V., et al., *Regulation of dendritic morphogenesis by Ras-PI3K-Akt-mTOR and Ras-MAPK signaling pathways*. *J Neurosci*, 2005. **25**(49): p. 11288-99.
28. Jossin, Y. and A.M. Goffinet, *Reelin signals through phosphatidylinositol 3-kinase and Akt to control cortical development and through mTor to regulate dendritic growth*. *Mol Cell Biol*, 2007. **27**(20): p. 7113-24.
29. Cota, D., et al., *Hypothalamic mTOR signaling regulates food intake*. *Science*, 2006. **312**(5775): p. 927-30.
30. Brugarolas, J., et al., *Regulation of mTOR function in response to hypoxia by REDD1 and the TSC1/TSC2 tumor suppressor complex*. *Genes Dev*, 2004. **18**(23): p. 2893-904.
31. Huang, J., et al., *The TSC1-TSC2 complex is required for proper activation of mTOR complex 2*. *Mol Cell Biol*, 2008. **28**(12): p. 4104-15.
32. Huang, J. and B.D. Manning, *A complex interplay between Akt, TSC2 and the two mTOR complexes*. *Biochem Soc Trans*, 2009. **37**(Pt 1): p. 217-22.
33. Hay, N. and N. Sonenberg, *Upstream and downstream of mTOR*. *Genes Dev*, 2004. **18**(16): p. 1926-45.
34. Raught, B., et al., *Phosphorylation of eucaryotic translation initiation factor 4B Ser422 is modulated by S6 kinases*. *Embo J*, 2004. **23**(8): p. 1761-9.
35. Holz, M.K., et al., *mTOR and S6K1 mediate assembly of the translation preinitiation complex through dynamic protein interchange and ordered phosphorylation events*. *Cell*, 2005. **123**(4): p. 569-80.
36. Jastrzebski, K., et al., *Coordinate regulation of ribosome biogenesis and function by the ribosomal protein S6 kinase, a key mediator of mTOR function*. *Growth Factors*, 2007. **25**(4): p. 209-26.
37. Nojima, H., et al., *The mammalian target of rapamycin (mTOR) partner, raptor, binds the mTOR substrates p70 S6 kinase and 4E-BP1 through their TOR signaling (TOS) motif*. *J Biol Chem*, 2003. **278**(18): p. 15461-4.
38. Mayer, C. and I. Grummt, *Ribosome biogenesis and cell growth: mTOR coordinates transcription by all three classes of nuclear RNA polymerases*. *Oncogene*, 2006. **25**(48): p. 6384-91.
39. Hannan, K.M., et al., *mTOR-dependent regulation of ribosomal gene transcription requires S6K1 and is mediated by phosphorylation of the carboxy-terminal activation domain of the nucleolar transcription factor UBF*. *Mol Cell Biol*, 2003. **23**(23): p. 8862-77.
40. Mayer, C., et al., *mTOR-dependent activation of the transcription factor TIF-IA links rRNA synthesis to nutrient availability*. *Genes Dev*, 2004. **18**(4): p. 423-34.

41. Kristof, A.S., et al., *Stimulation of signal transducer and activator of transcription-1 (STAT1)-dependent gene transcription by lipopolysaccharide and interferon-gamma is regulated by mammalian target of rapamycin*. J Biol Chem, 2003. **278**(36): p. 33637-44.
42. Cunningham, J.T., et al., *mTOR controls mitochondrial oxidative function through a YY1-PGC-1alpha transcriptional complex*. Nature, 2007. **450**(7170): p. 736-40.
43. Kim, J.E. and J. Chen, *regulation of peroxisome proliferator-activated receptor-gamma activity by mammalian target of rapamycin and amino acids in adipogenesis*. Diabetes, 2004. **53**(11): p. 2748-56.
44. Pattingre, S., et al., *Regulation of macroautophagy by mTOR and Beclin 1 complexes*. Biochimie, 2008. **90**(2): p. 313-23.
45. Sarbassov, D.D., et al., *Phosphorylation and regulation of Akt/PKB by the rictor-mTOR complex*. Science, 2005. **307**(5712): p. 1098-101.
46. Garcia-Martinez, J.M. and D.R. Alessi, *mTOR complex 2 (mTORC2) controls hydrophobic motif phosphorylation and activation of serum- and glucocorticoid-induced protein kinase 1 (SGK1)*. Biochem J, 2008. **416**(3): p. 375-85.
47. Jacinto, E., et al., *SIN1/MIP1 maintains rictor-mTOR complex integrity and regulates Akt phosphorylation and substrate specificity*. Cell, 2006. **127**(1): p. 125-37.
48. Fingar, D.C. and J. Blenis, *Target of rapamycin (TOR): an integrator of nutrient and growth factor signals and coordinator of cell growth and cell cycle progression*. Oncogene, 2004. **23**(18): p. 3151-71.
49. Hong, F., et al., *mTOR-raptor binds and activates SGK1 to regulate p27 phosphorylation*. Mol Cell, 2008. **30**(6): p. 701-11.
50. Rajan, P., et al., *BMPs signal alternately through a SMAD or FRAP-STAT pathway to regulate fate choice in CNS stem cells*. J Cell Biol, 2003. **161**(5): p. 911-21.
51. Verma, P., et al., *Axonal protein synthesis and degradation are necessary for efficient growth cone regeneration*. J Neurosci, 2005. **25**(2): p. 331-42.
52. Dash, P.K., S.A. Orsi, and A.N. Moore, *Spatial memory formation and memory-enhancing effect of glucose involves activation of the tuberous sclerosis complex-Mammalian target of rapamycin pathway*. J Neurosci, 2006. **26**(31): p. 8048-56.
53. Tischmeyer, W., et al., *Rapamycin-sensitive signalling in long-term consolidation of auditory cortex-dependent memory*. Eur J Neurosci, 2003. **18**(4): p. 942-50.
54. Colombani, J., et al., *A nutrient sensor mechanism controls Drosophila growth*. Cell, 2003. **114**(6): p. 739-49.
55. Glass, D.J., *Skeletal muscle hypertrophy and atrophy signaling pathways*. Int J Biochem Cell Biol, 2005. **37**(10): p. 1974-84.
56. Jackman, R.W. and S.C. Kandarian, *The molecular basis of skeletal muscle atrophy*. Am J Physiol Cell Physiol, 2004. **287**(4): p. C834-43.
57. Kandarian, S.C. and R.W. Jackman, *Intracellular signaling during skeletal muscle atrophy*. Muscle Nerve, 2006. **33**(2): p. 155-65.
58. Peng, X.D., et al., *Dwarfism, impaired skin development, skeletal muscle atrophy, delayed bone development, and impeded adipogenesis in mice lacking Akt1 and Akt2*. Genes Dev, 2003. **17**(11): p. 1352-65.
59. Ohanna, M., et al., *Atrophy of S6K1(-/-) skeletal muscle cells reveals distinct mTOR effectors for cell cycle and size control*. Nat Cell Biol, 2005. **7**(3): p. 286-94.
60. Izumiya, Y., et al., *Fast/Glycolytic muscle fiber growth reduces fat mass and improves metabolic parameters in obese mice*. Cell Metab, 2008. **7**(2): p. 159-72.

61. Lai, K.M., et al., *Conditional activation of akt in adult skeletal muscle induces rapid hypertrophy*. Mol Cell Biol, 2004. **24**(21): p. 9295-304.
62. Coleman, M.E., et al., *Myogenic vector expression of insulin-like growth factor I stimulates muscle cell differentiation and myofiber hypertrophy in transgenic mice*. J Biol Chem, 1995. **270**(20): p. 12109-16.
63. Wan, M., et al., *Muscle atrophy in transgenic mice expressing a human TSC1 transgene*. FEBS Lett, 2006. **580**(24): p. 5621-7.
64. Bodine, S.C., et al., *Akt/mTOR pathway is a crucial regulator of skeletal muscle hypertrophy and can prevent muscle atrophy in vivo*. Nat Cell Biol, 2001. **3**(11): p. 1014-9.
65. Pallafacchina, G., et al., *A protein kinase B-dependent and rapamycin-sensitive pathway controls skeletal muscle growth but not fiber type specification*. Proc Natl Acad Sci U S A, 2002. **99**(14): p. 9213-8.
66. Kimball, S.R. and L.S. Jefferson, *Signaling pathways and molecular mechanisms through which branched-chain amino acids mediate translational control of protein synthesis*. J Nutr, 2006. **136**(1 Suppl): p. 227S-31S.
67. Stitt, T.N., et al., *The IGF-1/PI3K/Akt pathway prevents expression of muscle atrophy-induced ubiquitin ligases by inhibiting FOXO transcription factors*. Mol Cell, 2004. **14**(3): p. 395-403.
68. Latres, E., et al., *Insulin-like growth factor-1 (IGF-1) inversely regulates atrophy-induced genes via the phosphatidylinositol 3-kinase/Akt/mammalian target of rapamycin (PI3K/Akt/mTOR) pathway*. J Biol Chem, 2005. **280**(4): p. 2737-44.
69. Han, J., et al., *Mammalian target of rapamycin (mTOR) is involved in the neuronal differentiation of neural progenitors induced by insulin*. Mol Cell Neurosci, 2008. **39**(1): p. 118-24.
70. Wang, B., et al., *Nogo-66 promotes the differentiation of neural progenitors into astroglial lineage cells through mTOR-STAT3 pathway*. PLoS ONE, 2008. **3**(3): p. e1856.
71. Swiech, L., et al., *Role of mTOR in physiology and pathology of the nervous system*. Biochim Biophys Acta, 2008. **1784**(1): p. 116-32.
72. Barnes, A.P., D. Solecki, and F. Polleux, *New insights into the molecular mechanisms specifying neuronal polarity in vivo*. Curr Opin Neurobiol, 2008. **18**(1): p. 44-52.
73. Bradke, F. and C.G. Dotti, *The role of local actin instability in axon formation*. Science, 1999. **283**(5409): p. 1931-4.
74. Li, Y.H., H. Werner, and A.W. Puschel, *Rheb and mTOR regulate neuronal polarity through Rap1B*. J Biol Chem, 2008. **283**(48): p. 33784-92.
75. Jaworski, J., et al., *Control of dendritic arborization by the phosphoinositide-3'-kinase-Akt-mammalian target of rapamycin pathway*. J Neurosci, 2005. **25**(49): p. 11300-12.
76. Lin, A.C. and C.E. Holt, *Local translation and directional steering in axons*. Embo J, 2007. **26**(16): p. 3729-36.
77. Tavazoie, S.F., et al., *Regulation of neuronal morphology and function by the tumor suppressors Tsc1 and Tsc2*. Nat Neurosci, 2005. **8**(12): p. 1727-34.
78. Schratt, G.M., et al., *BDNF regulates the translation of a select group of mRNAs by a mammalian target of rapamycin-phosphatidylinositol 3-kinase-dependent pathway during neuronal development*. J Neurosci, 2004. **24**(33): p. 7366-77.
79. Takei, N., et al., *Brain-derived neurotrophic factor induces mammalian target of rapamycin-dependent local activation of translation machinery and protein synthesis in neuronal dendrites*. J Neurosci, 2004. **24**(44): p. 9760-9.

80. Cammalleri, M., et al., *Time-restricted role for dendritic activation of the mTOR-p70S6K pathway in the induction of late-phase long-term potentiation in the CA1*. Proc Natl Acad Sci U S A, 2003. **100**(24): p. 14368-73.
81. Tang, S.J., et al., *A rapamycin-sensitive signaling pathway contributes to long-term synaptic plasticity in the hippocampus*. Proc Natl Acad Sci U S A, 2002. **99**(1): p. 467-72.
82. Vickers, C.A., K.S. Dickson, and D.J. Wyllie, *Induction and maintenance of late-phase long-term potentiation in isolated dendrites of rat hippocampal CA1 pyramidal neurones*. J Physiol, 2005. **568**(Pt 3): p. 803-13.
83. Gangloff, Y.G., et al., *Disruption of the mouse mTOR gene leads to early postimplantation lethality and prohibits embryonic stem cell development*. Mol Cell Biol, 2004. **24**(21): p. 9508-16.
84. Guertin, D.A., et al., *Ablation in mice of the mTORC components raptor, rictor, or mLST8 reveals that mTORC2 is required for signaling to Akt-FOXO and PKCalpha, but not S6K1*. Dev Cell, 2006. **11**(6): p. 859-71.
85. Murakami, M., et al., *mTOR is essential for growth and proliferation in early mouse embryos and embryonic stem cells*. Mol Cell Biol, 2004. **24**(15): p. 6710-8.
86. Graus-Porta, D., et al., *Beta1-class integrins regulate the development of laminae and folia in the cerebral and cerebellar cortex*. Neuron, 2001. **31**(3): p. 367-79.
87. Schwander, M., et al., *Beta1 integrins regulate myoblast fusion and sarcomere assembly*. Dev Cell, 2003. **4**(5): p. 673-85.
88. Hentges, K.E., et al., *FRAP/mTOR is required for proliferation and patterning during embryonic development in the mouse*. Proc Natl Acad Sci U S A, 2001. **98**(24): p. 13796-801.
89. Bentzinger, C.F., et al., *Skeletal muscle-specific ablation of raptor, but not of rictor, causes metabolic changes and results in muscle dystrophy*. Cell Metab, 2008. **8**(5): p. 411-24.
90. Polak, P., et al., *Adipose-specific knockout of raptor results in lean mice with enhanced mitochondrial respiration*. Cell Metab, 2008. **8**(5): p. 399-410.
91. Park, K.K., et al., *Promoting axon regeneration in the adult CNS by modulation of the PTEN/mTOR pathway*. Science, 2008. **322**(5903): p. 963-6.
92. Campbell, D.S. and C.E. Holt, *Chemotropic responses of retinal growth cones mediated by rapid local protein synthesis and degradation*. Neuron, 2001. **32**(6): p. 1013-26.
93. Zimmerman, L., et al., *Independent regulatory elements in the nestin gene direct transgene expression to neural stem cells or muscle precursors*. Neuron, 1994. **12**(1): p. 11-24.
94. Labarca, C. and K. Paigen, *A simple, rapid, and sensitive DNA assay procedure*. Anal Biochem, 1980. **102**(2): p. 344-52.
95. Easton, R.M., et al., *Role for Akt3/protein kinase Bgamma in attainment of normal brain size*. Mol Cell Biol, 2005. **25**(5): p. 1869-78.
96. Tschopp, O., et al., *Essential role of protein kinase B gamma (PKB gamma/Akt3) in postnatal brain development but not in glucose homeostasis*. Development, 2005. **132**(13): p. 2943-54.
97. Marthens, E.V., *Neonatal and adult brain parameters in mice selected for adult brain weight*. Dev Psychobiol, 1976. **9**(6): p. 587-93.
98. Reynolds, B.A. and S. Weiss, *Clonal and population analyses demonstrate that an EGF-responsive mammalian embryonic CNS precursor is a stem cell*. Dev Biol, 1996. **175**(1): p. 1-13.

99. Hartfuss, E., et al., *Characterization of CNS precursor subtypes and radial glia*. Dev Biol, 2001. **229**(1): p. 15-30.
100. Shu, T., A.C. Puche, and L.J. Richards, *Development of midline glial populations at the corticoseptal boundary*. J Neurobiol, 2003. **57**(1): p. 81-94.
101. Yokogami, K., et al., *Serine phosphorylation and maximal activation of STAT3 during CNTF signaling is mediated by the rapamycin target mTOR*. Curr Biol, 2000. **10**(1): p. 47-50.
102. Bonni, A., et al., *Regulation of gliogenesis in the central nervous system by the JAK-STAT signaling pathway*. Science, 1997. **278**(5337): p. 477-83.
103. Johe, K.K., et al., *Single factors direct the differentiation of stem cells from the fetal and adult central nervous system*. Genes Dev, 1996. **10**(24): p. 3129-40.
104. Cheng, A., et al., *Concurrent generation of subplate and cortical plate neurons in developing trisomy 16 mouse cortex*. Dev Neurosci, 2004. **26**(2-4): p. 255-65.
105. Crandall, J.E., M. Jacobson, and K.S. Kosik, *Ontogenesis of microtubule-associated protein 2 (MAP2) in embryonic mouse cortex*. Brain Res, 1986. **393**(1): p. 127-33.
106. Gillies, K. and D.J. Price, *The fates of cells in the developing cerebral cortex of normal and methylazoxymethanol acetate-lesioned mice*. Eur J Neurosci, 1993. **5**(1): p. 73-84.
107. Kessar, N., N. Pringle, and W.D. Richardson, *Specification of CNS glia from neural stem cells in the embryonic neuroepithelium*. Philos Trans R Soc Lond B Biol Sci, 2008. **363**(1489): p. 71-85.
108. Doetsch, F., *The glial identity of neural stem cells*. Nat Neurosci, 2003. **6**(11): p. 1127-34.
109. Forster, E., et al., *Reelin, Disabled 1, and beta 1 integrins are required for the formation of the radial glial scaffold in the hippocampus*. Proc Natl Acad Sci U S A, 2002. **99**(20): p. 13178-83.
110. Rickmann, M., D.G. Amaral, and W.M. Cowan, *Organization of radial glial cells during the development of the rat dentate gyrus*. J Comp Neurol, 1987. **264**(4): p. 449-79.
111. Zhao, S., et al., *Reelin is a positional signal for the lamination of dentate granule cells*. Development, 2004. **131**(20): p. 5117-25.
112. He, F., et al., *A positive autoregulatory loop of Jak-STAT signaling controls the onset of astroglialogenesis*. Nat Neurosci, 2005. **8**(5): p. 616-25.
113. Onda, H., et al., *Tsc2 null murine neuroepithelial cells are a model for human tuber giant cells, and show activation of an mTOR pathway*. Mol Cell Neurosci, 2002. **21**(4): p. 561-74.
114. Muller, S., et al., *Neurogenesis in the Dentate Gyrus Depends on CNTF and STAT3 Signaling*. Stem Cells, 2008.
115. Beck, K.D., et al., *Igf1 gene disruption results in reduced brain size, CNS hypomyelination, and loss of hippocampal granule and striatal parvalbumin-containing neurons*. Neuron, 1995. **14**(4): p. 717-30.
116. LoTurco, J.J. and J. Bai, *The multipolar stage and disruptions in neuronal migration*. Trends Neurosci, 2006. **29**(7): p. 407-13.
117. Bai, J., et al., *RNAi reveals doublecortin is required for radial migration in rat neocortex*. Nat Neurosci, 2003. **6**(12): p. 1277-83.
118. Nagano, T., S. Morikubo, and M. Sato, *Filamin A and FILIP (Filamin A-Interacting Protein) regulate cell polarity and motility in neocortical subventricular and intermediate zones during radial migration*. J Neurosci, 2004. **24**(43): p. 9648-57.

119. Tsai, J.W., et al., *LIS1 RNA interference blocks neural stem cell division, morphogenesis, and motility at multiple stages*. J Cell Biol, 2005. **170**(6): p. 935-45.
120. Ohshima, T., et al., *Cdk5 is required for multipolar-to-bipolar transition during radial neuronal migration and proper dendrite development of pyramidal neurons in the cerebral cortex*. Development, 2007. **134**(12): p. 2273-82.
121. Sirko, S., et al., *Chondroitin sulfate glycosaminoglycans control proliferation, radial glia cell differentiation and neurogenesis in neural stem/progenitor cells*. Development, 2007. **134**(15): p. 2727-38.
122. Tsang, C.K., et al., *Targeting mammalian target of rapamycin (mTOR) for health and diseases*. Drug Discov Today, 2007. **12**(3-4): p. 112-24.
123. Harrison, B.C. and L.A. Leinwand, *Fighting fat with muscle: bulking up to slim down*. Cell Metab, 2008. **7**(2): p. 97-8.
124. Shiota, C., et al., *Multiallelic disruption of the rictor gene in mice reveals that mTOR complex 2 is essential for fetal growth and viability*. Dev Cell, 2006. **11**(4): p. 583-9.
125. Rodriguez, C.I., et al., *High-efficiency deleter mice show that FLPe is an alternative to Cre-loxP*. Nat Genet, 2000. **25**(2): p. 139-40.
126. Popovic, Z.B., et al., *Differences in left ventricular long-axis function from mice to humans follow allometric scaling to ventricular size*. J Physiol, 2005. **568**(Pt 1): p. 255-65.
127. Laws, N. and A. Hoey, *Progression of kyphosis in mdx mice*. J Appl Physiol, 2004. **97**(5): p. 1970-7.
128. Ringelmann, B., et al., *Expression of laminin alpha1, alpha2, alpha4, and alpha5 chains, fibronectin, and tenascin-C in skeletal muscle of dystrophic 129ReJ dy/dy mice*. Exp Cell Res, 1999. **246**(1): p. 165-82.
129. Austyn, J.M. and S. Gordon, *F4/80, a monoclonal antibody directed specifically against the mouse macrophage*. Eur J Immunol, 1981. **11**(10): p. 805-15.
130. Sorokin, L.M., et al., *Developmental regulation of the laminin alpha5 chain suggests a role in epithelial and endothelial cell maturation*. Dev Biol, 1997. **189**(2): p. 285-300.
131. Sewry, C.A., et al., *The spectrum of pathology in central core disease*. Neuromuscul Disord, 2002. **12**(10): p. 930-8.
132. Um, S.H., et al., *Absence of S6K1 protects against age- and diet-induced obesity while enhancing insulin sensitivity*. Nature, 2004. **431**(7005): p. 200-5.
133. Harrington, L.S., et al., *The TSC1-2 tumor suppressor controls insulin-PI3K signaling via regulation of IRS proteins*. J Cell Biol, 2004. **166**(2): p. 213-23.
134. Sandri, M., et al., *Foxo transcription factors induce the atrophy-related ubiquitin ligase atrogin-1 and cause skeletal muscle atrophy*. Cell, 2004. **117**(3): p. 399-412.
135. Sakamoto, K. and L.J. Goodyear, *Invited review: intracellular signaling in contracting skeletal muscle*. J Appl Physiol, 2002. **93**(1): p. 369-83.
136. Kumar, A., et al., *Muscle-specific deletion of rictor impairs insulin-stimulated glucose transport and enhances Basal glycogen synthase activity*. Mol Cell Biol, 2008. **28**(1): p. 61-70.
137. Treves, S., et al., *Congenital muscle disorders with cores: the ryanodine receptor calcium channel paradigm*. Curr Opin Pharmacol, 2008.
138. Handschin, C., et al., *Skeletal muscle fiber-type switching, exercise intolerance, and myopathy in PGC-1alpha muscle-specific knock-out animals*. J Biol Chem, 2007. **282**(41): p. 30014-21.



139. Winkel, L.P., et al., *The natural course of non-classic Pompe's disease; a review of 225 published cases*. J Neurol, 2005. **252**(8): p. 875-84.
140. Song, X.M., et al., *Muscle fiber type specificity in insulin signal transduction*. The American journal of physiology, 1999. **277**(6 Pt 2): p. R1690-6.
141. Schieke, S.M., et al., *The mammalian target of rapamycin (mTOR) pathway regulates mitochondrial oxygen consumption and oxidative capacity*. J Biol Chem, 2006. **281**(37): p. 27643-52.
142. Lin, J., et al., *Transcriptional co-activator PGC-1 alpha drives the formation of slow-twitch muscle fibres*. Nature, 2002. **418**(6899): p. 797-801.
143. Wende, A.R., et al., *A Role for the Transcriptional Coactivator PGC-1{alpha} in Muscle Refueling*. J Biol Chem, 2007. **282**(50): p. 36642-51.
144. Leone, T.C., et al., *PGC-1alpha deficiency causes multi-system energy metabolic derangements: muscle dysfunction, abnormal weight control and hepatic steatosis*. PLoS Biol, 2005. **3**(4): p. e101.
145. Bassel-Duby, R. and E.N. Olson, *Signaling pathways in skeletal muscle remodeling*. Annual review of biochemistry, 2006. **75**: p. 19-37.
146. Potthoff, M.J., et al., *Histone deacetylase degradation and MEF2 activation promote the formation of slow-twitch myofibers*. J Clin Invest, 2007. **117**(9): p. 2459-67.
147. Wu, H., et al., *MEF2 responds to multiple calcium-regulated signals in the control of skeletal muscle fiber type*. Embo J, 2000. **19**(9): p. 1963-73.
148. Gollnick, P.D., et al., *Elongation of skeletal muscle relaxation during exercise is linked to reduced calcium uptake by the sarcoplasmic reticulum in man*. Acta Physiol Scand, 1991. **142**(1): p. 135-6.
149. Wiedmann, M., et al., *PI3K/Akt-dependent regulation of the transcription factor myocyte enhancer factor-2 in insulin-like growth factor-1- and membrane depolarization-mediated survival of cerebellar granule neurons*. Journal of neuroscience research, 2005. **81**(2): p. 226-34.
150. Rommel, C., et al., *Mediation of IGF-1-induced skeletal myotube hypertrophy by PI(3)K/Akt/mTOR and PI(3)K/Akt/GSK3 pathways*. Nat Cell Biol, 2001. **3**(11): p. 1009-13.
151. Manning, B.D., *Balancing Akt with S6K: implications for both metabolic diseases and tumorigenesis*. The Journal of cell biology, 2004. **167**(3): p. 399-403.
152. Beals, C.R., et al., *Nuclear export of NF-ATc enhanced by glycogen synthase kinase-3*. Science, 1997. **275**(5308): p. 1930-4.
153. Wu, H., et al., *NFAT signaling and the invention of vertebrates*. Trends Cell Biol, 2007. **17**(6): p. 251-60.
154. Alessi, D.R., et al., *Characterization of a 3-phosphoinositide-dependent protein kinase which phosphorylates and activates protein kinase Balpha*. Curr Biol, 1997. **7**(4): p. 261-9.
155. Bayascas, J.R. and D.R. Alessi, *Regulation of Akt/PKB Ser473 phosphorylation*. Mol Cell, 2005. **18**(2): p. 143-5.
156. Bozulic, L., et al., *PKBalpha/Akt1 Acts Downstream of DNA-PK in the DNA Double-Strand Break Response and Promotes Survival*. Mol Cell, 2008. **30**(2): p. 203-13.
157. Dunant, P., et al., *Expression of dystrophin driven by the 1.35-kb MCK promoter ameliorates muscular dystrophy in fast, but not in slow muscles of transgenic mdx mice*. Mol Ther, 2003. **8**(1): p. 80-9.
158. Osoegawa, K., et al., *Bacterial artificial chromosome libraries for mouse sequencing and functional analysis*. Genome Res, 2000. **10**(1): p. 116-28.

159. Casanova, E., et al., *Construction of a conditional allele of RSK-B/MSK2 in the mouse*. *Genesis*, 2002. **32**(2): p. 158-60.
160. Nagy, A., et al., *Derivation of completely cell culture-derived mice from early-passage embryonic stem cells*. *Proc Natl Acad Sci U S A*, 1993. **90**(18): p. 8424-8.
161. Delbono, O., et al., *Loss of skeletal muscle strength by ablation of the sarcoplasmic reticulum protein JP45*. *Proc Natl Acad Sci U S A*, 2007. **104**(50): p. 20108-13.
162. Brussee, V., F. Tardif, and J.P. Tremblay, *Muscle fibers of mdx mice are more vulnerable to exercise than those of normal mice*. *Neuromuscul Disord*, 1997. **7**(8): p. 487-92.
163. Moll, J., et al., *An agrin minigene rescues dystrophic symptoms in a mouse model for congenital muscular dystrophy*. *Nature*, 2001. **413**(6853): p. 302-7.
164. Briguet, A., et al., *Histological parameters for the quantitative assessment of muscular dystrophy in the mdx-mouse*. *Neuromuscul Disord*, 2004. **14**(10): p. 675-82.

## 6. Acknowledgements

First of all, I want to thank Professor Markus A. Rüegg for providing me with the opportunity to perform this PhD thesis in his laboratory.

I am grateful for the goodwill and the high degree of freedom which I experienced during this work. Also, I appreciate very much the commitment which he offered towards the project and his interest in the scientific education of us PhD students. He took a lot of time in promoting me to develop a better presentation style and encouraged me to meet public challenge.

I want to thank Professor Bernhard Bettler for accepting to be the coreferee of this thesis and Professor Martin Spiess for chairing the exam.

Further, I would like to thank all the people of Markus Rüegg's lab, especially the ones from the mTOR- and the brain-team who supported me with words and deeds. Many other colleagues from the 7<sup>th</sup> floor gave me valuable advice.

Finally, I want to thank Sibylle, my parents and all my family and friends for their support during the time of this work.

**Personal Details**

Name and Address: Dimitri Cloëtta  
Date of Birth: 23. April 1979  
Home Town: Zürich, Bergün  
Email: dimitri.cloetta@unibas.ch

**Education**

01/06/2009 – 30/04/2010 Postdoctoral studies.  
Analysis of neural stem cells that ectopically express activated Notch2.  
“The role of Notch2 in glioblastoma formation”.  
Department of Biomedicine Basel, University of Basel.

01/10/2004 – 31/05/2009 PhD thesis in neurobiology.  
Generation and analysis of mice which lack the mTOR complex 1 member raptor in the brain.  
“The Role of mTOR Complex 1 in Brain Development”.  
Biozentrum, University of Basel.

10/1999 – 04/2004 Diploma in natural sciences.  
Course of studies with specialization in Biochemistry and Molecular Biology/Biophysics at the Department of Biology, ETH Zürich.

Diploma thesis at the Institut für medizinische Mikrobiologie Zürich, in the field of *Mycobacterium tuberculosis* virulence:  
“Generation of Vectors for Allelic Replacement of *Mycobacterium tuberculosis* Prolipoprotein Diacylglycerol Transferase *lgt*”.

08/1992 – 02/1999 Secondary School in Zürich, matura typus B.

**Further Experience**

03/2000 – 06/2000 Temporary employment at UBS AG in Zürich.  
Trade processing.

**Languages**

German: native speaker  
English: fluent (written and spoken)  
French: good knowledge

### Talks and publications

“The role of mTOR complex 1 (mTORC1) and mTORC2 in skeletal muscle and brain”.

Presentation of the mTOR project of our group at the XXII<sup>nd</sup> International Winter Meeting of the Swiss Society of Neuropathology, St. Moritz, 27 – 30/03/2008.

“Investigation of the mTOR complex I in brain development”.

Poster at the 6<sup>th</sup> FENS Forum of European Neuroscience Geneva, 12. – 16. July, 2008.

“Skeletal Muscle-Specific Ablation of *raptor*, but Not of *rictor*, Causes Metabolic Changes and Results in Muscle Dystrophy”.

C. Florian Bentzinger, Klaas Romanino, Dimitri Cloëtta, Shuo Lin, Joseph B. Mascarenhas, Filippo Oliveri, Jinyu Xia, Emilio Casanova, Céline F. Costa, Marijke Brink, Francesco Zorzato, Michael N. Hall, Markus A. Rüegg. *Cell Metab.* 2008 Nov;8(5):411-424.

### References

Prof Bernhard Bettler (postdoctoral studies)  
Molecular Neurobiology  
DBM – Klingelbergstrasse  
Klingelbergstrasse 50/70  
CH-4056 Basel

Tel: 061 267 16 32  
Email: [bernhard.bettler@unibas.ch](mailto:bernhard.bettler@unibas.ch)

Prof Markus A. Rüegg (PhD studies)  
Neurobiology  
Biozentrum, University of Basel  
Klingelbergstrasse 50/70  
CH-4056 Basel

Tel: 061 267 22 23  
Email: [markus-a.ruegg@unibas.ch](mailto:markus-a.ruegg@unibas.ch)